# TOWARDS TRACTABLE PARAMETER-FREE STATISTICAL LEARNING

by

Aaron Angelo D'Souza

A Dissertation Presented to the
FACULTY OF THE GRADUATE SCHOOL
UNIVERSITY OF SOUTHERN CALIFORNIA
In Partial Fulfillment of the
Requirements for the Degree
DOCTOR OF PHILOSOPHY
(COMPUTER SCIENCE)

December 2004

## Dedication

This dissertation is dedicated to a woman of strength and beauty, who taught me much of what makes me the person I am; my grandmother, Benedicta Correia.

## Acknowledgements

It has been a privilege to have had Stefan Schaal as my *sensei* through this journey. As if finding a mentor who brings out the best in his students wasn't enough, I've been lucky to have one who has also grown to be a dear friend. He has provided direction and inspiration, while giving me the freedom to develop my own ideas and style of research. Under his wing, our little research group has become family, and our lab has become a home that I am loth to take leave of. I will miss our extended discussions on statistics, balrogs, and everything in between.

I could not have accomplished this body of work were it not for the wonderful advice and support from Sethu Vijayakumar, Andrew Moore, Chris Atkeson and Ashish Goel. I would especially like to thank Shun-ichi Amari and Mitsuo Kawato for the opportunities to spend very rewarding periods of time at the RIKEN Brain Science Institute and ATR Laboratories respectively.

I must also thank our (extended) lab: Aude Billard, Rick Cory, Auke Ijspeert, Shrija Kumari, Michael Mistry, Peyman Mohajerian, Srideep Musuvathy, Jan Peters & Ladan Shams for becoming family over the last four years. A special mention goes to Jo-Anne Ting, who has been a great help, and fabulous sounding board for many crazy research ideas in this last year. Also to Eric Coe, for providing the best mixture of caffeine, jazz, sarcasm and friendship anyone could ask for.

My parents Afra & Ayres D'Souza and sister Maria have provided me with the opportunities, encouragement and love which have allowed me to reach this far. I hope I have made them proud. My dear fiancée Jayita Bhojwani has been a pillar of strength, and the rest of my life with her will not be enough to thank her for loving, encouraging, prodding, scolding, inspiring and tolerating me during the ups and downs of graduate student life.

# Contents

# List Of Tables

# List Of Figures

## Abstract

The objectivity of statistical analysis hinges on the assumptions made about the form and complexity of the model used to fit the data. These usually take the guise of "nuisance parameters" which must be set based on some meta-level knowledge of the problem to be solved. This dissertation seeks to contribute statistical methods which require as little meta-level knowledge as possible, and yet are computationally and analytically tractable enough to operate on real-world datasets.

This goal is partially achieved within the framework of Bayesian statistics, which allows the specification of prior knowledge, and lets the data correctly constrain model complexity. However, for all but the simplest of statistical models, a full Bayesian treatment is often analytically and computationally intractable. We therefore explore the usefulness of approximation techniques; in particular, those stemming from variational calculus, to gain analytical tractability when performing statistical inference in complex graphical models.

We provide a novel, analytically closed-form solution to estimating the cardinality of mixture models, by locally approximating the evidence for splitting existing models, and thus growing complexity as needed. We contribute a solution to the problem of estimating forgetting rates for online learning by modeling the non-stationarity of the model as a set of drifting parameters, thus allowing a variational Kalman smoother to estimate the time scale of the process drift. We also address the estimation of Bayesian distance metrics for locally weighted regression — a problem commonly known as supersmoothing — by probabilistically modeling the kernel weights assigned to the data.

Another contribution of this dissertation is the development of statistical inference methods which are computationally scalable. We derive a probabilistic version of backfitting — a highly robust and scalable class of supervised non-parametric algorithms — and demonstrate that, among others, the framework of sparse Bayesian learning arises from this class as a special case.

We conclude that in several difficult statistical learning problems, principled approximation techniques, and careful model construction can create scalable and robust algorithms which eliminate the most difficult model complexity parameters, while retaining their applicability to large, complex and underconstrained data sets.

# Chapter 1

# Introduction

Humans and other biological learning "machines" demonstrate an immense amount of variability in learning strategies, along with an adaptive ability that spans a wide range of spatio-temporal scales. In this sense, they are truly autonomous learning entities since they require little outside intervention to configure the adaptive process.

The last several decades of research in the artificial intelligence and in particular, machine learning, have been working towards this goal of achieving greater autonomy in complex adaptive systems that can function in the real world with minimal monitoring and intervention. However, developing a machine learning framework that can display the same robustness as its biological counterpart, and operate without modification on the many noisy, large and underconstrained data sets that the real world has to offer has been an elusive goal. In some sense, we can regard the autonomy of an intelligent system at two levels:

**Task-level autonomy:** Autonomy at this level concerns itself with judging the correct actions to carry out based on the perceived state of an uncertain environment. A robot (for example) must choose between various actions or behavior modes that achieve goals or maximize expected rewards. Hierarchical plan generation, and decisions involving role and resource allocation in groups of intelligent entities also fall under this domain. Research on planning, reinforcement learning and POMDPs for example, addresses the autonomy required to accomplish these tasks.

**Inference-level autonomy:** Task-level autonomy relies on basic statistical operations such as regression, classification, clustering and density estimation to provide the building blocks of action and reasoning. For example, an autonomous humanoid robot requires that the statistical models of its inverse dynamics are constructed before the task of planning movements and trajectories is successful. This is fundamentally a regression problem from the representation of a desired movement, to the actuator commands required to achieve it. Autonomy at the inference level is concerned with the construction of such *models* of the observed data. This type of autonomy is the primary topic of this dissertation.

When discussing inference-level autonomy, it is important to note the distinction between *choosing* the correct model, and *optimizing* its parameters to fit the data. While there exists an extensive body of literature that deals with the optimization of model parameters, this process must necessarily rely on the appropriate model being chosen to begin with. In particular, a crucial aspect of model choice involves the specification of its complexity or modeling capacity which directly influences its capability to fit either simple or complex data sets. As we shall see, incorrectly specifying this "parameter" can lead to a failure to generalize correctly to unseen data. Even though setting the model complexity correctly is an important part of model construction, for an intelligent system

Figure 1.1: The Sarcos humanoid robot.

that functions in the real world and which faces the task of analyzing data that could arise from processes of varying complexity, having an oracle specify the correct model complexity at each instance does not result in a great deal of autonomy.

Besides the requirement of autonomy in specifying the model complexity, this determination must be achievable in an efficient manner, both in the use of data as well as computation time. As an example, when learning its own inverse dynamics, the Sarcos humanoid robot shown in figure 1.1 has a mere 2ms to incorporate new data in to the existing model and generate a motor command for the following timestep. Also, with training data being available at such high frequencies, and thus very large quantities, it becomes necessary to efficiently cache useful statistics from the data such that we are not burdened with processing the entire history every time we wish to generate a useful prediction.

Of the many approaches to machine learning, the field of *statistical* learning embodies some of the most promising features that we would expect from truly autonomous learning:

**Representation of uncertainty:** Learning machines are faced with numerous sources of ambiguity and uncertainty. Real-world data is frequently corrupted by noise and outliers due to sensor limitations. Taking into account this stochasticity is vital to the success of any learning system. Modeling the learning process as probabilistic inference can implicitly and explicitly represent the uncertainty in both our assumptions about the world and the inference results. In effect, modeling uncertainty gives us knowledge about the "lack of knowledge", allowing a learning system to focus on reducing this uncertainty.

**Meta-learning:** The ability to "learn how to learn" is a key element of producing robust learning systems that can adapt to varying degrees of problem type and complexity. For example, while conventional neural network research has taken inspiration from biology's computational structure, it has failed in creating a principled description of self-regulated learning so often found in biological systems. One of the main strengths of a statistical learning machine is its ability to mathematically quantify uncertainty in *itself*. As we shall see, this feature allows us to perform an important component of self-adaptation; automatic determination of statistical model complexity.

## 1.1 Nuisance Parameters in Statistical Learning

At the core of statistical analysis is the model used to fit the observed data. The most crucial decision facing the analyst is the structure of this model. Model structure encapsulates the key assumptions about the process that is believed to have generated the data, and hence constrains the analysis results such that it is possible to generalize from them in a meaningful manner. The exact definition of what constitutes "model structure" varies drastically as one moves between the various research sub-communities in machine learning, but a common thread seems to suggest that one should interpret structure as a set of *restrictions* on the space of possible hypotheses that can explain the data (Mitchell 1997). Without assumptions to constrain this space, one can do no better than to memorize the observed data — a solution that is as trivial as it is useless.

The assumptions used to develop a statistical model can be coarsely divided into two main categories:

1. Assumptions that describe model *form.*
2. Assumptions that restrict model *complexity.*

Often, the first category of assumptions are motivated by constraints of efficiency and representation ability. For example, efficiency constraints may require us to model a data set using a collection of computationally efficient locally linear models, while the knowledge that we are modeling periodic data may prompt us to use a basis space of sine and cosine functions or von Mises distributions[1]. Kernel methods, which include the popular support vector machine (SVM) (Schölkopf & Smola 2000), and Gaussian process regression (Williams & Rasmussen 1996), feature a particularly direct example of choice in model form, since their function analytic view requires the explicit choice of function class (polynomial, linear, Gaussian etc.) by choosing the corresponding (combination of) reproducing kernel Hilbert spaces (RKHSs) within which a solution is to be found.

What we will primarily concern ourselves with throughout this dissertation, is the second category of assumptions: those that determine the model *complexity.* Complexity parameters occur in many forms in statistical learning models. The following list is a small set of examples:

- Number of assumed latent dimensions for dimensionality reduction.
- Number of components in a mixture model.
- Number of relevant inputs or features for supervised learning.
- Spatio-temporal distance metrics for local learning.
- Size of the window of sufficient statistics in online learning.

A common property of all these parameters is that by tuning them, we can create a spectrum of models, which are able to fit data sets of various complexities. For example, assuming a small latent dimensionality in principal component analysis (PCA) allows the model to only fit a set of simple data sets of low dimensionality, while producing large errors on data sets with high-dimensional structure. The effects of underestimating model complexity are easy to detect since we observe poor modeling performance on the so-called *training* data set. Overestimating model complexity is a far more difficult problem to

[1]Defined as $p(x) = \frac{\exp(b\cos(x-a))}{2\pi I_0(b)}$ for $x \in [0, 2\pi)$ where $I_0(\cdot)$ is a modified Bessel function of first kind, the von Mises distribution is a circular analog of the Normal distribution

tackle since the model will perform extremely well on the training data, but fail miserably when generalizing to unseen examples. This phenomenon is well known in statistical learning literature as the *bias-variance tradeoff* (Geman et al. 1992). Essentially, an overly complex model will fit the (inevitable) noise in an observed data set, and successive re-training from multiple data sets will result in wildly differing estimates (high variance) of the model parameters.

In many cases, prior knowledge of the data-generating process may help us make an educated guess about the correct model complexity. For example, knowing sensor limitations may help us bound the frequency range of a measured signal, thus introducing smoothness constraints in the model used to analyze it. However, such knowledge is not always easy to come by, and may be difficult to infer *a priori*. Picking the correct values for these complexity parameters is therefore crucial to the outcome of the inference process, and yet these are the parameters for which we would most like to have the data tell us their value. It is little wonder that these complexity variables are often termed “nuisance parameters”.

As the following section will demonstrate, the framework of graphical modeling, in combination with the application of Bayesian statistics can provide an elegant solution to the problem of determining model complexity. However, as we will discuss in chapter 2, more often than not, this solution is analytically and computationally too difficult to apply to most real-world problems.

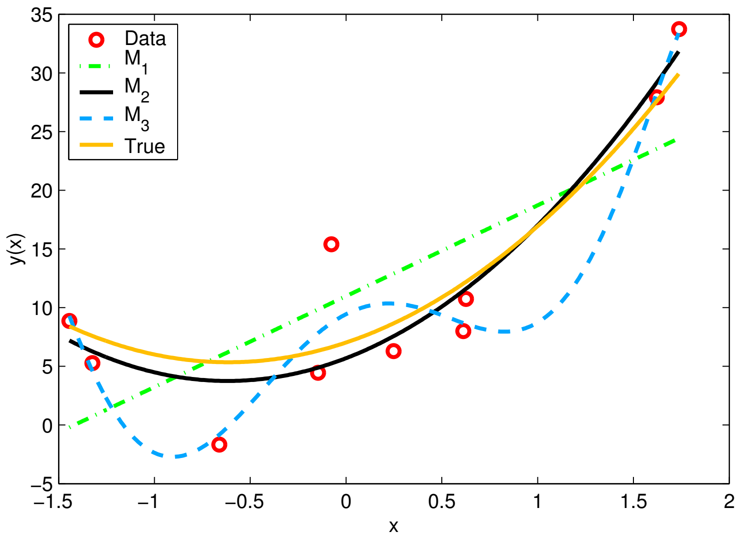

| Model | MSE | Log Evidence | LOO-CV |
|---|---|---|---|
| $\mathcal{M}_1$ | 44.85 | 100.25 | 78.05 |
| $\mathcal{M}_2$ | 15.55 | **104.38** | **25.84** |
| $\mathcal{M}_3$ | **7.92** | 59.91 | 901.06 |

Figure 1.2: A simple regression task, to which models $\mathcal{M}_1$, $\mathcal{M}_2$, and $\mathcal{M}_3$ (of increasing complexity) are applied. The table shows the scores assigned to the model by three metrics: mean squared error (MSE), log Bayesian evidence, and the leave-one-out cross validation error (LOO-CV). The best score (corresponding to the choice of model) is indicated in bold in each column.

## 1.2 Bayesian Model Complexity Estimation

Bayesian inference provides an elegant framework for the automatic determination of model complexity. Consider the simple regression task of figure 1.2. Assume that we have 3 models of increasing complexity $\mathcal{M}_1$, $\mathcal{M}_2$ and $\mathcal{M}_3$[2], and our goal is to find the complexity level that best explains our observed data $\mathbf{x}_\mathcal{D}$. As we can see from figure 1.2,

[2]In this example, polynomials of order 1, 2 and 6, respectively.

using a naive goodness-of-fit measure such as mean squared error (MSE) on the training data, would select the model with the highest complexity since it achieves the least MSE. The generalization ability (closeness to the true function) however, suffers greatly as the complexity is over/underestimated.

How can we best determine which of the three models has the correct complexity for this data set? As a Bayesian inference problem, this is best stated as finding the model $\mathcal{M}_i$ which maximizes:

$$p(\mathcal{M}_i|\mathbf{x}_\mathcal{D}) = \frac{p(\mathbf{x}_\mathcal{D}|\mathcal{M}_i)p(\mathcal{M}_i)}{p(\mathbf{x}_\mathcal{D})} \tag{1.1}$$

If we have no prior preference between the models, then $p(\mathcal{M}_1) = p(\mathcal{M}_2) = p(\mathcal{M}_3) = 1/3$, and it is the so called *evidence* $p(\mathbf{x}_\mathcal{D}|\mathcal{M}_i)$ that will decide between the models under consideration. This quantity is fairly polyonymous; statistics literature refers to it as the "marginal likelihood", while the physics community calls it the "partition function". Notably, this term also features as the normalization constant in the Bayesian inference of the posterior distribution over unobserved parameters (or hidden variables) $\mathbf{x}_\mathcal{H}$ in a model, conditioned on the observed variables $\mathbf{x}_\mathcal{D}$:

$$p(\mathbf{x}_\mathcal{H}|\mathbf{x}_\mathcal{D}, \mathcal{M}_i) = \frac{p(\mathbf{x}_\mathcal{D}|\mathbf{x}_\mathcal{H})p(\mathbf{x}_\mathcal{H}|\mathcal{M}_i)}{\underbrace{p(\mathbf{x}_\mathcal{D}|\mathcal{M}_i)}_{\text{evidence}}}$$

Does maximizing evidence arrive at the correct choice of model complexity? To answer this, consider the caricature scenario depicted in figure 1.3 (adapted from (Bishop 1995)). Each point on the horizontal axis represents a single data set. Low-complexity statistical

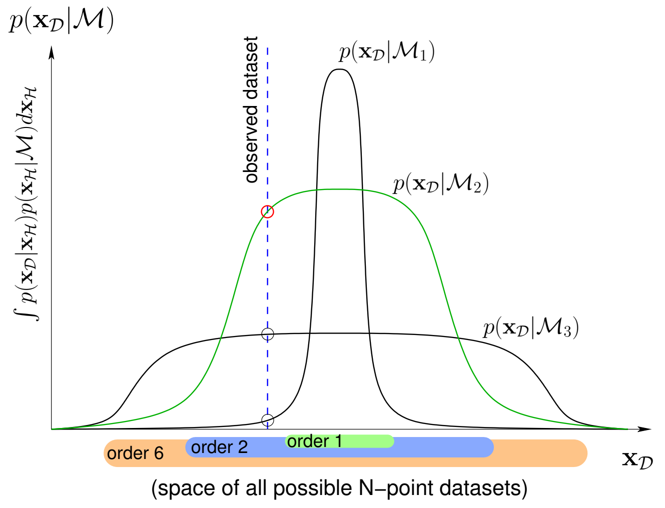

Figure 1.3: A caricature of why the evidence framework achieves model complexity regularization. Each of the three curves is the evidence that the corresponding model provides over the space of possible data sets.

models such as $\mathcal{M}_1$ are only able to give high probability to a small subset of data sets. As the complexity of the model increases, it is able to give high probability to a larger selection of data sets, however since the probability over all data sets must sum to 1, the probability mass is "spread thin" resulting in a lower numerical value for the evidence. Hence when a data set of intermediate complexity is observed, it falls outside the region modeled with high probability by $\mathcal{M}_1$, and although it is modeled equally well by both $\mathcal{M}_2$ and $\mathcal{M}_3$, the evidence for $\mathcal{M}_2$ is greater, giving us the correct choice of model complexity. In this way an idiom known as *Ockham's razor* is achieved, which seeks the simplest solution to a problem from a collection of solutions that model the data equally well. The "Log Evidence" column of the table in figure 1.2 reflects this choice in our toy regression problem. Note that this framework does not eliminate the ability to express our prior belief in a higher complexity class. If we have strong prior reason for believing that $\mathcal{M}_3$ is the true model, then this is merely reflected in the prior probability $p(\mathcal{M}_3)$, which weights the curves of figure 1.3 appropriately to generate the correct model choice in equation (1.1).

Thus, the key is to compare model structure by looking at the *evidence* $p(\mathbf{x}_\mathcal{D}|\mathcal{M}_i)$ that the data provides for the model.

While this framework seems like a very intuitive and reasonable solution to the problem of estimating model complexity, the detail that we have glossed over, is that in order to obtain the evidence, we must integrate over (or marginalize out) the unobserved parameters $\mathbf{x}_\mathcal{H}$ of the model:

$$p(\mathbf{x}_\mathcal{D}|\mathcal{M}_i) = \int p(\mathbf{x}_\mathcal{D}|\mathbf{x}_\mathcal{H})p(\mathbf{x}_\mathcal{H}|\mathcal{M}_i)d\mathbf{x}_\mathcal{H} \tag{1.2}$$

For variables in $\mathbf{x}_\mathcal{H}$ that are discrete, the marginalization takes the form of a summation. Immediately obvious are two difficulties: for discrete variables, even if the number of values each variable can take is small, the number of terms in the summation is exponential in the number of variables. Secondly, for continuous variables, the analytical integration itself may be intractable. While section 2.2 discusses some general algorithms for performing this marginalization in the context of graphical model representations, we shall see that in general, this problem is extremely difficult, both analytically and computationally.

## 1.3 Alternatives to the Evidence Framework

The quest for Ockham's razor is well documented in statistical learning literature. As the toy example in section 1.2 showed, given a noisy data set, it is very likely that for a model in which the complexity has been overestimated, the unneeded complexity will simply be used to fit the noise component of the training data, and thus will render the model's generalization capability to unseen data useless. Part of the problem also arises from the fact that we are dealing with an *inductive* setting, in which we do not know the exact set of data points on which we will eventually be evaluated[3].

While there are several techniques that can be used to regularize model complexity, the following sections will touch upon some of the most prevalent in current statistical learning literature.

### 1.3.1 Cross-Validation

Knowing that an overly complex model will perform well on training data, but badly on test data, an obvious solution is to keep aside a subset of data called the *validation set* on which the trained model is tested. All candidate models $\mathcal{M}_i$ are trained, and the model corresponding to the lowest error on the *validation* set is chosen. Varying the method of selecting the validation set gives rise to an entire spectrum of *cross-validation* methods (Stone 1974, Stone & Brooks 1990) in which the data set is split into $S$ disjoint subsets. Each model is repeatedly trained on $S-1$ chunks and validated on the subset that is left out. An extreme case is leave-one-out cross validation, in which a single data point is left

[3]Settings where this information is known, fall within the framework of *transductive* learning.

out as the validation set, and the error of the model is averaged over all training cycles that leave out each data point in the training set. The third column (LOO-CV) of the table in figure 1.2 shows that the cross-validation approach correctly selects the correct model complexity for the toy problem presented.

Although cross-validation is traditionally regarded as computationally expensive, real-time learning algorithms exist in which leave-one-out cross validation can be implemented exactly, and in an efficient manner (Vijayakumar et al. 2004, Vijayakumar & Schaal 2000, Vijayakumar et al. 2000). A related method which also uses a validation set is *early stopping* used in gradient based multi-layer neural network learning, in which training stopped when the error on a validation set increased thus preventing the network weights from taking on extreme values.

Another potential pitfall, is that when the observed data itself is sparse, it may not be feasible to leave out a portion of it for cross-validation. Indeed it is in such underconstrained situations when correct model regularization is of the utmost importance, and where Bayesian methods tend to excel.

### 1.3.2 Minimum Description Length

The basic idea underlying the Minimum Description Length (MDL) principle (Rissanen 1978, Rissanen 1996), is to view learning as a *data compression* problem. Intuitively, the probabilistic model that generated the data, is the most succinct description of the data set, and thus provides the most compression. Given a set of models $\{\mathcal{M}_1, \mathcal{M}_2, \ldots\}$ with varying complexities, we view each model $\mathcal{M}_i$ as a mechanism for compressing (or equivalently, describing in as short an encoding as possible) the observed data set $\mathbf{x}_\mathcal{D}$.

The choice of model is therefore the one that minimizes a quantity called the *stochastic complexity* $\bar{L}(\mathbf{x}_{\mathcal{D}}|\mathcal{M}_i)$ defined as:

$$\bar{L}(\mathbf{x}_{\mathcal{D}}|\mathcal{M}_i) = L(\mathbf{x}_{\mathcal{D}}|\mathbf{x}_{\mathcal{H}}{}^*; \mathcal{M}_i) + C(\mathcal{M}_i) \tag{1.3}$$

where $\mathbf{x}_{\mathcal{H}}{}^* = \arg\max_{\mathbf{x}_{\mathcal{H}}} L(\mathbf{x}_{\mathcal{D}}|\mathbf{x}_{\mathcal{H}} \in \mathcal{M}_i)$, and is equivalent to choosing the best "instance" of model within the class $\mathcal{M}_i$. The quantity $L(\mathbf{x}_{\mathcal{D}}|\mathbf{x}_{\mathcal{H}}{}^*; \mathcal{M}_i)$ is the encoding length of data $\mathbf{x}_{\mathcal{D}}$ under the best instance, and is defined by the *Shannon-Fano* code-length $L(\mathbf{x}_{\mathcal{D}}|M^* \in \mathcal{M}_i) = -\log p(\mathbf{x}_{\mathcal{D}}|\mathbf{x}_{\mathcal{H}}{}^*)$. The quantity $C(\mathcal{M}_i)$ is called the *parametric complexity* of $\mathcal{M}_i$ and relates to the overall complexity of the model. Intuitively then, we can interpret equation (1.3) as a two-part cost function; the first part which depends on the fit to the data, and the second, which penalizes the overall score proportional to the complexity of the model.

The crucial difference between MDL and Bayesian interpretations of inference, is that in the MDL framework, the probability distributions $p(\cdot|\mathcal{M}_i)$ are treated merely as encoding objects. Unlike Bayesian modeling where we interpret the probability distribution as being some plausible explanation of how the data was generated, the MDL framework does not concern itself with this plausibility at all. MDL accepts a candidate model, even if we know for sure that the data was not generated by that model, since even a completely implausible model is a perfectly valid (albeit probably very inefficient) encoder of the observed data.

How does MDL relate to Bayesian inference? Obviously, if the observed data was truly generated by a particular model's distribution $p(\cdot|\mathcal{M}_i)$, then this distribution also provides the optimal (minimum) encoding length under MDL. Also, for the exponential family of models, MDL selection coincides with Bayes factor model selection based on the non-informative *Jeffrey's prior* prior over the probability manifold (Jeffreys 1946, Bernardo & Smith 1994). Jeffrey's prior is derived from the consideration that any rule for determining the prior density $p(\mathbf{x}_{\mathcal{H}})$ over unknown variables should yield an equivalent result if applied to a transformation $\mathbf{x}_{\mathcal{H}}' = \phi(\mathbf{x}_{\mathcal{H}})$ of the variables. This choice of non-informative prior is $p(\mathbf{x}_{\mathcal{H}}) = J(\mathbf{x}_{\mathcal{H}})^{1/2}$ where $J(\mathbf{x}_{\mathcal{H}})$ is the *Fisher information* for $\mathbf{x}_{\mathcal{H}}$:

$$J(\mathbf{x}_{\mathcal{H}}) = \left\langle \left( \frac{d \log p\left(\mathbf{x}_{\mathcal{D}} | \mathbf{x}_{\mathcal{H}}\right)}{d\mathbf{x}_{\mathcal{H}}} \right)^2 \right\rangle = - \left\langle \left( \frac{d^2 \log p\left(\mathbf{x}_{\mathcal{D}} | \mathbf{x}_{\mathcal{H}}\right)}{d\mathbf{x}_{\mathcal{H}} d{\mathbf{x}_{\mathcal{H}}}^T} \right) \right\rangle$$

### 1.3.3 Bayesian/Akaike Information Criteria

We noted that the MDL method can be viewed as creating a two-part cost function which penalizes higher model complexity that does not justify a proportional increase in the efficacy of modeling the data. Both the Schwarz Bayesian Information Criterion (BIC or SBIC), and the Akaike Information Criterion (AIC) offer similar penalty terms, but are derived from very different considerations.

BIC (Schwarz 1978) can be derived by performing a Laplace approximation to the integral required in maximizing the posterior probability over a set of candidate models (c.f. equation (1.2)). Under a large sample assumption, the correct model is chosen by maximizing the following expression over the collection of candidate models.

$$BIC\left(\mathcal{M}_i\right) = \ln p(\mathbf{x}_{\mathcal{D}} | {\mathbf{x}_{\mathcal{H}}}^*, \mathcal{M}_i) - \frac{1}{2} \left|\mathcal{M}_i\right| \ln N \tag{1.4}$$

where $\mathbf{x}_{\mathcal{H}}{}^{*} = \arg\max_{\mathbf{x}_{\mathcal{H}}} \ln p(\mathbf{x}_{\mathcal{D}}|\mathbf{x}_{\mathcal{H}}, \mathcal{M}_i)$, $|\mathcal{M}_i|$ denotes the number of unknown parameters $\mathbf{x}_{\mathcal{H}}$ in $\mathcal{M}_i$, and $N$ denotes the number of observed data points. A more accurate version of BIC can be derived by retaining the second order derivative terms of the likelihood function:

$$BIC_2\left(\mathcal{M}_i\right) = \ln p(\mathbf{x}_{\mathcal{D}}|\mathbf{x}_{\mathcal{H}}{}^{*}, \mathcal{M}_i) - \frac{1}{2}\left|\mathcal{M}_i\right| \ln N - \frac{1}{2}\ln\left|J_i\left(\mathbf{x}_{\mathcal{H}}{}^{*}\right)\right| + \frac{1}{2}\left|\mathcal{M}_i\right| \ln 2\pi$$

where

$$J_i\left(\mathbf{x}_{\mathcal{H}}{}^{*}\right) = -\frac{1}{N}\left.\frac{\partial^2 \ln p(\mathbf{x}_{\mathcal{D}}|\mathbf{x}_{\mathcal{H}}, \mathcal{M}_i)}{\partial \mathbf{x}_{\mathcal{H}} \partial \mathbf{x}_{\mathcal{H}}{}^{T}}\right|_{\mathbf{x}_{\mathcal{H}}=\mathbf{x}_{\mathcal{H}}{}^{*}}$$

Note that the Fisher information term is identical to the one we saw in the previous section. An important property of BIC is that it can be shown to be a *consistent* model, i.e. if the true model $\mathcal{M}^*$ exists among the set of candidate models, then the probability of selecting the model of correct complexity approaches one as the sample size increases.

The Akaike Information Criterion (AIC) (Akaike 1974) is derived from an asymptotic minimization of the Kullback-Leibler (KL) divergence between the true model of the data, and an approximation to this model. Under a large sample assumption, and certain regularity conditions on the likelihood function, the correct model is selected by maximizing the following expression over the collection of candidate models:

$$AIC\left(\mathcal{M}_i\right) = \ln p(\mathbf{x}_{\mathcal{D}}|\mathbf{x}_{\mathcal{H}}{}^{*}, \mathcal{M}_i) - \left|\mathcal{M}_i\right| \tag{1.5}$$

where $|\mathcal{M}_i|$ is the number of open parameters in model $\mathcal{M}_i$. In settings where the sample size is small, AIC tends to overestimate the model complexity. Variants such as AICC — a corrected version of AIC (Hurvich & Tsai 1976) — have been shown to dramatically outperform AIC in such cases. Unfortunately there does not exist a proof of the consistency of AIC as in the BIC case.

The only difference between BIC and AIC in equations (1.4) and (1.5) is the complexity penalty term which leads to different model selection behavior. For large sample sizes, BIC is more conservative than AIC due to its higher penalty term. It will typically choose a model of complexity lesser than or equal to that chosen by AIC.

Both BIC and AIC would seem to provide an "automatic" model selection without the need to specify any prior distributions over the parameters space of the statistical models. While this may be seen as an advantage in some situations, it takes away both the freedom to incorporate prior knowledge about such model structure, as well as the responsibility of the statistical analyst to think carefully about the effect of a particular choice of prior. Note that there are also seemingly "prior-less" ways of achieving model regularization, such as the well-known *ridge* parameter in ridge regression. As with other forms of automatic regularization however, this can be easily interpreted in terms of a Bayesian prior. For ridge regression, the ridge parameter serves as the precision variable of a Gaussian prior over the regression coefficients (Hastie, Tibshirani & Friedman 2001).

### 1.3.4 Reversible Jump Markov Chain Monte Carlo

Markov Chain Monte Carlo (MCMC) is a term used for a class of sampling methods, in which the posterior distributions over the hidden variables $\mathbf{x}_{\mathcal{H}}$ is not represented parametrically, but instead as a collection of samples. This is done by constructing a Markov chain whose stationary distribution is the posterior distribution of interest. After sampling for a sufficiently long duration, the distribution approximated by the collection of samples approaches the true posterior distribution. Popular samplers include the Gibbs sampler (Geman & Geman 1984), and the Metropolis-Hastings method (Metropolis et al. 1953, Hastings 1970). Andrieu et al. (2003) provide an excellent review of MCMC techniques applied to machine learning.

In general, most statistical inference techniques (including traditional MCMC) assume that the structure of the statistical model is fixed, or equivalently, the size of the vector of unknown variables $\mathbf{x}_{\mathcal{H}}$ is a constant. For problems which concern model structure however, this is typically not the case. For example, if we wish to determine the cardinality of a mixture model, then adding a mixture component increases the number of unknown variables by the number of parameters required to describe the new component.

Since Gibbs samplers rely on successively sampling elements of $\mathbf{x}_{\mathcal{H}}$ conditioned on fixed values of the rest of the model, it makes no sense to generalize them to unknown numbers of these fixed variables. However, a variant of the Hastings method known as *reversible jump* MCMC (Green 1995, Richardson & Green 1997) allows us to achieve the required model selection between statistical models with potentially different numbers of unknown variables.

This is achieved by sampling from a countable set of *moves*, each of which could potentially switch between candidate models $\mathcal{M}_i$ and thus increase or decrease the size of the vector $\mathbf{x}_{\mathcal{H}}$. For a dimension (model structure) changing move $m$, a continuous random vector $\mathbf{u}$ is drawn (independent of $\mathbf{x}_{\mathcal{H}}$) and the state $\mathbf{x}_{\mathcal{H}}{}'$ in the new model is calculated as an invertible deterministic function of $\mathbf{x}_{\mathcal{H}}$ and $\mathbf{u}$. The acceptance probability for a move is given by:

$$\min\left\{1, \frac{p(\mathbf{x}_{\mathcal{H}}{}'|\mathbf{x}_{\mathcal{D}})r_m(\mathbf{x}_{\mathcal{H}}{}')}{p(\mathbf{x}_{\mathcal{H}}|\mathbf{x}_{\mathcal{D}})r_m(\mathbf{x}_{\mathcal{H}})q(\mathbf{u})}\left|\frac{\partial \mathbf{x}_{\mathcal{H}}{}'}{\partial(\mathbf{x}_{\mathcal{H}}, \mathbf{u})}\right|\right\}$$

where $r_m(\mathbf{x}_{\mathcal{H}})$ is the probability of choosing move $m$ in state $\mathbf{x}_{\mathcal{H}}$, and $q$ is the density from which $\mathbf{u}$ is drawn. For a move that does not change the dimension of $\mathbf{x}_{\mathcal{H}}$ this procedure reduces to the Metropolis-Hastings acceptance probability. Note that for models with a large number of parameters, the required computation of the Jacobian of transformations between models of different dimensionality is a non-trivial computational difficulty.

In general, sampling methods are potentially more accurate than others since they are unconstrained by the assumptions of parametric form in the probability distributions over variables. They are most appealing when samples are required from the predictive distribution, since no explicit parameterization of the posterior distribution is required. This same feature however, makes summarization of the inferred posterior distributions difficult since parametric summarizations can be misleading and distort the true nature of the distributions. Another disadvantage is that estimating the required length of the sampling process before we are assured that the chain has indeed converged to its stationary distribution, is still largely an unsolved problem.

### 1.3.5 Structural Risk Minimization

Assume we have a pattern recognition problem in which our training data consists of feature vectors $\mathbf{x}_i \in \Re^d$ describing each pattern and the corresponding $y_i \in \{1, -1\}$ give us the truth of the pattern's class. Assume we also have a learning machine (or class of functions) $f(\mathbf{x}, \boldsymbol{\alpha})$, which is parameterized by $\boldsymbol{\alpha}$. Any member of the class (indexed by a particular value of $\boldsymbol{\alpha}$) takes as input the feature vector $\mathbf{x}$ and returns a prediction of the class label $y$. If the data is generated according to some unknown distribution $p(\mathbf{x}, y)$, then the expected (true) risk for the prediction function under a given parameterization $\boldsymbol{\alpha}$ is:

$$R(\boldsymbol{\alpha}) = \int \frac{1}{2} \left| y - f\left(\mathbf{x}, \boldsymbol{\alpha}\right) \right| p(\mathbf{x}, y) d\mathbf{x} dy$$

The statistical inference problem can be thought of as seeking to reduce this expected risk by choosing the appropriate parameterization $\boldsymbol{\alpha}$. Unfortunately, since we do not know $p(\mathbf{x}, y)$, this quantity is impossible to compute directly. Given a particular data set $\{\mathbf{x}_i, y_i\}_{i=1}^{N}$ however, we can compute the *empirical* risk observed on this training data set:

$$R_{\text{emp}}(\boldsymbol{\alpha}) = \sum_{i=1}^{N} \frac{1}{2N} \left| y_i - f\left(\mathbf{x}_i, \boldsymbol{\alpha}\right) \right|$$

Note that this quantity does not require knowledge of the distribution $p(\mathbf{x}, y)$. For a fixed $\boldsymbol{\alpha}$ (i.e. particular function chosen from the function class), and the training set, this value is a constant. Under the assumption that the training data was generated from the true distribution $p(\mathbf{x}, y)$, the following bound (Vapnik 1995) holds:

$$R(\boldsymbol{\alpha}) \leq R_{\text{emp}}(\boldsymbol{\alpha}) + \underbrace{\sqrt{\frac{h\left(\ln\frac{2N}{h}+1\right)-\ln\frac{\eta}{4}}{N}}}_{\text{VC confidence}} \text{ with probability } 1-\eta \tag{1.6}$$

This equation tells us that given an empirical risk $R_{\text{emp}}(\boldsymbol{\alpha})$ calculated on a particular data set, with probability $1-\eta$ the true risk is bounded by the quantity on the right hand side of equation (1.6). The quantity $h$ is known as the Vapnik-Chervonenkis (VC) dimension, and is a measure of the "capacity" (related to model complexity) of the family of functions $f(\mathbf{x}, \boldsymbol{\alpha})$. Note that the VC dimension is not associated with any particular instance of a function within a class (even though $R(\boldsymbol{\alpha})$ and $R_{\text{emp}}(\boldsymbol{\alpha})$ are), but instead with the entire class of functions. Structural risk minimization (SRM) (Vapnik 1982) therefore "structures" the space of functions as nested subsets, and computes $h$ (or at least a bound for it) for each subset of functions. While in simple situations, one can relate the VC dimension $h$ to the number of open parameters in the model (as is done directly in the penalty term of AIC), we are cautioned against this naïve interpretation. As the simple "sine" function example can demonstrate, a single parameter function can have infinite classification (or "shattering") power on the real line, and therefore must be treated specially when analyzing its complexity.

To use the SRM framework, we select a set of candidate function classes, and for each we pick the instance within that class that minimizes the empirical training error. We then pick the one that minimizes the sum of its empirical risk and its VC confidence. Intuitively, this procedure makes sense, since, if we have a set of models, each of which fits the training data equally well (i.e. results in the same empirical risk), the bound in equation (1.6) is minimized by choosing the function class with the lowest VC dimension (or complexity). Note that the bound is a probabilistic bound (i.e. it is true with probability $1 - \eta$), and is thus related to what is known as a *Monte Carlo method* in the field of randomized algorithms (Motwani & Raghavan 1995). If the bound is tight for at least one of the candidate function classes, then we are guaranteed that we can do no better, but if the bound is not tight for any class under consideration, then we can do no better than to hope for the best.

This relatively abstract notion serves as the basis for the highly popular support vector machine (SVM). The SVM is a linear classifier, which finds a hyperplane that (for linearly separable problems) maximally separates the two classes (which is why this class of methods is also known as maximum-margin methods). For problems which are not linearly separable, there exist variants (C-SVM and $\nu$-SVM) which feature a tradeoff parameter which allows simpler decision boundaries, at the expense of some training classification errors. Interestingly, all inference in the SVM can be derived solely using inner products in the data space. This allows us to easily extend its applicability to nonlinear settings by the use of the *kernel trick* (Schölkopf & Smola 2000).

While the support vector machine is certainly considered to be a state-of-the-art machine learning tool, its inability to give true probabilistic predictions is a disadvantage. In addition, the requirement of cross-validation to determine the correct values of the tradeoff parameter becomes prohibitively expensive for large data sets, and is not naturally generalizable to online learning settings.

In general, the SRM framework does not explicitly deal with probability distributions over the hypothesis space, but only concerns itself with picking the correct function (class) that minimizes the expected risk. It is difficult to map the framework of SRM into equivalent notions in Bayesian statistical learning, or vice-versa. As such, it forms a parallel body of work that is very effective at doing principled machine learning. While proponents of the Bayesian methods value the flexibility of being able to introduce prior knowledge about the hypothesis space, the SRM framework sidesteps the explicit modeling of probability distributions, since ultimately we are only concerned with the expected error obtained by our learning machine.

## 1.4 Dissertation Outline

The remainder of this dissertation is organized as follows:

- Chapter 2 reviews graphical models as an intuitive tool for describing the probabilistic relationships between variables in a statistical model. It discusses basic inference techniques such as the junction tree algorithm for estimating marginal distributions in such models, and highlights the analytical and computational difficulties that arise as the complexity of the models increase. We also discuss the parameter optimization framework of expectation-maximization (EM), and show that an elegant approximation technique known as the factorial variational approximation can be derived very naturally as an extension.

- Chapter 3 introduces three algorithms contributed by this dissertation which tackle especially difficult problems of model complexity estimation. The first deals with estimating the cardinality of mixture models using a novel technique that approximates the statistical evidence for splitting local models. The second algorithm deals with the problem of estimating the size of the temporal "window" of sufficient statistics in online learning problems. We show that by tracking the drifting process using a variational Kalman smoother, we can obtain a principled estimate of this window size. The third algorithm deals with estimating the spatial extent of locally weighted learning components — a problem known as supersmoothing. We show that by placing distributions over the kernel weighting parameters and by using properties of convex duality to derive a lower bound, we can obtain a probabilistic estimate of a local component's spatial extent.

- Chapter 4 discusses the issue of the computational complexity of inference for supervised learning. We review several efficient algorithms, some of which form the inspiration for a novel derivation of backfitting — an efficient family of supervised learning algorithms. By deriving backfitting with probabilistic underpinnings, we can leverage the computational robustness of the original algorithm, while introducing the benefits of Bayesian inference and model selection. Using bounds derived from convex duality, we extend the algorithm to classification tasks, and show that the framework of sparse Bayesian learning can be derived using Bayesian backfitting at its core. The popular relevance vector machine (RVM) is an example of such an algorithm which can benefit from the scalability and robustness of Bayesian backfitting.

- Chapter 5 concludes with a summary of the research presented in this thesis, and a discussion of its future direction.

# Chapter 2

# The Quest for Analytical Tractability

In this chapter, we will briefly introduce graphical models, their types and the terminology we will use to refer to them through the rest of this dissertation. We also review some of the algorithms that are used to perform Bayesian inference in graphical models. In particular, we will revisit the well-known expectation-maximization (EM) algorithm, and show that an important class of approximate algorithms can be derived as a natural generalization of this method.

## 2.1 Graphical Models

Probabilistic inference has been intimately tied to graph theory through the representation tool of *graphical models* (Pearl 1988, Lauritzen 1996). Given a graph $\mathcal{G} = (\mathcal{V}, \mathcal{E})$, with vertices $\mathcal{V}$ and edges $\mathcal{E}$ (directed or undirected), we associate a random variable $x$ with each vertex $i \in \mathcal{V}$. The random variables may be discrete or continuous. Associated with this graph, is a probability distribution over the set of random variables which factorizes according to the structure of the graph. For discrete variables this distribution is a mass function (a density with respect to a counting measure), while for continuous variables, it is a density with respect to the Lebesgue measure. For any subset $\mathcal{A} \subseteq \mathcal{V}$ we define $\mathbf{x}_\mathcal{A} = \{x_i | i \in \mathcal{A}\}$.

The structure of a graphical model imposes a factorization over the probability distribution, and elegantly captures the structure of conditional independence between the variables in a statistical model. Variable $x_i$ is conditionally independent of another variable $y$, given a third variable $z$, if we can write $p(x, y|z) = p(x|z)p(y|z)$. Graphical models representing the conditional independence relationships between random variables can be broadly classified into two categories: undirected graphs (Markov networks or Markov random fields), and directed acyclic graphs (DAGs, or Bayesian networks). The reader is referred to (Lauritzen 1996) for an excellent formal treatise on graphical models in their various representation forms.

In an undirected graphical model, we define a set of cliques $\mathcal{C}_1 \ldots \mathcal{C}_M$ to be a set of maximally fully connected subsets of vertices in $\mathcal{V}$, such that $\cup_{m=1}^{M} \mathcal{C}_m = \mathcal{V}$. A clique $\mathcal{C}_m$ is maximally fully connected if the addition of any vertex not already in $\mathcal{C}_m$ destroys the fully connected property. In such a graphical model, the joint probability distribution over the variables in the model is represented by a normalized product of *clique potential functions* $\psi_m$ over cliques $\mathcal{C}_m$:

$$p(\mathbf{x}) = \frac{1}{Z} \prod_{m=1}^{M} \psi_m \left(\mathbf{x}_{\mathcal{C}_m}\right)$$

Each clique potential function depends only on the variables in its corresponding clique, and is restricted to be non-negative. The normalizing constant $Z$ is chosen such that the sum of probabilities over all possible configurations of the random variables is one.

Conditional independence in an undirected graphical model is represented by the concept of graph separability. For three mutually disjoint sets of vertices $\mathcal{A}$, $\mathcal{B}$ and $\mathcal{C}$, we say that $\mathbf{x}_{\mathcal{A}}$ and $\mathbf{x}_{\mathcal{B}}$ are conditionally independent given $\mathbf{x}_{\mathcal{C}}$ if all paths between a vertex in $\mathcal{A}$ and another vertex in $\mathcal{B}$ must pass through a vertex in $\mathcal{C}$ (also known as the Markov property). By the Hammersley-Clifford theorem (Hammersley & Clifford 1971), for strictly positive density functions $p(\mathbf{x})$, the factorization property across clique potentials, and the Markov property are equivalent.

In a directed acylic graph, an edge from node $x_i$ to $x_j$ establishes that $x_i$ is the *parent* of $x_j$ and equivalently, $x_j$ is the *child* of $x_i$. If we denote by $\mathcal{P}_i$ the set of all parents of vertex $i$, then the probability distribution over all variables in a graphical model is represented by a product over conditional probability distributions over each child variable given the set of its parents. Since the graph is acyclic, it establishes a partial ordering over the variables, thus guaranteeing that this product is over a finite set of terms:

$$p(\mathbf{x}) = \prod_{i \in \mathcal{V}} p\left(x_i | \mathbf{x}_{\mathcal{P}_i}\right)$$

If we recursively define the *descendents* of a set of nodes to be the set of their children and their children's descendents, then the conditional independence that falls out of the structure of a DAG is easily described: in a DAG, a set of variables is conditionally independent of all its non-descendents given its parents.

Graphical models are a simple yet elegant tool for representing the structure of a statistical model. As mentioned before however, we are primarily concerned with the elimination of nuisance parameters from the statistical inference process, which can be achieved using Bayesian inference. Unfortunately, using this framework often necessitates an increase in the complexity of the graphical model, thus rendering it difficult or impossible to derive analytically closed-form solutions to the posterior updates of the unobserved variables in the model.

### 2.1.1 Graphical Model Conventions in this Dissertation

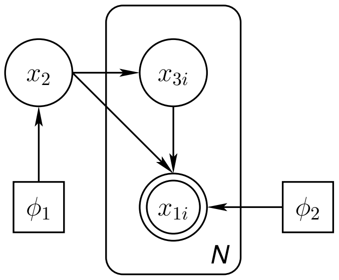

Figure 2.1: An example graphical model. This particular model is represented by a directed acyclic graph (DAG).

Figure 2.1 shows an example graphical model, which serves to illustrate some of the conventions we will use throughout this dissertation when we use graphical models to represent the structure of our statistical models.

1. Random variables in the model ($x_1$, $x_2$, and $x_3$ in figure 2.1) will be drawn as circular nodes. We will distinguish between observed and unobserved variables by giving nodes corresponding to observed variables a double border. The collection of these nodes is the observed data set $\mathbf{x}_\mathcal{D} = \{x_1\}$. We will typically be interested in inferring marginal posterior distributions over the unobserved random variables. We will collectively refer to these unobserved variables using the symbol $\mathbf{x}_\mathcal{H} = \{x_2, x_3\}$.

2. Parameters which do not have distributions will be drawn as square nodes. We will sometimes be interested in optimizing *point estimates* of these parameters such that the model best fits the data. We will collectively refer to these parameters with the symbol $\boldsymbol{\phi} = \{\phi_1, \phi_2\}$.

3. Edges in the graph are used to indicate dependencies between variables. A directed edge from $x_2$ to $x_1$ implies that the distribution of $x_1$ is conditioned on $x_2$.

4. Repeated sets of variables (e.g. multiple samples from the same distribution) are denoted by the use of a rectangular box around the variables called a *plate*. The variables inside the plate ($x_1$ and $x_3$ in figure 2.1) will typically have subscripts denoting iteration over the repetitions. Unless otherwise specified, the variables in each copy of the plate is conditionally i.i.d. (independently, identically distributed) given all *parent* nodes outside the plate. In our example, this corresponds to $\{x_{1i}, x_{3i}\}$ being conditionally independent of $\{x_{1j}, x_{3j}\}$ for $j \neq i$, given $\{x_2\}$.

## 2.2 Inference in Graphical Models

Consider a graphical model represented by a graph $\mathcal{G} = (\mathcal{V}, \mathcal{E})$, and let $\{\mathcal{D}, \mathcal{H}\}$ be a partition over $\mathcal{V}$ such that the random variables $\mathbf{x}_{\mathcal{D}}$ associated with the nodes in partition $\mathcal{D}$ are *observed*, while the random variables $\mathbf{x}_{\mathcal{H}}$ in $\mathcal{H}$ are *hidden*. Additionally we consider a set of *variables* $\boldsymbol{\phi}$ which parameterize the distributions in the graphical model, or otherwise relate to model structure and complexity. Importantly we assume that these variables $\boldsymbol{\phi}$ are not modeled as random variables, but rather as fixed parameters for which we would like an estimate (such as the choice of model complexity).

Given a data set $\mathbf{x}_\mathcal{D}$ of observations corresponding to observed nodes in the model $\mathcal{D}$, we can classify our inferential requirements of a graphical model into two main categories:

1. Inference of the posterior distributions over the unobserved variables $p(\mathbf{x}_\mathcal{H}|\mathbf{x}_\mathcal{D};\boldsymbol{\phi})$ given the observed data and a particular setting of the parameters $\boldsymbol{\phi}$.

2. Optimization of the parameters $\boldsymbol{\phi}$ such that the model best explains the observed data, i.e. maximizes $p(\mathbf{x}_\mathcal{D};\boldsymbol{\phi})$.

### 2.2.1 Inferring Marginal Distributions

Although most of this dissertation will deal with statistical models that are represented by DAGs, we will review inference in undirected graphs (Markov networks) since this turns out to be a more general framework for inference in graphical models which can then be applied to DAGs as well.

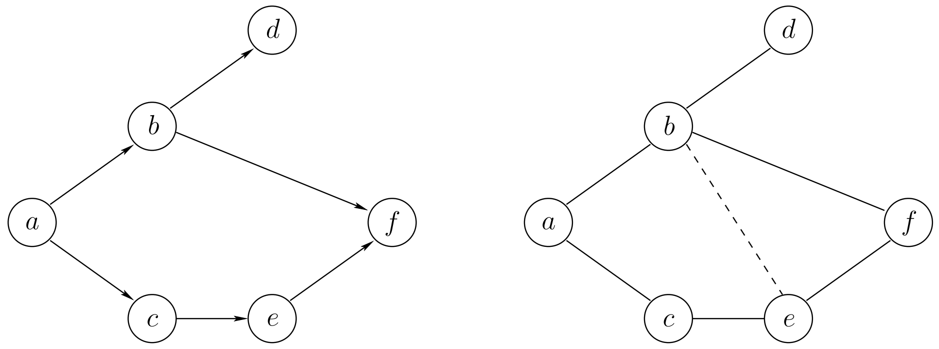

(a) Directed acyclic graph (b) Resulting *moralized* MRF

Figure 2.2: The process of converting a DAG into an MRF proceeds by making sure that the parents $\mathcal{P}_i$ of each node $i$ are connected — a process called *moralization*

A DAG can be converted into an undirected graph by the process of *moralization*. For each node $i \in \mathcal{V}$, we connect its parents $\mathcal{P}_i$ and remove direction from all edges involved. Figure 2.2(b) shows the moralized undirected graph corresponding to the DAG in figure 2.2(a). The additional edge $(b, e)$ was added by moralizing the parents of node $f$. Moralization ensures that the "explaining away" property of a fan-in in a belief network is preserved in the resulting Markov network.

#### 2.2.1.1 Variable Elimination

As simple algorithm for obtaining the marginal distribution over variables in a graphical model is the process of *variable elimination*. As we described in section 2.1, the distribution over variables in an undirected graph is represented by a product of potential functions defined over maximal cliques of the graph. For example, for the moralized MRF shown in Figure 2.2(b), these potential functions are $\psi(x_b, x_e, x_f)$, $\psi(x_b, x_d)$, $\psi(x_c, x_e)$, $\psi(x_a, x_c)$ and $\psi(x_a, x_b)$. Given our knowledge of the directed graph in figure 2.2(a), one possible valid assignment of the potential functions could be:

$$\begin{aligned}
\psi(x_b, x_e, x_f) &= p(x_f|x_b, x_e) \\
\psi(x_b, x_d) &= p(x_d|x_b) \\
\psi(x_c, x_e) &= p(x_e|x_c) \\
\psi(x_a, x_c) &= p(x_c|x_a) \\
\psi(x_a, x_b) &= p(x_b|x_a)p(a)
\end{aligned}$$

allowing us to write the joint probability distribution as a product of potentials:

$$p(\mathbf{x}) = \psi\left(x_b, x_e, x_f\right)\psi\left(x_b, x_d\right)\psi\left(x_c, x_e\right)\psi\left(x_a, x_c\right)\psi\left(x_a, x_b\right)$$

To obtain the marginal probability of a single variable $x_i$ in the graphical model, it suffices to choose an ordering of the remaining variables for "elimination" which is equivalent to summing or integrating them out of the model. As each node in the sequence is eliminated, it creates a dependency between its neighbors which is reflected by our addition of edges between all neighbors of the eliminated node at each step.

Figure 2.3 shows the sequence of elimination steps for an elimination ordering of $f, e, d, c, a$. Mathematically the sequence of eliminations is equivalent to the following summations:

$$\begin{aligned}
p(x_b) &= \sum_{x_a}\psi\left(x_a, x_b\right)\sum_{x_c}\psi\left(x_a, x_c\right)\sum_{x_d}\psi\left(x_b, x_d\right)\sum_{x_e}\psi\left(x_c, x_e\right)\sum_{x_f}\psi\left(x_b, x_e, x_f\right) \qquad (2.1)\\
&= \sum_{x_a}\psi\left(x_a, x_b\right)\sum_{x_c}\psi\left(x_a, x_c\right)\sum_{x_d}\psi\left(x_b, x_d\right)\sum_{x_e}\psi\left(x_c, x_e\right)m_f\left(x_b, x_e\right)\\
&= \sum_{x_a}\psi\left(x_a, x_b\right)\sum_{x_c}\psi\left(x_a, x_c\right)m_e\left(x_b, x_c\right)\sum_{x_d}\psi\left(x_b, x_d\right)\\
&= m_d\left(x_b\right)\sum_{x_a}\psi\left(x_a, x_b\right)\sum_{x_c}\psi\left(x_a, x_c\right)m_e\left(x_b, x_c\right)\\
&= m_d\left(x_b\right)\sum_{x_a}\psi\left(x_a, x_b\right)m_c\left(x_a, x_b\right)
\end{aligned}$$

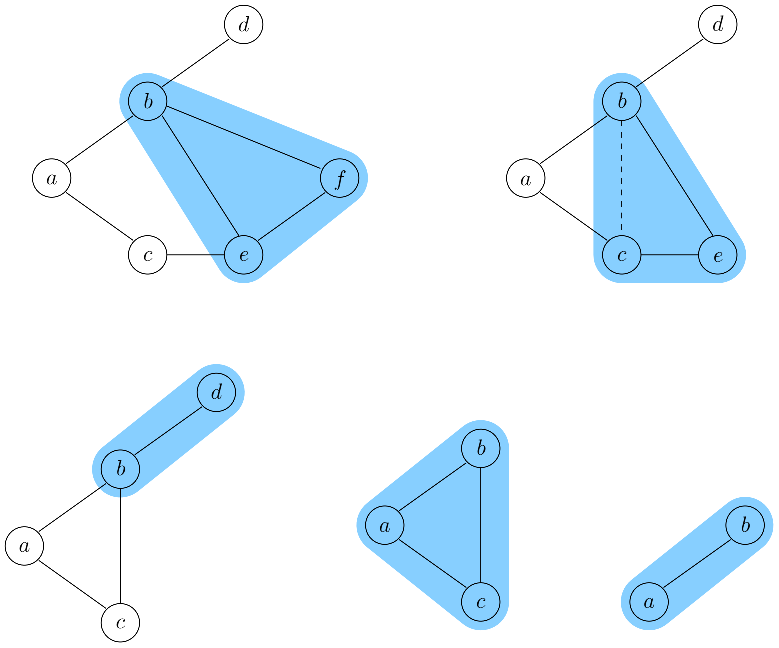

Figure 2.3: Each step in variable elimination picks a node, connects its neighbors, and marginalizes that node out from the graph. In the figure, the sequence of eliminated nodes is $f, e, d, c, a$. The shaded region indicates the *elimination clique* created by the node eliminated at each step. The dashed edge is introduced during the elimination of node $e$ which requires that we connect its neighbors.

$$= m_d\left(x_b\right) m_a\left(x_b\right)$$

The shaded region in each step of figure 2.3 is the *elimination clique* associated with the node being eliminated. This set contains all the nodes involved in the summation at that step in the elimination. Incorporating observed data into the elimination algorithm is easy. For each observed variable $x_i$ where $i \in \mathcal{D}$, we simply instantiate it in all the potential functions in which $x_i$ appears. Summing over an evidence variable now reduces to a single term.

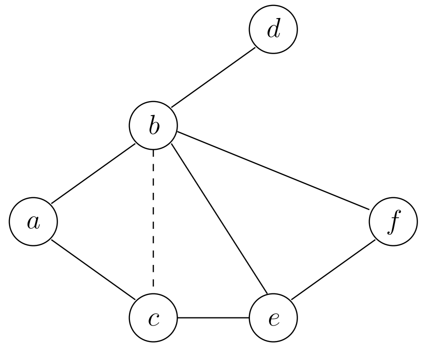

(a) Triangulated MRF

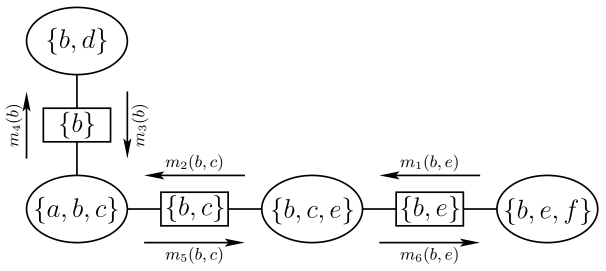

(b) Junction tree with sequence of messages

Figure 2.4: A triangulated Markov network and its junction tree.

Variable elimination is *query sensitive*, i.e. we need to know which are the query variables before we begin eliminating the others. Unfortunately this means that for each node whose marginal posterior is required, the algorithm must be restarted from scratch. This process is wasteful since many intermediate results are re-used across elimination sequences for different query nodes. The junction tree algorithm described in the next section can be thought of as a dynamic programming version of the elimination algorithm, which enables us to get the marginal posteriors over collections of variables simultaneously.

#### 2.2.1.2 Junction Trees

In the junction tree algorithm (Lauritzen & Spiegelhalter 1988) we start with the moralized graph of figure 2.2(b) and add any edges that were added during the elimination phase. This process results in a graph that is *triangulated*[1]. Triangulated graphs are also

[1]A triangulated graph is one in which every cycle of length greater than 3 has a chord.

known as *chordal* graphs, and form a subset of graphical models in which both directed and undirected graphical models have the same expressive power to represent statistical relationships (Pearl 1988). From the maximal cliques of this triangulated graph, we can create its *cluster tree* representation, by connecting the cliques via *separator nodes*. A separator node between cliques $\mathcal{C}_i$ and $\mathcal{C}_j$ contains $\mathcal{C}_i \cap \mathcal{C}_j$. A cluster tree is a *junction tree* if for any pair of cluster nodes $\mathcal{C}_i$ and $\mathcal{C}_j$, all nodes (cluster and separator) on the path between $\mathcal{C}_i$ and $\mathcal{C}_j$ all contain $\mathcal{C}_i \cap \mathcal{C}_j$. This is also known as the *running intersection property*. One can show that the triangulation step ensures that the running intersection property holds and that the cluster tree formed is indeed a junction tree. Figure 2.4 shows a junction tree corresponding to the triangulated moral graph from the previous section. It is easy to verify its running intersection property. We define potentials over the clique nodes in this new graph: $\psi\left(x_b, x_e, x_f\right)$, $\psi\left(x_b, x_c, x_e\right)$, $\psi\left(x_a, x_b, x_c\right)$ and $\psi\left(x_b, x_d\right)$. In addition, we also have potentials over the variables in the separator nodes: $\psi\left(x_b, x_e\right)$, $\psi\left(x_b, x_c\right)$ and $\psi\left(x_b\right)$.

Inference in a junction tree proceeds as follows:

- Choose a clique node as the root. In figure 2.4(b) we choose the root to be the node representing clique $\{a, b, c\}$.
- Pass messages from leaf-nodes up towards the root, and then from the root back down to the leaves. A message from clique $\mathcal{C}_i$ to an adjacent clique $\mathcal{C}_j$ is a two-step update of the potential of a separator node $\mathcal{S}_{ij}$, as well as the destination clique node $\mathcal{C}_j$:

$$\psi^*\left(\mathbf{x}_{\mathcal{S}_{ij}}\right) = \sum_{\mathbf{x}_{\mathcal{C}_i \setminus \mathcal{S}_{ij}}} \psi\left(\mathbf{x}_{\mathcal{C}_i}\right)$$

$$\psi^*\left(\mathbf{x}_{\mathcal{C}_j}\right) = \psi\left(\mathbf{x}_{\mathcal{C}_j}\right) \frac{\psi^*\left(\mathbf{x}_{\mathcal{S}_{ij}}\right)}{\psi\left(\mathbf{x}_{\mathcal{S}_{ij}}\right)}$$

- The algorithm terminates when each edge in the graph has transmitted a message exactly once in each direction. At this point, the potential at each cluster is the marginal distribution over the variables in that cluster, i.e. $\psi\left(\mathbf{x}_{\mathcal{C}_i}\right) = p(\mathbf{x}_{\mathcal{C}_i})$.

Note that the maximal cliques nodes in the junction tree of figure 2.4(b) are the same elimination cliques we observed formed during the variable elimination method (c.f. figure 2.3). Also, our notation for the intermediate terms in equation (2.1) is no coincidence. Messages $m_1$, $m_2$ and $m_3$ in figure 2.4(b) are identical to the intermediate terms $m_f$, $m_e$ and $m_d$ respectively, in the elimination algorithm. While these messages allow us to compute the marginals in the root clique (including $p(x_b)$ in the elimination example), the remaining messages $m_4$, $m_5$, and $m_6$ allow the marginals in the other cliques to be obtained as well.

The computational complexity of the junction tree method depends heavily on the structure of the graphical model, and the particular tree structure chosen. This in turn depends on the edges added in the triangulation step. In general, finding the optimal triangulation and tree structure is an NP-hard problem. For a junction tree with discrete variables, the computational complexity is exponential in the size of the largest clique node (also known as *tree width*), which stems from having to iterate over a possibly large number of states for each variable. For continuous variables, the summation is replaced by integration over the state space, which — depending on the form of the distributions involved — may be analytically intractable.

#### 2.2.1.3 Monte Carlo Methods

An alternative to approximating the posterior distributions in a statistical model is to produce a representation composed of samples from these distributions. Monte Carlo methods are computational techniques that seek to carry out probabilistic inference using representative sets of samples from probability distributions. There are two main problems that demand attention when using sampling methods. Firstly, the distribution of interest must be sampled from. Several methods exist such as importance sampling (Rubin 1988), which relies on an *importance distribution* which can be sampled from easily. An alternative is to construct a Markov chain having the distribution of interest as its stationary distribution. The Metropolis-Hastings algorithm (Metropolis et al. 1953, Hastings 1970), and Gibbs sampling (Geman & Geman 1984) are two examples of this approach. MacKay (2003*a*) and Fearnhead (1998) provide a succinct review of several sampling strategies.

An interesting subset of research in the sampling community has been that of *sequential* sampling methods, also known as *particle filters.* It is well known that Kalman filters (Kalman 1960) are a simplification of the general Bayesian state estimation problem in which the state and observation equations are assumed linear with Gaussian distributions. The seminal paper of Gordon, Salmond & Smith (1993) showed that by creative use of importance sampling, one could relax the linear and Gaussian assumptions and still retain the sequential nature of the algorithm. Doucet, de Freitas & Gordon (2001) provide a comprehensive summarization of the current state of theoretical and practical sequential state estimation research. One of the very successful applications of this set of statistical tools is in creating solutions to the simultaneous localization and mapping (SLAM) problem in mobile robotics (Thrun 2002). Recently Deutscher, Blake & Reid (2000) have demonstrated the use of this technique for motion capture applications as well.

### 2.2.2 Parameter Estimation and the EM Algorithm

The algorithms described in the preceding section allowed us to compute marginal distributions over sets of variables in a graphical model. Frequently however, we are also often interested in optimizing the parameterization $\boldsymbol{\phi}$ of the model itself such that we are most *likely* to generate our observations $\mathbf{x}_{\mathcal{D}}$. This most naturally expressed as a maximization of the marginal likelihood function (or evidence) $p(\mathbf{x}_{\mathcal{D}}; \boldsymbol{\phi})$, and is appropriately called the *maximum likelihood* (ML) framework.

Within the ML framework it is customary to refer to the quantity $p(\mathbf{x}_{\mathcal{D}}; \boldsymbol{\phi})$ as the *incomplete* likelihood since it assumes that only a subset of the nodes in the model corresponding to $\mathbf{x}_{\mathcal{D}}$ are observed. In contrast the quantity $p(\mathbf{x}_{\mathcal{D}}, \mathbf{x}_{\mathcal{H}}; \boldsymbol{\phi})$ is called the *complete* likelihood, since we must assume that the values of the hidden variables $\mathbf{x}_{\mathcal{H}}$ are known as well.

Given our observations $\mathbf{x}_{\mathcal{D}}$, the graph structure, and the mathematical form of the probability distributions over the random variables, we require to find the parameter value that maximizes the incomplete likelihood $\boldsymbol{\phi}^* = \arg\max_{\boldsymbol{\phi}} p(\mathbf{x}_{\mathcal{D}}; \boldsymbol{\phi})$. Note that this is typically a non-trivial task for the following reasons:

1. As we discussed in section 2.2, the quantity $p(\mathbf{x}_{\mathcal{D}}; \boldsymbol{\phi})$ is sometimes difficult to obtain since it involves marginalization over the hidden variables $\mathbf{x}_{\mathcal{H}}$:

$$p(\mathbf{x}_{\mathcal{D}}; \boldsymbol{\phi}) = \int p(\mathbf{x}_{\mathcal{D}}, \mathbf{x}_{\mathcal{H}}; \boldsymbol{\phi}) d\mathbf{x}_{\mathcal{H}} = \int p(\mathbf{x}_{\mathcal{D}} | \mathbf{x}_{\mathcal{H}}; \boldsymbol{\phi}) p(\mathbf{x}_{\mathcal{H}}; \boldsymbol{\phi}) d\mathbf{x}_{\mathcal{H}} \tag{2.2}$$

2. Even when the marginal is analytically expressed, the subsequent optimization of the parameters $\boldsymbol{\phi}$ requires solving:

$$\frac{\partial p(\mathbf{x}_{\mathcal{D}}; \boldsymbol{\phi})}{\partial \boldsymbol{\phi}} = \mathbf{0}$$

   In all but the most trivial models, the parameters $\boldsymbol{\phi}$ are inextricably linked, thus making an analytical expression for the optimal parameters purely in terms of the observed variables $\mathbf{x}_{\mathcal{D}}$ impossible. A well-known example of this is the simple model of density estimation using a mixture of Gaussians.

The expectation-maximization (EM) algorithm of Dempster, Laird & Rubin (1977) is a parameter optimization algorithm that operates within the framework of ML parameter estimation. Due to the conditional independencies induced by the graphical model structure, it is much more convenient to express the complete likelihood $p(\mathbf{x}_{\mathcal{D}}, \mathbf{x}_{\mathcal{H}}; \boldsymbol{\phi})$ (as a product of conditional distributions or clique potentials) than it is to compute the marginalized likelihood integral of equation (2.2). The important contribution of the EM algorithm is the ability to perform the optimization of the model parameters $\boldsymbol{\phi}$, while still working with the analytical convenience of the complete likelihood $p(\mathbf{x}_\mathcal{D}, \mathbf{x}_\mathcal{H}; \boldsymbol{\phi})$. While several derivations of the EM algorithm exist, we shall briefly summarize one which relies on creating a lower bound to the incomplete likelihood using Jensen's inequality. As we shall show in the next section, this particular route is an interesting precursor to an elegant variational approximation technique known as the factorial variational approximation.

Given a partition of the vertices in the graph into observed and unobserved sets$\{\mathcal{D}, \mathcal{H}\}$, let us hypothesize the existence of an arbitrary distribution $Q(\mathbf{x}_\mathcal{H})$ over the unobserved variables $\mathbf{x}_\mathcal{H}$, which allows us to derive the following lower bound on the incomplete log likelihood[2]:

$$\begin{aligned}
\ln p(\mathbf{x}_\mathcal{D}; \boldsymbol{\phi}) &= \ln \int p(\mathbf{x}_\mathcal{D}, \mathbf{x}_\mathcal{H}; \boldsymbol{\phi}) d\mathbf{x}_\mathcal{H} \\
&= \ln \int Q(\mathbf{x}_\mathcal{H}) \left[ \frac{p(\mathbf{x}_\mathcal{D}, \mathbf{x}_\mathcal{H}; \boldsymbol{\phi})}{Q(\mathbf{x}_\mathcal{H})} \right] d\mathbf{x}_\mathcal{H} \\
&\geq \int Q(\mathbf{x}_\mathcal{H}) \ln \left[ \frac{p(\mathbf{x}_\mathcal{D}, \mathbf{x}_\mathcal{H}; \boldsymbol{\phi})}{Q(\mathbf{x}_\mathcal{H})} \right] d\mathbf{x}_\mathcal{H} \qquad \text{(Jensen's inequality)} \qquad (2.3) \\
&= \langle \ln p(\mathbf{x}_\mathcal{D}, \mathbf{x}_\mathcal{H}; \boldsymbol{\phi}) \rangle_Q + \mathcal{H}\left[Q\right] \\
&= \mathcal{F}(Q, \boldsymbol{\phi}) \qquad (2.4)
\end{aligned}$$

where $\langle \cdot \rangle_Q$ denotes expectation with respect to the distribution $Q$, and $\mathcal{H}\left[Q\right]$ denotes its entropy. A crucial element of the functional lower bound $\mathcal{F}(Q, \boldsymbol{\phi})$ in equation (2.4), is that for the special case in which the distribution $Q(\mathbf{x}_\mathcal{H}) = p(\mathbf{x}_\mathcal{H} | \mathbf{x}_\mathcal{D}; \boldsymbol{\phi})$ (the posterior distribution of the hidden variables under the current parameter settings), the lower

[2]Maximizing the logarithm of the likelihood is justified due to the monotonic nature of the logarithm. In addition, it will facilitate the use of Jensen's inequality — $\ln \langle x \rangle \geq \langle \ln x \rangle$ — in deriving the bound.

bound becomes an equality. This is easily verified by substituting $p(\mathbf{x}_{\mathcal{H}}|\mathbf{x}_{\mathcal{D}};\boldsymbol{\phi})$ for $Q$ in equation (2.3). In fact, it is easy to exactly quantify the tightness of the bound as being the Kullback-Leibler (KL) divergence between $Q(\mathbf{x}_{\mathcal{H}})$ and $p(\mathbf{x}_{\mathcal{H}}|\mathbf{x}_{\mathcal{D}};\boldsymbol{\phi})$:

$$\begin{aligned}
\ln p(\mathbf{x}_{\mathcal{D}};\boldsymbol{\phi}) &= \int Q(\mathbf{x}_{\mathcal{H}}) \ln p(\mathbf{x}_{\mathcal{D}};\boldsymbol{\phi}) d\mathbf{x}_{\mathcal{H}} \\
&= \int Q(\mathbf{x}_{\mathcal{H}}) \ln \left[\frac{p(\mathbf{x}_{\mathcal{D}},\mathbf{x}_{\mathcal{H}};\boldsymbol{\phi})}{p(\mathbf{x}_{\mathcal{H}}|\mathbf{x}_{\mathcal{D}};\boldsymbol{\phi})} d\right] \mathbf{x}_{\mathcal{H}} \\
&= \int Q(\mathbf{x}_{\mathcal{H}}) \ln \left[\frac{p(\mathbf{x}_{\mathcal{D}},\mathbf{x}_{\mathcal{H}};\boldsymbol{\phi})}{Q(\mathbf{x}_{\mathcal{H}})}\right] d\mathbf{x}_{\mathcal{H}} + \int Q(\mathbf{x}_{\mathcal{H}}) \ln \left[\frac{Q(\mathbf{x}_{\mathcal{H}})}{p(\mathbf{x}_{\mathcal{H}}|\mathbf{x}_{\mathcal{D}};\boldsymbol{\phi})}\right] d\mathbf{x}_{\mathcal{H}} \\
&= \mathcal{F}(Q,\boldsymbol{\phi}) + KL\left[Q(\mathbf{x}_{\mathcal{H}})||p(\mathbf{x}_{\mathcal{H}}|\mathbf{x}_{\mathcal{D}};\boldsymbol{\phi})\right] \qquad (2.5)
\end{aligned}$$

```
1: Init: $\boldsymbol{\phi} \leftarrow \boldsymbol{\phi}_0$
2: repeat
3:     E-step
       $l_c(\boldsymbol{\phi}) \leftarrow \langle \ln p(\mathbf{x}_{\mathcal{D}},\mathbf{x}_{\mathcal{H}};\boldsymbol{\phi})\rangle_{p(\mathbf{x}_{\mathcal{H}}|\mathbf{x}_{\mathcal{D}};\boldsymbol{\phi})}$
4:     M-step
       $\boldsymbol{\phi} \leftarrow \arg\max_{\boldsymbol{\phi}} l_c(\boldsymbol{\phi})$
5: until convergence
```

**Algorithm 1:** Expectation Maximization algorithm

Algorithm 1 gives the general procedure for using EM. Rather than maximize the incomplete log likelihood $\ln p(\mathbf{x}_{\mathcal{D}};\boldsymbol{\phi})$ directly, EM operates on the functional $\mathcal{F}(Q,\boldsymbol{\phi})$, alternately performing a coordinate ascent in its two arguments: the space of probability distributions $Q(\mathbf{x}_{\mathcal{H}})$ (E-step), and the space of parameter values $\boldsymbol{\phi}$ (M-step). By evaluating the expectation $\langle \ln p(\mathbf{x}_{\mathcal{D}},\mathbf{x}_{\mathcal{H}};\boldsymbol{\phi})\rangle_Q$ under the specific distribution $Q(\mathbf{x}_{\mathcal{H}}) = p(\mathbf{x}_{\mathcal{H}}|\mathbf{x}_{\mathcal{D}};\boldsymbol{\phi})$, the E-step ensures that the functional lower bound $\mathcal{F}$ is raised to an equality. The M-step then maximizes w.r.t. $\boldsymbol{\phi}$, the only term in $\mathcal{F}$ with a dependency on $\boldsymbol{\phi}$; namely $\langle \ln p(\mathbf{x}_{\mathcal{D}},\mathbf{x}_{\mathcal{H}};\boldsymbol{\phi})\rangle_Q$. Since the E-step makes the bound an equality, we are guaranteed that maximizing $\mathcal{F}$ in the M-step also increases the incomplete log likelihood $\ln p(\mathbf{x}_\mathcal{D}; \boldsymbol{\phi})$. Under general conditions (Wu 1983), EM is guaranteed to converge to a local maximum in the incomplete likelihood $p(\mathbf{x}_\mathcal{D}; \boldsymbol{\phi})$.

Several variants of the EM algorithm exist. To address computational issues, Neal & Hinton (1998) have theoretically justified incremental and sparse variants, in which only a subset of the hidden variables and/or parameters are updated in each EM cycle. There also exist variants that seek to overcome the problem of local minima, such as Deterministic Annealing EM (DAEM) (Ueda & Nakano 1998), and in the context of mixture models, Split-and-Merge EM (SMEM) (Ueda et al. 1999). Minagawa et al. (2002) showed however, that the SMEM mechanism may actually settle on suboptimal solutions.

It is important to realize that the efficacy of the M-step depends upon being able to successfully compute the expectation of the complete log likelihood $\ln p(\mathbf{x}_\mathcal{D}, \mathbf{x}_\mathcal{H}; \boldsymbol{\phi})$ with respect to the *true posterior* $p(\mathbf{x}_\mathcal{H}|\mathbf{x}_\mathcal{D}; \boldsymbol{\phi})$. This is because only the true posterior raises the bound of equation (2.4) to an equality, and thereby guarantees that the M-step is actually maximizing $p(\mathbf{x}_\mathcal{D}; \boldsymbol{\phi})$ — the quantity of interest.

What happens when we cannot express the posterior $p(\mathbf{x}_\mathcal{H}|\mathbf{x}_\mathcal{D}; \boldsymbol{\phi})$ analytically? Or when the required E-step expectation $\langle \ln p(\mathbf{x}_\mathcal{D}, \mathbf{x}_\mathcal{H}; \boldsymbol{\phi}) \rangle$ with respect to this posterior is intractable? This is where the realm of approximation methods plays a crucial role. In the next section, we will derive an approximation method that stems naturally from the EM formulation that we have just described.

## 2.3 The Factorial Variational Approximation

Often in statistical models, the marginal posterior distributions over variables is analytically intractable due to the structure of the individual conditional distributions. Even using the junction tree methods of section 2.2 does not help since propagating and absorbing messages involves the marginalization of variables in the cliques, which pose the same analytical restrictions. Additionally exacerbating the problem is the process of variable elimination, which typically adds additional dependency relations in the graph, further complicating subsequent marginalizations.

An alternative way of addressing the issue is to make the *a priori* assumption that the *posterior* distribution factorizes over certain sets of variables in the model (Beal 2003). In some sense, this can be thought of as artificially restricting the *clique size* in the junction tree of section 2.2.1.2. We can then restrict our search to families of posterior distributions that satisfy this constraint. This approximation is therefore known as the *factorial* variational approximation.

### 2.3.1 An Update Mechanism for Factored Posterior Distributions

Let us start with the lower bound derived in equation (2.4) of the preceding section:

$$\begin{aligned} \ln p(\mathbf{x}_{\mathcal{D}};\boldsymbol{\phi}) &\geq \int Q(\mathbf{x}_{\mathcal{H}}) \ln \left[ \frac{p(\mathbf{x}_{\mathcal{D}},\mathbf{x}_{\mathcal{H}};\boldsymbol{\phi})}{Q(\mathbf{x}_{\mathcal{H}})} \right] d\mathbf{x}_{\mathcal{H}} \\ &= \left\langle \ln p(\mathbf{x}_{\mathcal{D}},\mathbf{x}_{\mathcal{H}};\boldsymbol{\phi}) \right\rangle_Q + \mathcal{H}\left[Q\right] \end{aligned}$$

We know that maximizing the lower bound implies maximizing the functional $\mathcal{F}(Q, \boldsymbol{\phi})$ over the space of probability distributions $Q(\mathbf{x}_{\mathcal{H}})$. Another way of formulating the problem is by noting that the tightness of the bound is quantified by the KL divergence between the true posterior and its approximation, as shown in equation (2.5). This KL divergence is also known as the *variational free energy.* Minimizing this free energy is equivalent to tightening the lower bound, and bringing the approximation $Q(\mathbf{x}_{\mathcal{H}})$ closer to the true posterior $p(\mathbf{x}_{\mathcal{H}}|\mathbf{x}_{\mathcal{D}}; \boldsymbol{\phi})$. Moreover, we know that this a constrained variational optimization problem since we must maintain that $\int Q(\mathbf{x}_{\mathcal{H}})d\mathbf{x}_{\mathcal{H}} = 1$ over the space of possible solutions.

If we do not impose any additional constraints, maximization of $\mathcal{F}(Q, \boldsymbol{\phi})$ w.r.t. $Q(\mathbf{x}_{\mathcal{H}})$ will lead to the true posterior distribution $p(\mathbf{x}_{\mathcal{H}}|\mathbf{x}_{\mathcal{D}}; \boldsymbol{\phi})$ which we have assumed is analytically intractable. If however, we impose the additional constraint that the distribution $Q(\mathbf{x}_{\mathcal{H}})$ must factorize over some partition $\{\mathbf{x}_{\mathcal{H}1}, \mathbf{x}_{\mathcal{H}2}, \ldots, \mathbf{x}_{\mathcal{H}p}\}$, i.e.:

$$Q(\mathbf{x}_{\mathcal{H}}) = \prod_{i=1}^{p} Q_i(\mathbf{x}_{\mathcal{H}i})$$

then using the calculus of variations (see (Rustagi 1976) for example,) we can derive (see appendix B.1) the following update equation for the marginal posterior over each individual partition $\mathbf{x}_{\mathcal{H}i}$:

$$Q_i(\mathbf{x}_{\mathcal{H}i}) = \frac{\exp \langle \ln p(\mathbf{x}_{\mathcal{D}}, \mathbf{x}_{\mathcal{H}}; \boldsymbol{\phi}) \rangle_{Q_{k\neq i}}}{\int \exp \langle \ln p(\mathbf{x}_{\mathcal{D}}, \mathbf{x}_{\mathcal{H}}; \boldsymbol{\phi}) \rangle_{Q_{k\neq i}} d\mathbf{x}_{\mathcal{H}i}} \tag{2.6}$$

or equivalently:

$$\ln Q_i(\mathbf{x}_{\mathcal{H}i}) = \langle \ln p(\mathbf{x}_{\mathcal{D}}, \mathbf{x}_{\mathcal{H}}; \boldsymbol{\phi}) \rangle_{Q_{k \neq i}} + const_{\mathbf{x}_{\mathcal{H}i}} \tag{2.7}$$

where $\langle \cdot \rangle_{Q_{k \neq i}}$ denotes expectation taken w.r.t. all distributions $Q_k$ except $Q_i$. This is a particularly appealing formulation, since it allows us (once again) to work with the complete joint distribution over our statistical model as we did before in the EM algorithm, without the need for explicit marginalization. Successive application of the update (2.6) to each distribution $Q_i(\mathbf{x}_{\mathcal{H}i})$ for $1 \leq i \leq p$ guarantees that each update monotonically decreases the KL divergence between the approximated (factored) posterior $Q(\mathbf{x}_{\mathcal{H}})$ and the true posterior $p(\mathbf{x}_{\mathcal{H}}|\mathbf{x}_{\mathcal{D}}; \boldsymbol{\phi})$.

### 2.3.2 Solution for Partial Factorization

If we drop the assumption of complete factorization and allow dependencies between partitions then our result changes only slightly (see appendix B.1.1). Assume, for example, that $Q(\mathbf{x}_{\mathcal{H}1}, \mathbf{x}_{\mathcal{H}2}) = Q(\mathbf{x}_{\mathcal{H}1}|\mathbf{x}_{\mathcal{H}2})Q(\mathbf{x}_{\mathcal{H}2})$. In this case, the update equations for $Q(\mathbf{x}_{\mathcal{H}2})$ become:

$$Q_2(\mathbf{x}_{\mathcal{H}2}) \propto \exp\left( \langle \ln p(\mathbf{x}_{\mathcal{D}}, \mathbf{x}_{\mathcal{H}}; \boldsymbol{\phi}) \rangle_{Q_{j \neq 2}} - \int Q(\mathbf{x}_{\mathcal{H}1}|\mathbf{x}_{\mathcal{H}2}) \ln Q(\mathbf{x}_{\mathcal{H}1}|\mathbf{x}_{\mathcal{H}2}) d\mathbf{x}_{\mathcal{H}1} \right) \tag{2.8}$$

or equivalently

$$\ln Q_2(\mathbf{x}_{\mathcal{H}2}) = \langle \ln p(\mathbf{x}_{\mathcal{D}}, \mathbf{x}_{\mathcal{H}}; \boldsymbol{\phi}) \rangle_{Q_{j \neq 2}} + \text{entropy}\left\{Q(\mathbf{x}_{\mathcal{H}1}|\mathbf{x}_{\mathcal{H}2})\right\} + const_{\mathbf{x}_{\mathcal{H}2}} \tag{2.9}$$

The factorial variational approximation has only recently gained attention in the machine learning community although it has its roots in statistical physics and mean field theory (Parisi 1988). MacKay (1999) provides an insightful comparison of these so-called *approximating ensemble* methods with the traditional exact methods, and shows that in cases where we are inclined to summarize the posterior distributions with point estimates, ensemble methods are a more accurate representation of the location of overall posterior mass.

The analytical simplicity of the variational approximation has found several applications in the statistical learning literature. Saul, Jaakkola & Jordan (1996) use a mean field approximation to create tractable inference in sigmoid belief networks. Ghahramani & Beal (2000) have extended probabilistic factor analysis (FA) models (Ghahramani & Hinton 1997) to incorporate automatic estimation of the number of latent dimensions. Identical formulations have also been presented in the context of principal component analysis (PCA) (Bishop 1999*b*, Bishop & Winn 2000). Ghahramani & Beal (2001) also show that the variational approximation can be used in the general case of conjugate-exponential belief networks (i.e. models in which the conditional distributions are from the exponential family, and whose priors are conjugate), as well as Markov networks. In fact, it can be formulated as a form of message-passing or *propagation* algorithm similar to the junction tree method described in section 2.2.1.2. They also demonstrate its use in several statistical learning problems such as a Bayesian treatment of Kalman filter parameter estimation. Sato (2001) shows for the case of conjugate exponential models, that one can use the variational approximation to derive posterior distributions that retain their prior form, thus enabling observed data to be summarized by the sufficient statistics of these distributions. Observing new data is then naturally incorporated into the model by the update of these statistics, thus enabling efficient online learning implementations.

Other forms of variational approximations exist which do not necessarily include a factorization. Variational calculus has been used to find the optimal parameterization of a functional lower bound to a true posterior distribution in each node of sigmoid belief networks (Saul et al. 1996, Jordan, Ghahramani, Jaakkola & Saul 1999). Prior to the use of variational approximations, a popular method for approximating intractable distributions has been the Laplacian approximation (also known as the Gaussian approximation), which uses a second-order Taylor series expansion at the maximum of the distribution (Bishop 1999*a*). The Hessian matrix of the quadratic surface at the location of the maximum serves as the covariance matrix of the Gaussian approximation. Gelman et al. (1995) present several asymptotic justifications for this approach, as well as counterexamples where it does not work well. Wainwright & Jordan (2003) show that by using the theory of convex duality, one can derive several approximate inference algorithms, including the factorial variational approximation, loopy belief propagation, and Bethe/Kikuchi approximations.

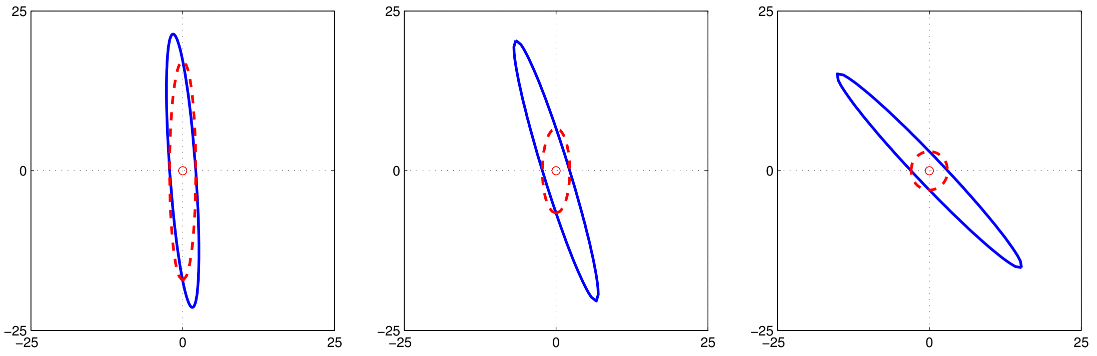

Figure 2.5: This figure shows the factorial variational approximation (dashed line) to the true distribution (solid line), as the independence assumption between the two variables is successively invalidated. In general the approximation is worsened as the assumption is more incorrect, and tends to be more compact than the true distribution.

### 2.3.3 The Effect of Making Independence Assumptions

In this section, we try to present some intuition for the consequences of the factorial approximation, and its implications for the solution of marginal posteriors over the factorized sets of variables. Let us consider a simple example where we shall approximate a bivariate Gaussian distribution $p(\mathbf{x})$ over $\mathbf{x} = \begin{bmatrix} x_1 & x_2 \end{bmatrix}^T$ with a factorial variational approximation that assumes independence, i.e., $Q(\mathbf{x}) = Q(x_1)Q(x_2)$, where each $Q(x_i)$ is a univariate Gaussian. From our derivation of the lower bound to the evidence (c.f. equation (2.5)), we know that the best approximation under the factorized constraint is one that minimizes the KL divergence:

$$\int Q(\mathbf{x}) \ln \frac{Q(\mathbf{x})}{p(\mathbf{x})} d\mathbf{x}$$

Figure 2.5 shows the resulting approximation for different distributions $p(\mathbf{x})$ which have increasing degrees of dependence between $x_1$ and $x_2$. MacKay (2003*b*) points out that the variational approximation will always tend to produce more compact distributions than the true posterior. This is also evident in figure 2.5 where the resulting approximation tends to put most of the probability mass on the subset of the domain which has support under both the true posterior distribution and the approximation.

Interestingly, MacKay (2003*b*) notes that if we instead minimize the following KL divergence:

$$\int p(\mathbf{x}) \ln \frac{p(\mathbf{x})}{Q(\mathbf{x})} d\mathbf{x}$$

we get the opposite effect, in which the resulting approximation tends to put most of the probability mass on the *superset* of the domain which has support under the approximation and the true distribution (i.e. we obtain an axis-aligned Gaussian which encompasses the true distribution), and thus obtain a less compact approximation.

The interesting question is what this result would seem to imply in terms of model complexity estimation. A more compact distribution may seem to suggest that the model overfits since it gives higher probability than it should to a particular solution. However, it should be noted that whether this behavior corresponds to overfitting or underfitting depends on the space of models that is given high probability in the posterior. If a compact approximation puts more probability mass on the subspace of models which have lower complexity then we would in fact have the effect of *underfitting* the model since the true complexity cannot be accurately represented with our approximation.

Additional support for this idea of underfitting is given by MacKay (2001), who notes that in the presence of fewer data points, variational approximations tend to prune away additional model complexity, and require large amounts of data to justify retaining more complex models.

As a last point, it should be mentioned that certain dependencies in a statistical model take the form of *symmetries* in the parameter space; for example, permutations of mixture component labels and parameters. The joint posterior distributions are therefore notoriously multimodal. By neglecting these dependencies, the factorial variational approximation will settle on one of the modes, but the choice of mode is highly dependent on initialization of the inference process. In situations like mixture modeling for example, this is typically not a problem since from a model evidence point of view, the solutions at all the symmetric modes are equivalent.

# Chapter 3

# Algorithms for Analytical Tractability

Armed with the analytical methodology presented in chapter 2, and in particular, the framework of variational approximations, we seek to tackle some of the particularly difficult problems that require a careful consideration of model complexity in order for inference to be successful. Section 3.1 develops a novel algorithm that addresses the issue of determining the appropriate number of components in mixture modeling. Using the factorial variational approximation, we create a closed form solution to the problem of modeling local evidence, which allows us to grow a collection of mixture components to suit the complexity of the data set.

In section 3.2 we deal with the problem of estimating the window of sufficient statistics (or equivalently, the forgetting factor) used in online learning situations where we must model a time-varying system. By modeling the parameters of the time-varying system as a set of drifting parameters, we derive an algorithm that extends the Kalman filter to determine the appropriate size of the window of sufficient statistics required in online learning problems.

Finally, section 3.3 addresses the analogous problem of determining the spatial extent of kernels in locally weighted learning — a problem also known in the statistics literature as *supersmoothing*. By modeling the kernel weights probabilistically, we can achieve both an automatic estimation of the kernel width, as well as gain robustness to outliers.

## 3.1 Mixture Model Cardinality

Mixture modeling (McLachlan & Peel 2000) is a well-established, powerful tool for modeling complex data using a collection of simple, local models. It intuitively describes situations in which each observation is modeled as having been produced by one of a set of alternative mechanisms. This is not the only useful interpretation, however, since mixtures of analytically simple distributions (such as Gaussians) can be used to model arbitrarily complex density functions, and mixtures of computationally efficient locally linear regressors can be used to fit arbitrarily nonlinear regression data. Thus mixture modeling is also a useful tool of composition.

The optimization of model parameters in finite mixture models often seeks to maximize a measure of goodness of fit (or equivalently, minimize an error measure), between the model and the observed data. This typically involves a joint optimization of the parameters that define the locality of each model (for example, the parameters of the gating network as used by Jordan & Jacobs (1994)), along with the parameters that fit each local model to the data (for example, the parameters of a local factor analyzer or local linear regression parameters).

If we merely wished to estimate the parameters of a collection of components of *known* cardinality, then the problem can be tackled using the expectation-maximization (EM) algorithm (Dempster et al. 1977) mentioned in section 2.2.2, and its many variants (Neal & Hinton 1998, Ueda & Nakano 1998, Ueda et al. 1999), which provide a clean optimization mechanism within the maximum likelihood (ML) framework. Estimating the *number* of mixture components however, is an issue of determining the statistical model complexity and is still a largely unsolved problem. It is well known that increasing the number of mixture components monotonically increases the fit to the observed data (Li & Barron 2001, Cadez & Smyth 2001), since each model with $k+1$ components contains the $k$-component model as a special case, and consequently, must have a likelihood greater than or equal to a $k$-component model. This increased likelihood, however, comes at a price of poor generalization ability due to the increase in model complexity; another manifestation of the classic bias-variance dilemma (Geman et al. 1992).

There have been various approaches to estimating and/or regularizing model complexity with respect to the number of mixture components. Some have included evaluating the fitness function for various numbers of components and then performing a statistical hypothesis test to determine the most appropriate complexity (Chuang & Mendell 1997, Mendell et al. 1993). An alternative approach penalizes the fitness function with a term that scales with model complexity. The approaches discussed in section 1.3 such as the minimum description length (MDL) principle (Rissanen 1978), and Bayesian/Akaike information criteria (BIC/AIC) (Schwarz 1978, Akaike 1974, Roeder & Wasserman 1995, Mengerson & Robert 1996) fall in this category.

Cross-validation for selecting the number of mixture components, although, in general, computationally intensive, has also been attempted. Smyth (2000) compares a particular implementation of cross-validated methodologies called Monte Carlo cross validation (MCCV) and compares it to other non-Bayesian approaches including BIC and bootstrap methods. In addition, there are several non-parametric clustering methods (see, for example, (Zhang & Liu 2002) and references therein) that also attempt to automatically discover the number of clusters. One of the more exciting of these approaches has been the use of semi-parametric Bayesian models and the family of Pitman-Yor processes to model a countably infinite number of mixture components (Pitman & Yor 1997, Escobar & West 1995, Ishwaran & James 2002). Solutions to these models however are obtained via MCMC sampling techniques, and are prohibitively expensive for high-dimensional data. For the remainder of this section, we shall restrict ourselves, however, to model-based approaches, and attempt to derive an algorithm using the approximation techniques mentioned in chapter 2.

There has already been some research that makes steps in this direction. In the context of mixtures of factor analyzers, Ghahramani & Beal (2000) have used variational calculus to approximate the model evidence, and hence successfully discover the local dimensionality within each factor analyzer. Their approach to inferring the number of model components, however, involves a heuristic which stochastically chooses a candidate model for splitting based on its contribution to the overall (approximated) evidence.

The idea of using a local measure to determine a splitting criterion, however, is a promising one. And it is this approach that we will explore in the remainder of this section.

### 3.1.1 Growing Mixture Models

One possible solution to estimating the cardinality of a mixture model is to overestimate the complexity by creating far more models than is necessary, and then allowing the evidence maximization process to prune away the excess model complexity (Blei & Jordan 2004). Ideally however, we would like to use a *growing* rather than a *pruning* approach to determining mixture model cardinality since this reduces the initial computational burden, and removes the decision of the initial overestimate in the number of components.

#### 3.1.1.1 1 or 2 Models?

As a starting point, consider the simple problem of deciding between one or two mixture components given the observed data. Let us assume we have a data set $\mathbf{x}_{\mathcal{D}} = \{\mathbf{x}_i\}_{i=1}^N$ consisting of $d$-dimensional input vectors $\mathbf{x}_i$. Our task is to model the probability distribution $p(\mathbf{x})$ using either one, or two Gaussians (it is straightforward to modify the following discussion such that it is applicable to classification or regression tasks). We represent a $K$-component mixture of Gaussians by the following equations:

$$\begin{aligned} \mathbf{x}|s_{im} = 1 &\sim \text{Normal}\left(\mathbf{x}; \boldsymbol{\mu}_m, \mathbf{P}_m^{-1}\right) \\ \mathbf{s}_i &\sim \text{Multinomial}\left(\mathbf{s}_i; \boldsymbol{\pi}\right) \\ p(\mathbf{x}) &= \sum_{k=1}^{K} p(\mathbf{x}|s_{ik} = 1)\pi_k \end{aligned} \tag{3.1}$$

In equations 3.1, each $\mathbf{s}_i$ is a $K$-component vector of indicator variables and $\boldsymbol{\pi}$ is a vector of prior probabilities for each component. $\boldsymbol{\mu}_m$, and $\mathbf{P}_m$ represent the mean and

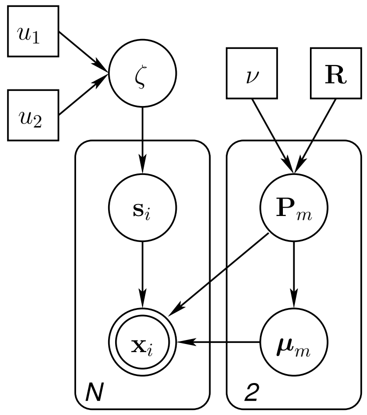

Figure 3.1: This statistical model determines whether a local patch of data requires one or two components to be modeled. By recursively splitting models, we hope to grow a collection of mixture components that best models the data with minimum complexity.

precision of the $m$th Gaussian for $1 \leq m \leq K$. For our present discussion, we restrict $K = 2$. If we use *likelihood* as a model fitness criterion, then it is obvious that the 2-Gaussian model will always have performance better-than or equal-to that of the 1-Gaussian model (Cadez & Smyth 2001). If however, we compute the *marginal* likelihood, and integrate over the parameters for each $K$-component model, then we should be able to correctly determine the appropriate complexity required to model the data $\mathbf{x}_\mathcal{D}$ without over fitting. This implies computing the integral for the model evidence:

$$p(\mathbf{x}_\mathcal{D}; \mathcal{M}_K) = \int p(\mathbf{x}_\mathcal{D}|\mathbf{x}_\mathcal{H}) p(\mathbf{x}_\mathcal{H}; \mathcal{M}_K) d\mathbf{x}_\mathcal{H}$$

We use $\mathbf{x}_\mathcal{H}$ to represent the collective set of model parameters that we must integrate over. In order to compute the marginal evidence, we alter the statistical model by placing the following prior distributions:

$$\boldsymbol{\mu}_m | \mathbf{P}_m \sim \text{Normal}\left(\boldsymbol{\mu}_m; \mathbf{0}, \mathbf{P}_m^{-1}/\alpha_0\right) \tag{3.2}$$

$$\mathbf{P}_m \sim \text{Wishart}_\nu\left(\mathbf{P}_m; \mathbf{R}\right) \tag{3.3}$$

$$p(s_{i1} = 1) = \zeta \quad \text{and} \quad p(s_{i2} = 1) = 1 - \zeta \tag{3.4}$$

$$\zeta \sim \text{Beta}\left(\zeta; u_1, u_2\right) \tag{3.5}$$

In equations (3.2) and (3.3) we place a joint Normal-Wishart prior over $\{\boldsymbol{\mu}_m, \mathbf{P}_m\}$. Gelman et al. (1995) provide several justifications for this choice of joint prior. In addition, as shown in equation (3.4), our indicator variable $\mathbf{s}_i$ is now just a binomially distributed 2-component vector $\begin{bmatrix} s_{i1} & s_{i2} \end{bmatrix}^T$, while we represent our uncertainty about the knowledge of the binomial parameter with the Beta prior in equation (3.5). This model is graphically represented by the DAG in figure 3.1.

The joint distribution over the variables in this model factorize according to the structure in the graphical model as follows:

$$p(\mathbf{x}_\mathcal{D}, \mathbf{x}_\mathcal{H}; \mathcal{M}_2) = \left[\prod_{i=1}^{N} \prod_{m=1}^{2} \left[p\left(\mathbf{x}_i | \boldsymbol{\mu}_m, \mathbf{P}_m\right) p\left(s_{im} = 1\right)\right]^{s_{im}}\right] \left[\prod_{m=1}^{2} p(\boldsymbol{\mu}_m | \mathbf{P}_m) p(\mathbf{P}_m)\right] p(\zeta)$$

In order to compute the model evidence $p(\mathbf{x}_\mathcal{D}; \mathcal{M}_2)$, the collective set of parameters that we have to integrate over is $\mathbf{x}_\mathcal{H} = \left\{\{\boldsymbol{\mu}_m, \mathbf{P}_m\}_{m=1,2}, \{\mathbf{s}_i\}_{i=1}^N, \zeta\right\}$. As mentioned before, this integral is analytically intractable, and although exact solutions can be found using Markov Chain Monte Carlo (MCMC) (Neal 1994), we choose to find an analytical solution using the factorial variational approximation of section 2.3. We make the following factorial assumption over the posterior distribution of unknown variables:

$$\begin{aligned} Q(\mathbf{x}_{\mathcal{H}}) &= Q(\boldsymbol{\mu}, \mathbf{P}, \mathbf{S}, \zeta) \\ &= Q(\boldsymbol{\mu}, \mathbf{P}) Q(\mathbf{S}) Q(\zeta) \end{aligned}$$

If we substitute the conditional distributions, take logarithms, and lump all irrelevant terms into an additive constant, we get:

$$\begin{aligned} \ln p(\mathbf{x}_{\mathcal{D}}, \mathbf{x}_{\mathcal{H}}; \mathcal{M}_2) = \sum_{i=1}^{N} s_{i1} & \left[ \frac{1}{2} \ln |\mathbf{P}_1| - \frac{1}{2} (\mathbf{x}_i - \boldsymbol{\mu}_1)^T \mathbf{P}_1 (\mathbf{x}_i - \boldsymbol{\mu}_1) + \ln \zeta \right] \\ &+ s_{i2} \left[ \frac{1}{2} \ln |\mathbf{P}_2| - \frac{1}{2} (\mathbf{x}_i - \boldsymbol{\mu}_2)^T \mathbf{P}_2 (\mathbf{x}_i - \boldsymbol{\mu}_2) + \ln (1 - \zeta) \right] \\ &+ \sum_{m=1,2} \left[ \frac{d}{2} \ln \alpha_0 + \frac{1}{2} \ln |\mathbf{P}_m| - \frac{\alpha_0}{2} {\boldsymbol{\mu}_m}^T \mathbf{P}_m \boldsymbol{\mu}_m \right] \\ &+ \sum_{m=1,2} \left[ \left( \frac{\eta - d - 1}{2} \right) \ln |\mathbf{P}_m| - \frac{1}{2} \operatorname{Tr} \left[ \mathbf{R}^{-1} \mathbf{P}_m \right] \right] \\ &+ (u_1 - 1) \ln \zeta + (u_2 - 1) \ln (1 - \zeta) + const_{\mathbf{x}_{\mathcal{D}}, \mathbf{x}_{\mathcal{H}}} \end{aligned} \tag{3.6}$$

Using the update equation for factored distributions in equation (2.6), we can derive the following updates (see appendix B.2) to each of the marginal distributions that maximize the functional lower bound to the true evidence:

$$
\begin{aligned}
Q(\boldsymbol{\mu}_m|\mathbf{P}_m) &= \text{Normal}\left(\boldsymbol{\mu}_m; \mathbf{m}_{\boldsymbol{\mu}}^{(m)}, \boldsymbol{\Sigma}_{\boldsymbol{\mu}}^{(m)}\right)\\
Q(\mathbf{P}_m) &= \text{Wishart}_{\tilde{\nu}_m}\left(\mathbf{P}_m; \tilde{\mathbf{R}}_m\right)\\
Q(\zeta) &= \text{Beta}\left(\zeta; \tilde{u}_1, \tilde{u}_2\right)
\end{aligned}
$$

where

$$
\begin{aligned}
\bar{\mathbf{x}}_m &= \frac{\sum_{i=1}^N \langle s_{im}\rangle \mathbf{x}_i}{\sum_{i=1}^N \langle s_{im}\rangle}\\
\boldsymbol{\Sigma}_{\boldsymbol{\mu}}^{(m)} &= \left(\sum_{i=1}^N \langle s_{im}\rangle + \alpha_0\right)^{-1} \mathbf{P}_m^{-1}\\
\mathbf{m}_{\boldsymbol{\mu}}^{(m)} &= \boldsymbol{\Sigma}_{\boldsymbol{\mu}_m}\left(\sum_{i=1}^N \langle s_{im}\rangle\right)\mathbf{P}_m\bar{\mathbf{x}}_m = \frac{\sum_{i=1}^N \langle s_{im}\rangle}{\sum_{i=1}^N \langle s_{im}\rangle + \alpha_0}\bar{\mathbf{x}}_m\\
\tilde{\mathbf{R}}_m^{-1} &= \mathbf{R}^{-1} + \sum_{i=1}^N \langle s_{im}\rangle \left(\mathbf{x}_i - \bar{\mathbf{x}}_m\right)\left(\mathbf{x}_i - \bar{\mathbf{x}}_m\right)^T + \frac{\sum_{i=1}^N \langle s_{im}\rangle \alpha_0}{\sum_{i=1}^N \langle s_{im}\rangle + \alpha_0}\bar{\mathbf{x}}_m\bar{\mathbf{x}}_m^T\\
\tilde{\nu}_m &= \nu + \sum_{i=1}^N \langle s_{im}\rangle\\
\tilde{u}_1 &= u_1 + \sum_{i=1}^N \langle s_{i1}\rangle; \qquad \tilde{u}_2 = u_2 + \sum_{i=1}^N \langle s_{i2}\rangle\\
\ln Q(s_{i1}=1) &= \frac{1}{2}\langle \ln|\mathbf{P}_1|\rangle - \frac{1}{2}\left\langle \left(\mathbf{x}_i - \boldsymbol{\mu}_1\right)^T \mathbf{P}_1 \left(\mathbf{x}_i - \boldsymbol{\mu}_1\right)\right\rangle + \langle \ln\zeta\rangle + const\\
\ln Q(s_{i2}=1) &= \frac{1}{2}\langle \ln|\mathbf{P}_2|\rangle - \frac{1}{2}\left\langle \left(\mathbf{x}_i - \boldsymbol{\mu}_2\right)^T \mathbf{P}_2 \left(\mathbf{x}_i - \boldsymbol{\mu}_2\right)\right\rangle + \langle \ln(1-\zeta)\rangle + const
\end{aligned}
$$

Repeatedly applying these updates until convergence guarantees that the KL divergence between the factored approximation $Q(\mathbf{x}_{\mathcal{H}})$ and the true posterior $p(\mathbf{x}_{\mathcal{H}}|\mathbf{x}_{\mathcal{D}}; \mathcal{M}_2)$ is monotonically decreased. In addition, the functional approximation to the evidence is

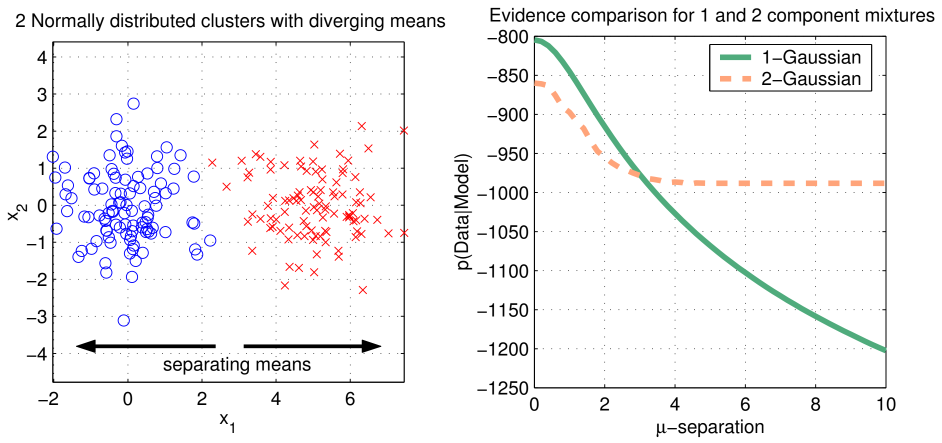

Figure 3.2: A comparison of the functional $\mathcal{F}$ for the data set consisting of two Gaussian clusters with increasing mean separation.

also maximized, and the appropriate model complexity regularization is achieved since integration over the parameter space automatically penalizes model complexity that is not given adequate data support. In other words, the data may support a simpler model (with a single mixture component) since it would have higher evidence than a more complex model (with two or more components) that fit the data just as well.

We can demonstrate this regularization intuitively with the following example. Consider two sets of 100 data points each generated from unit variance 2-dimensional Gaussians. We combine the two clusters such that they initially have identical means, but slowly increase the separation between their means. Initially the combined data set will appear to have been generated by a single Gaussian, but as the separation increases, we should start to see more evidence for two mixture components.

Figure 3.2 plots the evidence as a function of increasing separation between the means of the two data sets. Two cases are plotted:

- The solid line shows the evidence when the model is constrained to use only a *single* Gaussian (by appropriately constraining its priors) to model the data. As expected, the evidence monotonically decreases as the separation between the two clusters is increased.

- The dashed line shows the evidence when the model is free to use two Gaussians. Initially, although the 2-Gaussian model chooses to retain only a single Gaussian, its evidence is lower due to its higher model complexity. As the separation increases however, the 2-Gaussian case has enough evidence to warrant the existence of 2 components, after which its evidence stays essentially constant.

We also notice a distinct crossover point at which the evidence for the 2-Gaussian model becomes higher than that of the 1-Gaussian model. This is a crucial observation since we can effectively use the evidence (or in this case, the approximation $\mathcal{F}$ to the evidence) as a distinction mechanism to make an automatic choice between using 1 or 2 Gaussians to model the given data.

We can now embed this result in a framework that provides us with a principled way of increasing the number of models to account for structure in the data.

### 3.1.2 An Algorithm for Growing Mixture Model Cardinality

We are now in a position to formulate an algorithm based on the results of the previous section. Given a $K$-component mixture model, the 1-component v/s 2-component decision that we discussed in the previous section can be applied to each of the $K$ components, to make a local decision about splitting a local model into 2 components. In

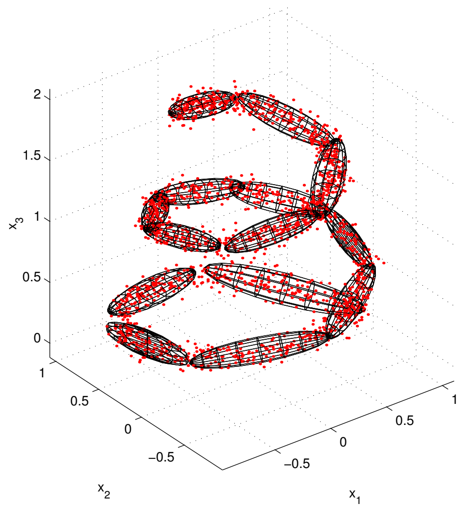

Figure 3.3: Starting with an initial set of 5 components, the model grows in complexity to settle on a final estimate of 14 components.

this way, starting with a very small number of components (or even a *single* component), we can grow the number of components until the local evidence at each component votes in favor of 1 model instead of 2. Algorithm 2 details this procedure.

Although in the previous section, we explicitly evaluated the evidence of the 1-component and 2-component models separately, practically we only need to start with the

```
1: Init: $K = 1$, $\mathbf{x}_{\mathcal{H}} = \left\{\boldsymbol{\mu}_1, \mathbf{P}_1, \{s_{i1}\}_{i=1}^{N}, \zeta\right\}$
2: **repeat**
3:   **for** $m = 1$ to $K$ **do**
4:     Hypothesize an $\mathcal{M}_2$ model covering the same data $\mathbf{x}_{\mathcal{D}_m}$ as component $m$
5:     Maximize $p(\mathbf{x}_{\mathcal{D}_m}; \mathcal{M}_2)$
6:     **if** split **then**
7:       $K \leftarrow K + 1$
8:       $\mathbf{x}_{\mathcal{H}} \leftarrow \mathbf{x}_{\mathcal{H}} \cup \left\{\boldsymbol{\mu}_K, \mathbf{P}_K, \{s_{iK}\}_{i=1}^{N}\right\}$
9:     **end if**
10:   **end for**
11: **until** no split occurs
```

**Algorithm 2:** Growing Mixture Models

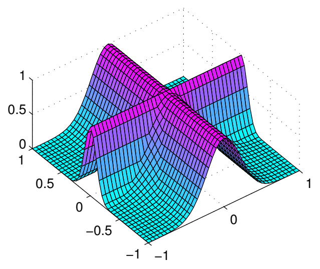

(a) The cross function

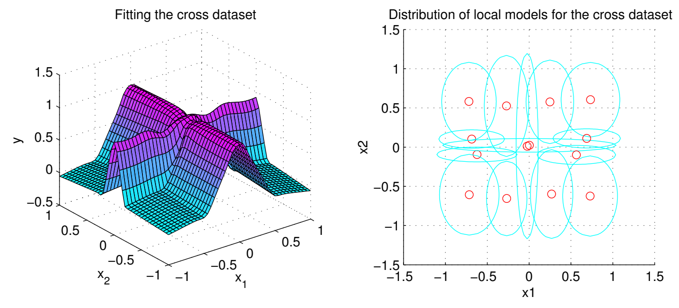

(b) Final learned function and localization of 14 components after starting with an initial 4 components

Figure 3.4: Bayesian estimation of mixture model complexity applied to regression. 2000 points from the function $y = \max\left[e^{-10x_1^2}, e^{-50x_2^2}, e^{-5(x_1^2+x_2^2)}\right]$ are sampled and rotated into a 15-dimensional space. The learned function is shown rotated back into the original 2-dimensional input space.

assumption of the 2-component model, and allow the evidence maximization procedure automatically adjust our parameter space to allow or disallow the additional complexity such that the local evidence is always maximized. The mathematics of the previous section can be extended to incorporate the additional "expert" parameters in a mixture-of-experts setting (Jordan & Jacobs 1994). For example, in maximizing the local evidence, we can integrate over the parameter spaces of a local regression or classification model, while still keeping the resulting posteriors analytically tractable with the factorial assumption. Figure 3.3 shows the result of applying this algorithm on a 3-dimensional shrinking spiral for mixtures of Gaussians density estimation, while figure 3.4 demonstrates its use on a toy regression problem.

One of the main advantages of this approach is the fact that we can start with an underestimate of the number models, and allow the data to automatically increase the model complexity as required. Secondly, since each splitting decision is based on local evidence, the computation does not have to take into account the entire data set and hence is efficient. Finally, the splitting decision is based on the much more principled criterion of evidence maximization compared to previous approaches, which is guaranteed to locally regularize model complexity.

One potential pitfall of this method is the phenomenon of “sudden death” which happens when the complexity of the data covered by a single model is too great to be modeled by just two components. In such a situation, both the 1-component and 2-component choices model the data equally *badly* resulting in the choice of a simpler model (no split) to maximize evidence at the current level of (bad) fit. In such a case, one solution would be to attempt a split into more than 2 components in regions where the data distribution seems to warrant additional complexity. Reliably detecting these situations is a topic of further research.

### 3.1.3 Application to Non-linear Latent Dimensionality Estimation

Recent research has provided increasingly more evidence for the existence of internal models in biological motor control — either as forward models or inverse models. For example, an inverse model of the body’s dynamics allows the generation of appropriate muscle activations when supplied with a desired movement trajectory. In the most visionary theories, internal models of the entire body dynamics and kinematics are required to accomplish motor competence. However, from a statistical learning viewpoint, the acquisition of such large internal models is very complex due to the hundreds of (possibly irrelevant/redundant) input dimensions from various afferent and efferent sources — a similar problem as that which seems to be solved by the mammalian cerebellum. Early theories in computational motor control rejected internal model-based control due to the daunting complexity of the differential equations that govern such models, and the high dimensionality of the input spaces from which these models are learned.

From a control theoretic point of view, *model-based* feed-forward control has been highly successful, particularly for fast movements with significant feedback loop delays. In recent years however there has been mounting evidence (Kawato 1999) that internal models are used in biological motor control (e.g., from force field experiments, neurophysiology of oculomotor control, lesion and clinical studies of the cerebellum). An open theoretical research question is therefore: what is the complexity of the learning task that needs to be tackled for motor control? Clearly, the hope is that even though the movement system is extremely high-dimensional, kinematic and other constraints will restrict movement data to reside in a very low dimensional manifold within this space, thus providing a simpler learning task when expressed in terms of these low-dimensional variables.

To answer this question, we performed a local dimensionality analysis of a significant amount of movement data (D'Souza, Vijayakumar & Schaal 2001). If indeed, the data was discovered to exist in locally low dimensional manifolds, then this would imply that learning a model of movement data would only need to operate in this low dimensional space — thus providing evidence that it is indeed feasible to learn internal models. The data is analyzed using two statistical methods: singular value decomposition (SVD) and our growing mixture model with each component being a variational Bayesian factor

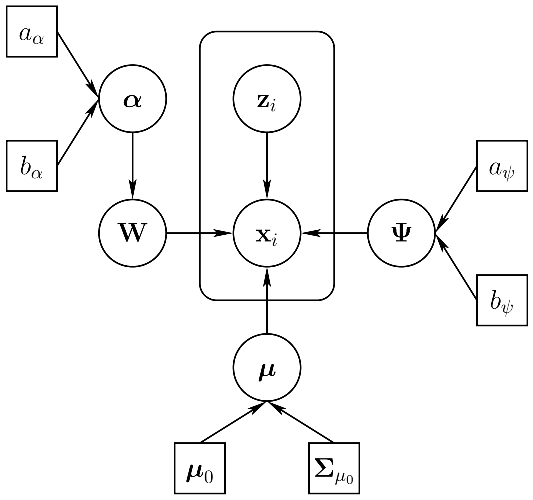

Figure 3.5: Graphical model for Bayesian factor analysis.

analyzer (Ghahramani & Beal 2000). Bayesian factor analysis treats the latent dimensionality of the model as an unknown model complexity parameter which must be estimated. While several methods exist to estimate this latent dimensionality (Ghahramani & Hinton 1997, Bishop 1999*a*, Bishop 1999*b*), we choose to extend the model presented in (Ghahramani & Beal 2000) since it fits well with our variational scheme.

The graphical model for variational factor analysis is shown in figure 3.5. The observed high-dimensional data $\mathbf{x}$ is assumed to be a linear combination $\mathbf{W}$ of a low-dimensional set of latent variables $\mathbf{z}$ with additive axis-aligned noise:

$$\mathbf{x}_i = \mathbf{W}\mathbf{z}_i + \boldsymbol{\mu} + \boldsymbol{\eta}_i \quad \text{where } \boldsymbol{\eta}_i \text{ is i.i.d. Normal}\left(\boldsymbol{\eta}_i; \mathbf{0}, \boldsymbol{\Psi}\right)$$

By placing priors over each column of $\mathbf{W}$, we can regularize over the number of latent variables that are required to reconstruct $\mathbf{x}$. This model serves as a single component

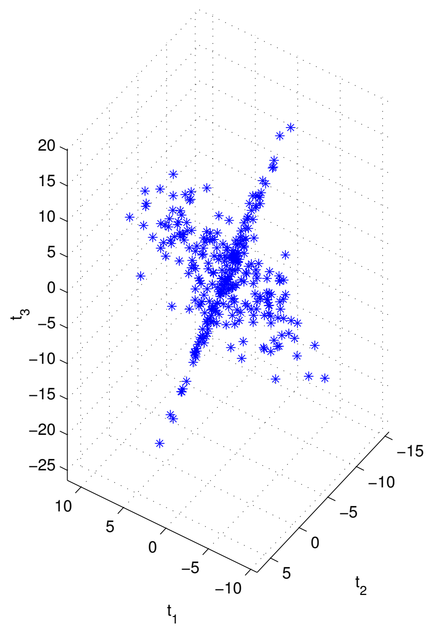

(a) Non-linear data set with locally low-dimensional manifolds

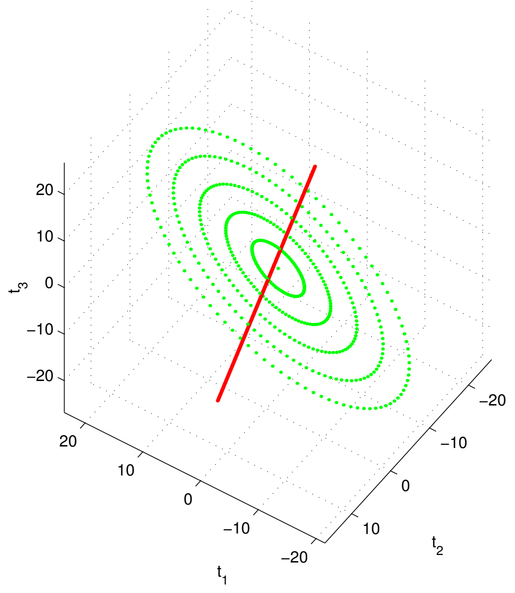

(b) Inferred manifolds

Figure 3.6: Mixture modeling with factor analyzers allows us to examine the local dimensionality structure in potentially highly non-linear data. In this example, the data is clearly 3-dimensional, with strong evidence for local 1-dimensional, and 2-dimensional structure.

in our mixture model used to analyze the human movement data. An analysis of a toy example is shown in figure 3.6.

Several subjects were recorded performing a wide variety of everyday tasks such as walking, picking-and-placing objects, etc., to obtain an unbiased sample of movement data generated during normal activity. The data was collected using the Sarcos SenSuit, which is an exoskeleton that can record 35 degrees of freedom of the human body at 100Hz (see figure 3.7). The following preprocessing steps were performed on the captured motion data:

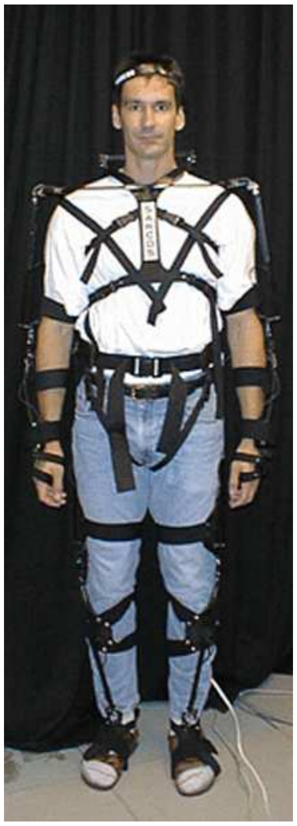

Figure 3.7: The Sarcos SenSuit is an exoskeleton that can record position data of 35 degrees of freedom of the human body at 100Hz.

- The recorded joint angle data was low-pass filtered using a second-order Butterworth filter with cutoff at 5Hz to eliminate sensor noise.
- Filtered data was numerically differentiated to obtain velocity and acceleration resulting in an input dimensionality of $35 \times (\theta, \dot{\theta}, \ddot{\theta}) = \Re^{105}$

The final data set consisted of 126,000 data points in 105 dimensions.

As a baseline estimate, we determine the underlying *global* dimensionality of the movement data using Singular Value Decomposition. As shown in figure 3.8(a), we find that 32 dimensions are required to explain 99% of the observed variance in the data.

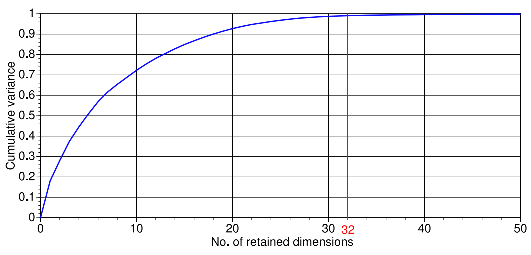

(a) Estimation using SVD

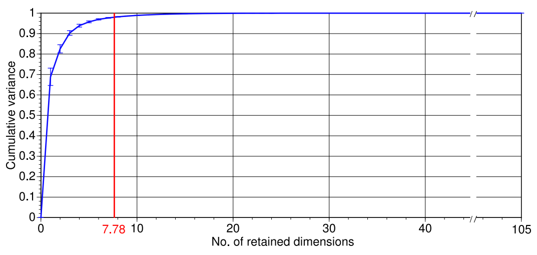

(b) Estimation with Bayesian mixtures of factor analyzers

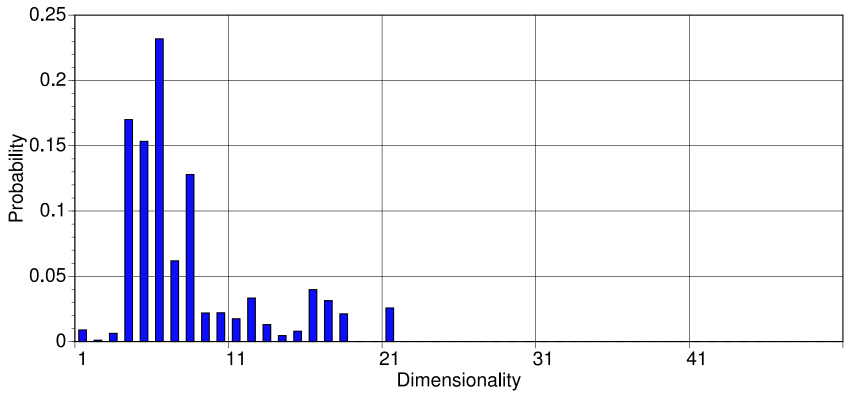

(c) Distribution of latent dimensionality

Figure 3.8: A histogram of the latent dimensionality of movement collected with the SenSuit. The weight of each bin is the ratio of the total amount of data that is modeled by a factor analyzer of that dimensionality.

In a sense, the global dimensionality estimate is the maximum that we can expect the local dimensionality of the data to be. This figure however is an overestimate since it fails to take into account local structure. By analyzing the same data set with mixtures of Bayesian factor analyzers, we address the issue of local structure, as well as create a mathematically principled estimate of local dimensionality within each model. As shown in figure 3.8(b), when local structure is taken into account, our estimate of the average dimensionality of the movement data drops to 7.78. The dimensionality of each local model automatically falls out of the inference process, and the overall dimensionality calculated as a weighted average over all models.

Figure 3.8(c) plots a histogram of the local dimensionality found in each model. We can see that in spite of the global data dimensionality being 105, the bulk of the probability mass lies between 6 to 9 dimensions. From these results we can conclude the following:

- Biological movement data seems to lie on low-dimensional distributions that are embedded in very high-dimensional spaces.
- Such low-dimensional distributions can be exploited efficiently by learning (in particular function approximation) algorithms that use spatially localized receptive fields, and dimensionality reduction techniques inside these localized receptive fields.

What are the potential reasons for the locally low-dimensional distributions of biological movement data? It is useful to examine well-known *invariances* of human movement in the light of the dimensionality of movement data that they produce:

**Minimum Jerk / Torque-Change / Variance Criteria:** These criteria assume that human movement is created out of optimizing a general, biologically useful cost criterion. A typical characteristic of these criteria is that the velocity of movement is unimodal and bell-shaped. Therefore, the trajectories in different joints are (to a first approximation) just a scaling of each other. Thus if all DOFs would move in minimum jerk trajectories, the local dimensionality of the space spanned by position velocity and acceleration of all DOFs would be just 3, since the scaling of trajectories between each DOF makes their positions linearly dependent (as would be the velocity and accelerations).

**Rhythmic pattern generators:** In rhythmic movement, most joint angle trajectories are either first or second order sinusoids (e.g., the knee joint performs second order oscillations in locomotion), the only difference being amplitude and phase of the oscillations. The linear superposition of two sinusoids with different phase can reproduce arbitrary sinusoids in terms of phase and amplitude. Thus, if all joints would perform first order oscillations, the space spanned by position, velocity, and acceleration of all DOFs will be at most 6-dimensional, globally or locally! Some joints performing higher order oscillations may add some modest amount of additional dimensionality.

**Consistent resolution of redundancy:** Redundancy in human movement is mostly resolved in a very consistent manner, e.g., reaching movements are invariantly straight-line trajectories with highly repeatable resolution of redundancy within an individual. Thus, from the end effector trajectory, the resolution of redundancy of the human body can approximately be inferred, and the dimensionality of the joint space movements is approximately that of the end effector movement, i.e., at most 9-dimensional for 3D position, velocity and acceleration of the end effector.

**2/3 power law:** The 2/3 power law can be interpreted as an epiphenomenon of sinusoidal joint space trajectories (Schaal & Sternad 2001). Hence the comments under "Rhythmic Pattern Generators" can be applied to how the 2/3 power law may lead to low dimensional distributions in joint space.

### 3.1.4 Mixture Modeling with Dirichlet Process Priors

Recently, the use of semi-parametric techniques such as Dirichlet processes have gained popularity as a method of dealing with the question of mixture model cardinality. Dirichlet processes were introduced as a means of placing probability distributions over the space of density functions in statistical models (Ferguson 1973, Ferguson 1974). Formally, the Dirichlet process can be defined as follows:

*If $\alpha$ is a finite measure on $(\mathcal{X}, \Omega)$, and $\mathcal{B}_1, \ldots, \mathcal{B}_k$ is any partition of $\mathcal{X}$ by Borel sets, then there exists a unique probability measure $D(\alpha)$ on the space of probability measures over $\mathcal{X}$, called the Dirichlet process with parameter $\alpha$ satisfying:*

$$\big(p(\mathcal{B}_1), \ldots, p(\mathcal{B}_k)\big) \sim \mathrm{Dirichlet}\big(\alpha(\mathcal{B}_1), \ldots, \alpha(\mathcal{B}_k)\big) \tag{3.7}$$

The only parameter of the Dirichlet process is the base measure $\alpha(\cdot)$, which is sometimes written as a product $\alpha(\cdot) = \alpha_0 p_0(\cdot)$ where $\alpha_0$ is a scalar, known as the "concentration", and $p_0(\cdot)$ is a probability measure. A Dirichlet process with base measure $\alpha(\cdot)$ establishes a distribution over the space of density functions $p(\cdot)$ over the domain $\mathcal{X}$, such that the following properties hold:

- The expected value of the density $p(\cdot)$ is given by:

$$\langle p(\cdot) \rangle = \frac{\alpha(\cdot)}{\alpha(\mathcal{X})} = p_0(\cdot) \tag{3.8}$$

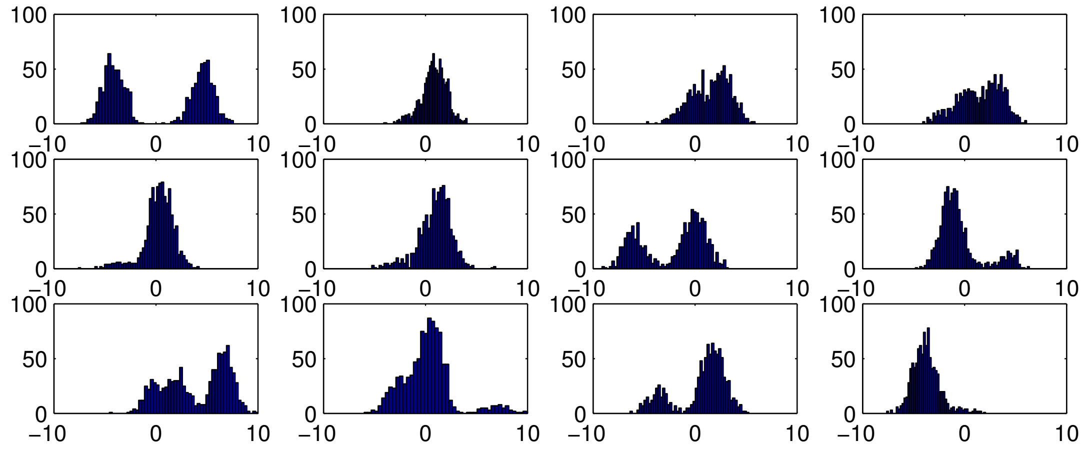
Figure 3.9: Samples from a Dirichlet process. The base distribution is a Gaussian Normal $(x; 0, 10)$ with zero mean and variance 10. The concentration parameter $\alpha = 1$ allows a fair amount of variation in sampled distributions.

- The posterior distribution of $p(\cdot)$ given an observation of $x_1, \ldots, x_n$ is also a Dirichlet process:

$$p(\cdot)|x_1, \ldots, x_n \sim \mathrm{DP}\left(\alpha(\cdot) + \sum_{i=1}^{n} \delta_{x_i}(\cdot)\right) \tag{3.9}$$

Where $\delta_{x_i}(x) = 1$ when $x = x_i$ and zero otherwise. Hence we can write the mean posterior distribution as follows:

$$\langle p(\cdot)|x_1, \ldots, x_n \rangle = \frac{\alpha(\mathcal{X})}{\alpha(\mathcal{X}) + n} \underbrace{\left(\frac{\alpha(\cdot)}{\alpha(\mathcal{X})}\right)}_{p_0(\cdot)} + \frac{n}{\alpha(\mathcal{X}) + n} \left(\frac{\sum_{i=1}^{n} \delta_{x_i}(\cdot)}{n}\right)$$

This has an intuitive appeal as a Bayesian estimate since it is a convex combination of "prior guess" and "empirical estimate". Hence, given a set of observed samples $x_1, \ldots, x_n$, with probability $\alpha(\mathcal{X})/(\alpha(\mathcal{X}) + n)$, the next sample is a new, distinct value chosen according to the "prior guess". Otherwise, it is drawn uniformly from among the first $n$ samples. The applicability of the term "concentration parameter" to $\alpha_0$ is apparent here, since for large values of $\alpha_0$, the sampled distributions will tend to be very similar to the base distribution, while smaller values of $\alpha_0$ allow more variation. Figure 3.9 shows sample distributions from a Dirichlet process with a relatively low concentration parameter $\alpha_0 = 1$ which allows a fair amount of deviation from the base distribution $p_0(x) = \text{Normal}\,(x; 0, 10)$.

- The probability of a new observation $x_{n+1}$ can be derived from the corresponding result for Dirichlet distributions by taking the limit as $\alpha_j \to 0$ and $k \to \infty$ such that $\alpha(\mathcal{X})$ is constant.

$$\begin{aligned} p(x_{n+1} = x_i \text{ for some } 1 \leq i \leq n | x_1, \ldots, x_n, \alpha) &= \frac{\sum_{i=1}^{n} \delta_{x_i}(x_{n+1})}{\alpha(\mathcal{X}) + n} \\ p(x_{n+1} \neq x_i \text{ for all } 1 \leq i \leq n | x_1, \ldots, x_n, \alpha) &= \frac{\alpha(\mathcal{X})}{\alpha(\mathcal{X}) + n} \end{aligned} \tag{3.10}$$

The tractability of equation (3.10) is crucial for sampling methods used to solve DP models.

Any realization of a Dirichlet process is (with probability 1) a discrete distribution (Blackwell 1973), since there is always a non-infinitesimal probability of observing a sample that we have seen before. In this sense, the Dirichlet process can be thought of as an infinite-dimensional extension of the standard Dirichlet distribution, and its connection to the Pólya urn representation is also well documented (Blackwell & MacQueen 1973, Chun et al. 2003, Ghosh & Ramamoorthi 2003). While the discreteness of the Dirichlet process might seem to curb its applicability to modeling continuous distributions, this is easily remediedby simply convolving it with a simple continuous distribution such as the popular Gaussian, resulting in the Dirichlet process mixture model (Antoniak 1974, Escobar 1994, MacEachern & Müller 1998):

$$
\begin{aligned}
x_i &\sim \int \text{Normal}\left(x_i; \mu, \sigma^2\right) p_\mu(\mu) d\mu \\
p_\mu &\sim DP\left(\alpha_0 p_0\right)
\end{aligned}
$$

Initially, the use of such models was limited because the posteriors quickly become intractable for modest numbers of observations. However, the development of Gibbs sampling techniques which could solve these models exactly (Escobar 1994, Escobar & West 1995) made them popular density estimation techniques. See (Neal 1998) for an excellent overview of sampling methods for Dirichlet processes.

An example using a density estimation task is shown in figure 3.1.4. A 1000-sample data set is presented with the histogram shown in figure 3.10(a). Using the sampling techniques outlined in (Neal 1998), we can generate samples from the posterior distribution over the space of probability measures over $x$. These samples (along with the mean and one standard deviation bars) are shown in figure 3.10(b). The key aspect of the algorithm is that even though we implicitly use a mixture model, we do not need to explicitly specify the number of mixture components. Indeed, the Dirichlet process model allows for an infinite number of components, which can be instantiated based on the complexity of the data set.

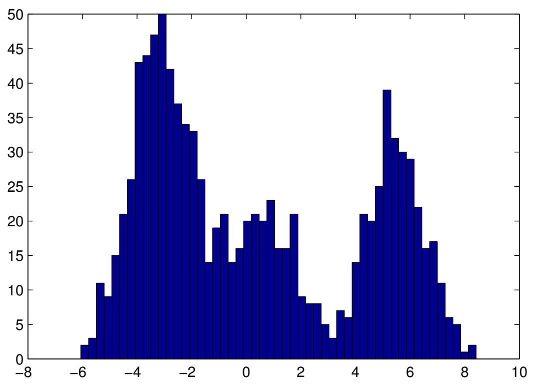
(a) Histogram of 1000 samples of data.

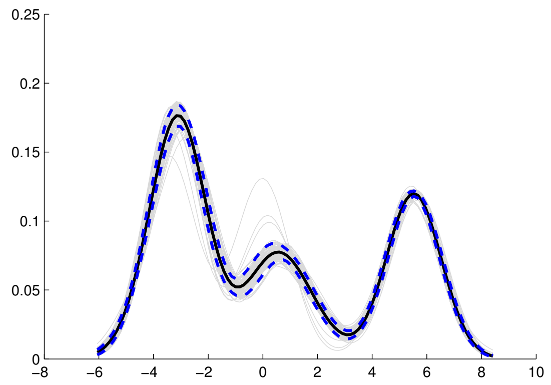
(b) Samples from the estimated distribution.

Figure 3.10: The right sub-figure shows samples from the posterior distribution over probability densities (light grey lines), estimated from the data on the left using a Dirichlet process prior. Also shown are the mean (thick dark line) and standard deviation (thick dashed lines) of the sampled distributions.

An alternate set of sampling methods using the stick-breaking construction of the Dirichlet process by Sethuraman (1994) has also gained in popularity, leading to the truncated versions of the Dirichlet process (Ishwaran & James 2001, Ishwaran & Zarepour 2002). Variational methods for the Dirichlet process which use this truncated representation also exist (Blei & Jordan 2004), although algorithmically, they reduce again to the existing methods proposed in (Beal 2003) which initially overestimate the number of components, and then allow the inference mechanism to prune away the unneeded model complexity.

Some of our recent efforts have been directed towards examining whether locally weighted projection regression (LWPR) (Vijayakumar et al. 2000), an extremely efficient supervised learning algorithm based on the creation of fixed local models, can be interpreted in the framework of Dirichlet process mixtures.

The key similarity is the generation of new local models. As Neal (1998) intuitively describes, in the Gibbs sampling algorithm, a data point has a higher probability of spawning a new Dirichlet process mixture component if it cannot be explained satisfactorily by existing components. This is exactly the same heuristic that is used by LWPR for the creation of new local models.

At this time the Dirichlet process model is still computationally unattractive due to the Gibbs sampling procedure which limits its applicability to higher-dimensional parameter spaces. Although it has been used with limited success in some supervised learning settings (Rasmussen 2000, Rasmussen & Ghahramani 2002, Beal et al. 2002), the variational approach of Blei & Jordan (2004) and our growing mixture formulation presented in this section seem more promising and empirically seem to require fewer iterations to converge.

## 3.2 Online Learning with Automatic Forgetting Rates

While there exists a large body of statistical learning literature that deals with Bayesian techniques for batch learning, many of these techniques are not naturally applicable to sequential learning tasks that are often embedded in dynamic, non-stationary environments. Two aspects of online learning make statistical learning especially hard. Firstly, the parameters of interest (e.g. the parameters of a classification/regression function) may themselves vary with time. In addition, a complex learning algorithm with multiple parameters in flux, may cache statistics based on only partially converged estimates of these parameters. It therefore becomes necessary to “forget” past data and statistics, in favor of more recent observations, such that the learning system is responsive to new conditions at an appreciable rate, as the learning model and environment evolve.

In the context of regression, the popular Recursive Least Squares (RLS) algorithm (Ljung & Söderström 1983) has received considerable attention. Crucial to this framework is the notion of a "forgetting rate" $\gamma$ (where $0 \leq \gamma \leq 1$), which controls the extent to which past data contributes towards the current estimate of the process parameters. In a sense, the forgetting rate $\gamma$ can be thought of as defining an effective window of size $\gamma/(1-\gamma)$ over the data. Several algorithms adapt this strategy to limit the horizon of accumulated "sufficient statistics", including the recent model estimation framework using variational Bayes (Sato 2001).

Recently, an alternative view within the framework of Bayes filtering has been proposed (de Freitas et al. 1999, Sykacek & Roberts 2003). This framework treats the estimation of the parameters of a non-stationary process as a Bayesian state estimation problem. Several algorithms exist for performing state estimation including the well-known Kalman filter. Indeed, statistical signal processing literature often highlights the relationship between RLS based system identification, and Kalman filters (Proakis et al. 2002). In (Sykacek & Roberts 2003), an algorithm for online classification is presented that uses the variational Bayes framework in conjunction with a Kalman filter, to automatically estimate the process noise variance — a crucial parameter in determining the extent of non-stationarity. The algorithm however, only considers causal information flow (Kalman *filtering*), even though a windowing approach is used which could potentially take advantage of anti-causal information flow (Kalman *smoothing*) as well.

### 3.2.1 Using a Kalman Filter to Track Non-Stationarity

A simple way of dealing with a non-stationary parameter, is to formulate it as a "drifting" random variable (Sykacek & Roberts 2003), and track it with a Bayes filter. For the purposes of this exposition, let us consider a simple regression problem, in which each data point $(y_n|x_n)$ is generated according to the following model:

$$w_n = w_{n-1} + \eta_n \tag{3.11}$$

$$y_n = w_n x_n + \epsilon_n \tag{3.12}$$

where $\eta_n$ and $\epsilon_n$ are additive Gaussian noise distributed as $\eta_n \sim \text{Normal}\left(\eta_n; 0, 1/\lambda\right)$ and $\epsilon_n \sim \text{Normal}\left(\epsilon_n; 0, 1/\psi_y\right)$. Note the subscript $n$ for the regression coefficient $w$ indicates that we treat it as a drifting parameter whose value changes with time according to equation (3.11). Since these equations represent a linear, Gaussian state-space model, a Bayes filter reduces to the well known Kalman filter (Kalman 1960).

Knowledge of the precision $\lambda$ is crucial if we wish to track $w_n$ accurately, since it constrains the amount that $w_n$ is allowed to vary at each time step. As shown in figure 3.11, an incorrect estimate of $\lambda$ can result in a learning system that is too sluggish to adapt to changes (if $\lambda$ is too high), or one that is excessively responsive, and highly susceptible to noise (if $\lambda$ is too low). Thus $\lambda$ can be interpreted as an inverse *process adaptation rate*, or perhaps more accurately, an inverse *drift step size*. Estimating $\lambda$ (and also $\psi_y$) is potentially achievable if we retain a moving window of $N$ data points (we shall revisit the question of window size later) in conjunction with a Kalman smoothing

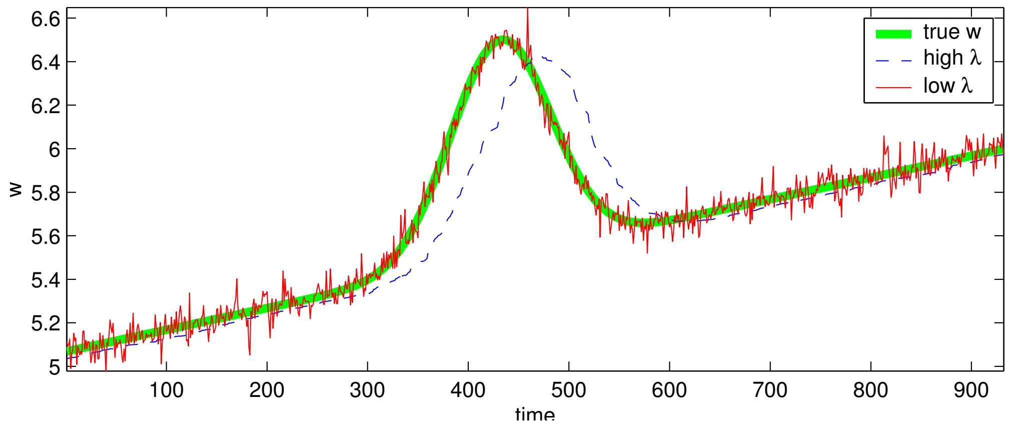

Figure 3.11: Overestimating the precision $\lambda$ results in sluggish tracking of rapid changes in $w$, while underestimating it introduces a hyper-sensitivity to noise.

procedure to estimate true posteriors over the $w_n$ within the window. Clearly, a naive Maximum-Likelihood (ML) estimation of both $\lambda$ and $\psi_y$ simultaneously, is impossible without arriving at degenerate Gaussian distributions over $w_n$. This is partially because $\lambda$ and $\psi_y$ are essentially model complexity parameters, since they restrict the possible space of Markov chains of $w_n$ given a starting distribution $p(w_0)$. Consequently, they also restrict the possible space of data sets that could be observed under this model structure. Hence, we look towards the evidence framework to provide the necessary regularization ability such that we can obtain principled estimates of these quantities from the point of view of maximizing model *evidence*.

We therefore place prior distributions over $\lambda$ and $\psi_y$. Since they are essentially *scale* parameters, we choose the prior distributions to be broad (non-informative) Gamma distributions, which are theoretically justified as being relatively uniform over a log scale (Gelman et al. 1995), as well as analytically convenient due to their conjugacy with Normal distributions:

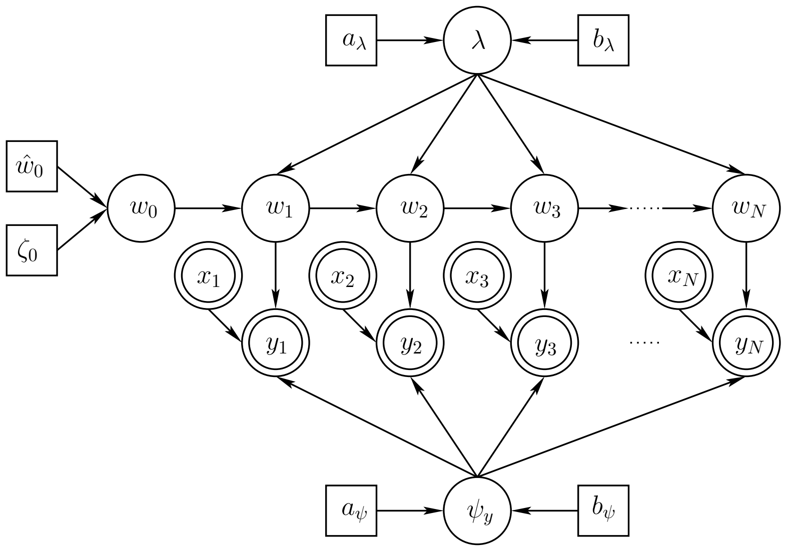

Figure 3.12: Graphical model for variational Kalman filtering

$$\lambda \sim \mathrm{Gamma}\left(\lambda; a_\lambda, b_\lambda\right) = \frac{b_\lambda^{a_\lambda}}{\Gamma\left(a_\lambda\right)} \lambda^{a_\lambda - 1} \exp\left(-b_\lambda \lambda\right) \tag{3.13}$$

$$\psi_y \sim \mathrm{Gamma}\left(\psi_y; a_\psi, b_\psi\right) = \frac{b_\psi^{a_\psi}}{\Gamma\left(a_\psi\right)} \psi_y^{a_\psi - 1} \exp\left(-b_\psi \psi_y\right) \tag{3.14}$$

The graphical model incorporating these distributions is shown in figure 3.12. Given the conditional independencies implied by this model, the log complete evidence can be written as follows:

$$
\begin{aligned}
\ln p(\mathbf{y}, \mathbf{w}, \lambda, \psi_y | \mathbf{x}) = \sum_{n=1}^{N} \Bigg[ & \frac{1}{2} \ln \frac{\psi_y}{2\pi} - \frac{\psi_y}{2} (y_n - w_n x_n)^2 \\
& + \frac{1}{2} \ln \frac{\lambda}{2\pi} - \frac{\lambda}{2} (w_n - w_{n-1})^2 \Bigg] \\
& + \frac{1}{2} \ln \frac{\zeta_0}{2\pi} - \frac{\zeta_0}{2} (w_0 - \hat{w}_0)^2 \\
& + a_\lambda \ln b_\lambda - \ln \Gamma(a_\lambda) + (a_\lambda - 1) \ln \lambda - b_\lambda \lambda \\
& + a_\psi \ln b_\psi - \ln \Gamma(a_\psi) + (a_\psi - 1) \ln \psi_y - b_\psi \psi_y
\end{aligned}
\tag{3.15}
$$

where we define $\mathbf{y} = \begin{bmatrix} y_1 & \cdots & y_N \end{bmatrix}^T$, $\mathbf{x} = \begin{bmatrix} x_1 & \cdots & x_N \end{bmatrix}^T$, $\mathbf{w} = \begin{bmatrix} w_1 & \cdots & w_N \end{bmatrix}^T$. Ultimately, we are interested in the posterior distribution over the regression coefficient at the current (last) time step, i.e. $p(w_N | \mathbf{x}_{\mathcal{D}_N})$, which is obtained by marginalizing out all the other random variables from the true posterior $p(\mathbf{w}, \lambda, \psi_y | \mathbf{x}_{\mathcal{D}_N})$. From the structure of equation (3.15), we see that this is an analytically intractable proposition. We therefore turn to the factorial variational approximation methods described in chapter 2 to allow tractable inference of the model parameters.We shall choose to approximate the true posterior $p(\mathbf{w}, \lambda, \psi_y | \mathbf{x}_{\mathcal{D}_N})$ with the factored approximating ensemble:

$$
Q(\mathbf{w}, \lambda, \psi_y) = Q(\mathbf{w}) Q(\lambda, \psi_y) \tag{3.16}
$$

The factorization between $Q(\mathbf{w})$ and $Q(\lambda, \psi_y)$ is the approximation we introduce to allow tractable inference. As it turns out, an additional factorization $Q(\lambda)Q(\psi_y)$ falls out of the conditional independencies in the model itself (the graph vertices corresponding to $\lambda$ and $\psi_y$ are separated by $\mathbf{w}$).

Inference of the individual posterior distributions proceeds by iteratively updating each $Q_i(\cdot)$ in equation (3.16) according to equation (2.6). Given the factorization in equation (3.16), estimating the posterior distribution $Q(\mathbf{w})$ over the regression coefficients is equivalent to performing the forward (filtering) and backward (smoothing) recursions of a Kalman smoother, given current estimates of $Q(\lambda)$ and $Q(\psi_y)$. If we assume that the filtered distribution of $w_n$ is $Q(w_n|\mathbf{x}_{\mathcal{D}_{1:n}}) = \text{Normal}\left(w_n; \left\langle w_n \right\rangle_n, 1/\zeta_n\right)$, and the smoothed distribution is $Q(w_n|\mathbf{x}_{\mathcal{D}_{1:N}}) = \text{Normal}\left(w_n; \left\langle w_n \right\rangle_N, 1/\varphi_n\right)$, then we can derive the following forward recursion:

$$\begin{aligned}
\zeta_n &= \left\langle \psi_y \right\rangle x_n^2 + \frac{\zeta_{n-1} \left\langle \lambda \right\rangle}{\zeta_{n-1} + \left\langle \lambda \right\rangle} \\
\left\langle w_n \right\rangle_n &= \frac{1}{\zeta_n} \left[ \left\langle \psi_y \right\rangle x_n y_n + \frac{\left\langle \lambda \right\rangle \zeta_{n-1} \left\langle w_{n-1} \right\rangle_{n-1}}{\zeta_{n-1} + \left\langle \lambda \right\rangle} \right]
\end{aligned}$$

as well as the backward recursion:

$$\begin{aligned}
\varphi_{n-1} &= \frac{\varphi_n \big(\zeta_{n-1} + \left\langle \lambda \right\rangle\big)^2}{\varphi_n \big(\zeta_{n-1} + \left\langle \lambda \right\rangle\big) + \left\langle \lambda \right\rangle^2} \\
\left\langle w_{n-1} \right\rangle_N &= \frac{\varphi_n}{\varphi_{n-1}} \left[ \frac{\big(\zeta_{n-1} \left\langle w_{n-1} \right\rangle_{n-1} + \left\langle \lambda \right\rangle \left\langle w_n \right\rangle_N\big)\big(\zeta_{n-1} + \left\langle \lambda \right\rangle\big)}{\varphi_n \big(\zeta_{n-1} + \left\langle \lambda \right\rangle\big) + \left\langle \lambda \right\rangle^2} \right]
\end{aligned}$$

The update equations for the distributions of $Q(\lambda)$ and $Q(\psi_y)$ are easily derived as Gamma distributions from equations (3.15) and (2.6). This results in the following update equations (see appendix B.3) for the parameters of the posterior Gamma marginals $Q(\lambda)$ and $Q(\psi_y)$:

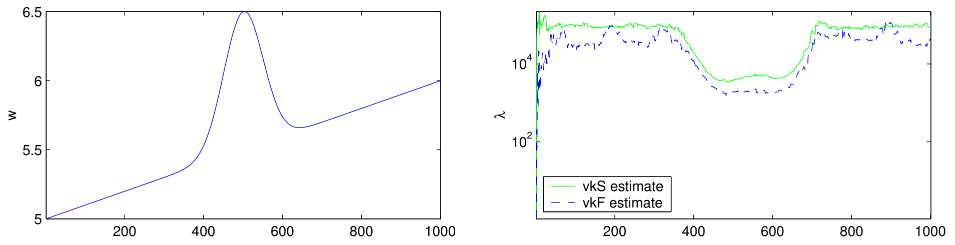

(a) True (drifting) $w$ (b) Estimating $\lambda$

Figure 3.13: In our artificial data set, the regression parameter drifts as shown in 3.13(a). The estimates of $\lambda$ obtained by the vkS and vkF algorithms (for $\psi_y = 10^4$) are shown in 3.13(b)

$$\begin{aligned}
\hat{a}_\psi &= a_\psi + \frac{N}{2} \\
\hat{b}_\psi &= b_\psi + \frac{1}{2}\sum_{n=1}^{N}\left[\left(y_n - \langle w_n\rangle_N x_n\right)^2 + \frac{1}{\varphi_n}\right] \\
\hat{a}_\lambda &= a_\lambda + \frac{N}{2} \\
\hat{b}_\lambda &= b_\lambda + \frac{1}{2}\sum_{n=1}^{N}\left[\left(\langle w_n\rangle_N - \langle w_{n-1}\rangle_N\right)^2 + \frac{1}{\varphi_n} + \frac{1}{\varphi_{n-1}} - 2\,\mathrm{Cov}\left(w_{n-1}, w_n\right)\right]
\end{aligned}$$

where $\mathrm{Cov}\left(w_{n-1}, w_n\right)$ is the cross-time covariance that can be derived using Schur complements (see appendix A.1) as:

$$\mathrm{Cov}(w_{n-1}, w_n) = \frac{\langle\lambda\rangle\left(\zeta_{n-1} + \langle\lambda\rangle\right)}{\varphi_{n-1}\left[\varphi_n\left(\zeta_{n-1} + \langle\lambda\rangle\right) + \langle\lambda\rangle^2\right]}$$

### 3.2.2 Bayesian Forgetting Rates Evaluation

To evaluate our algorithm we considered the simple linear regression system outlined in section 3.2.1. We allow $w$ to drift over 1000 time steps according to the plot in figure 3.13(a). At each time step we sample $x_n$ according to $\text{Normal}\,(x_n; 0, 1)$, a zero mean, unit variance Gaussian, and generate $y_n$ according to equation (3.12). We generate 50 such data sets in each of three categories, corresponding to the observation noise precision set at $\psi_y = 10^2$, $\psi_y = 10^3$, and $\psi_y = 10^4$, for a total of 150 data sets.

We evaluated our variational Kalman *smoother* (vkS) algorithm against two others on the generated data sets: the variational Kalman *filter* (vkF) algorithm of (Sykacek & Roberts 2003) (adapted for regression instead of classification), and RLS. In order to select the optimum value for the window size parameter $N$ in vkF, it was evaluated at several values ranging from 10 to 200 time steps, and the window size giving the smallest mean-squared error with the true $w$ was chosen. In a similar manner the forgetting rate $\gamma$ for RLS was chosen using a line search to minimize the mean-squared error between the estimated and the true $w$.

Note that our vkS algorithm did not have access to the true $w$, but as figure 3.14 shows, it performs the best of the 3 algorithms across all noise ranges. As the results show, the vkS algorithm tends to outperform RLS significantly. The vkF algorithm performs comparably at estimating $w$, but as figure 3.13(b) shows, it tends to underestimate $\lambda$ due to the lack of anti-causal information that is useful in smoothing out past estimates. Underestimating $\lambda$ causes it to be slightly more susceptible to output noise than our vkS method.

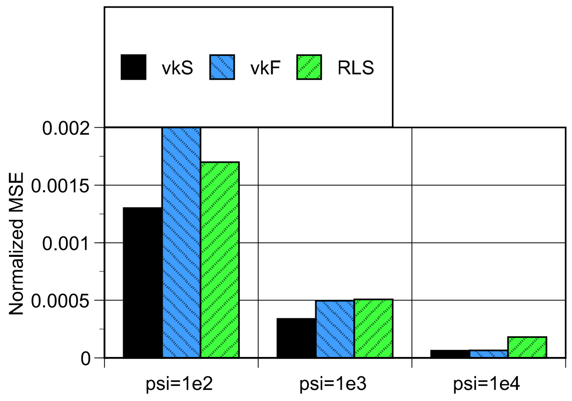

Figure 3.14: A comparison of the mean squared error between the estimated $w$ and the true $w$ obtained for the 3 algorithms for different values of observation noise. Results are tested for statistical significance with $p < 0.05$.

A second set of experiments was carried out by integrating the vkS formulation with the Bayesian backfitting regression algorithm (introduced in chapter 4)[1]. Each experiment consisted of a regression task with a set of 5000 pairs $\{\mathbf{x}_i, y_i\}$ presented to the algorithm sequentially. The goal of the algorithm at each step $i$ is to predict an unseen $y_i$ based on $\mathbf{x}_i$ and the past observations $\{\mathbf{x}_1, y_1\} \ldots \{\mathbf{x}_{i-1}, y_{i-1}\}$. As an additional difficulty, we construct the input data set to live in a low dimensional (5-dimensional) manifold which is embedded in a 105-dimensional space. Two different embeddings are created:

1. The first embedding (corresponding to results in figures 3.15(a) and 3.15(c)) added 50 irrelevant (noise) dimensions, as well as 50 redundant copies of the true input dimensions.

2. The second embedding (corresponding to results in figures 3.15(b) and 3.15(d)) also added the 50 noise dimensions, but this time the 50 redundant inputs were linear combinations of the true inputs.

[1]Many thanks to Jo-Anne Ting for carrying out these evaluations

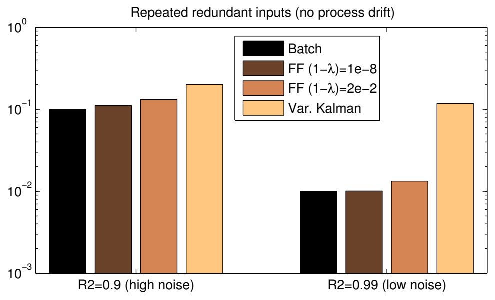

(a)

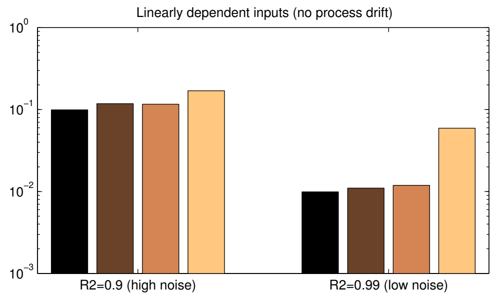

(b)

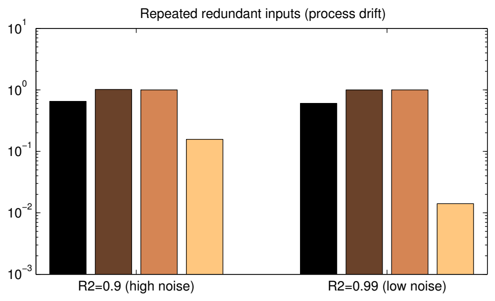

(c)

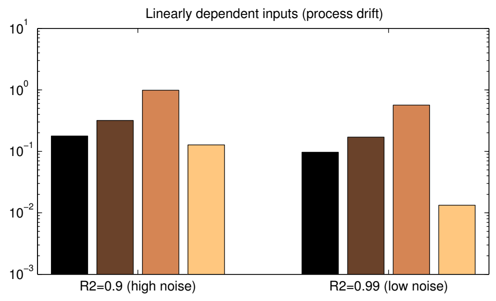

(d)

Figure 3.15: Bayesian forgetting rates applied to a high-dimensional regression task, in conjunction with the Bayesian backfitting algorithm (discussed in chapter 4). Note that all errors are reported on a log scale. The legend in the first graph serves for all. Results are statistically significant with $p < 0.05$.

For each of these embeddings, two different sets of $y$ data was generated by linearly combining the the 5 true dimensions of $\mathbf{x}$: the first using a fixed regression vector, and the second using a drifting regression vector. This resulted in the four scenarios shown in figure 3.15. The results for each of the algorithms compared were averaged over 50 simulation runs for each scenario.

Four algorithms were compared during the simulations: Standard batch regression, two instances of RLS with different forgetting rates $\lambda$ such that $(1 - \lambda_1) = 1e - 8$ and $(1 - \lambda_2) = 2e - 2$, and our variational kalman smoother. Figure 3.15 shows the results of the experiments. In the case where the underlying process is indeed stationary, the batch algorithm does the best job since it takes into account all the data. This is reflected in the top two graphs of figure 3.15. The bottom two graphs on the other hand, show a marked improvement on the performance of the variational Kalman smoother when the process is indeed drifting. The smoother is able to automatically able to determine the appropriate window size required to correctly generalize from the sequential data presented.

#### 3.2.2.1 On Selecting the Window Size "$N$"

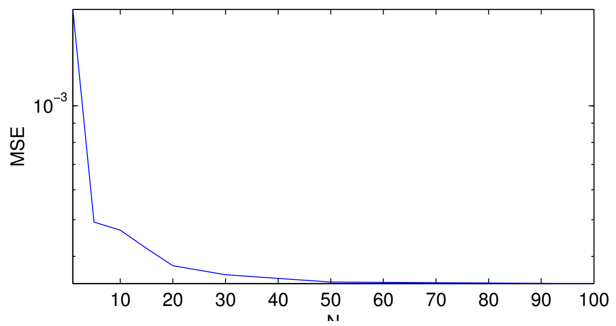

Figure 3.16: Effect of increasing window size on the estimation error

One could argue that we have simply replaced the problem of determining $\lambda$, with the problem of guessing the appropriate number of steps $N$ that we wish to compute a backward (smoothing) pass over. Indeed, while the method proposed in (Sykacek & Roberts 2003) also uses a windowing procedure, it does not give a clear indication as to how the window size should be selected. In general, we find that increasing the window size allows greater robustness when observation noise is high. This is evident from figure 3.16, which shows that the estimation accuracy increases with the window size. It is

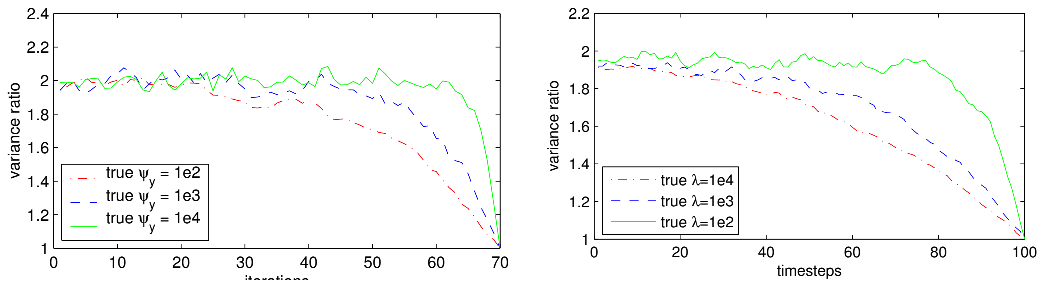

(a) Varying $\psi_y$ (b) Varying $\lambda$

Figure 3.17: Estimating the influence of past data

important to note however, that the gain in accuracy quickly saturates, after which the increase in estimation accuracy is negligible.

Can we obtain an estimate of the "correct" window size from the data itself? It turns out that we can at least obtain a valuable hint in this regard, from the precision estimates of $w_n$ after the filtering (the $\zeta_n$ values), and smoothing (the $\varphi_n$ values) steps. If we plot the ratio $\varphi_n/\zeta_n$, we note that at the final time step, the ratio must be 1 (since the filtered and smoothed distributions are identical for the final time step), but as we go further back in time, the ratio settles to a stable average value (figure 3.17). Note however that the number of time steps over which the ratio settles to this stable value reflects the time horizon over which successive values of $w_n$ have an influence over each other, and give us a clue as to the required window size $N$.

From figure 3.17(a) we see that given a fixed process drift rate, the time horizon should be larger when the value of $\psi_y$ is small (data is noisy), while higher $\psi_y$ (more precise data) allows more trustworthy recent data to take precedence over past estimates that are too far back in time. Similarly, figure 3.17(b) shows us that for a fixed noise level in the output, a higher value of $\lambda$ (slowly changing process) tends to stretch the window, while a lower value of $\lambda$ (rapidly changing process) tends to require a smaller window. Our evaluations of vkS in the previous section monitor this quantity to ensure an appropriately large window size.

Thus we essentially have a parameter-free algorithm that is able to automatically determine its own adaptation rate within a principled framework.

## 3.3 Bayesian Supersmoothing

Kernel-based methods have been highly popular in statistical learning, starting with Parzen windows, kernel regression, locally weighted regression, radial basis function networks, and more recently in formulations involving RKHS such as support vector machines, and Gaussian process regression. In general, most algorithms start out with kernel parameterizations that are the same for all kernels, independent of where in the data space the kernel is used, but later recognize the advantage of locally adaptive kernels, e.g. (Friedman 1984, Poggio & Girosi 1990, Schaal & Atkeson 1998, Paciorek & Schervish 2004). This progression of algorithms is motivated by a large class of learning problems in which the properties of learning data vary strongly throughout the data space, for instance, as in regression problems with different frequency characteristics in different parts of the work space, or, as phrased in Gaussian process regression, with non-stationary covariance functions. However, while optimization of the parameters of one globally shared kernel is already quite expensive for most algorithms — e.g., it constitutes the bulk of the computation in Gaussian process regression (Williams 1997) —

performing such optimization for every kernel individually becomes rather complex and prone to overfitting due to the flood of open parameters. It thus seems natural to seek a completely Bayesian treatment of local kernel adaptation, i.e., to integrate out complexity parameters, ideally with an EM-like algorithm such that gradient descent and sampling problems can be avoided.

For non-parametric locally weighted regression (Atkeson, Moore & Schaal 1997), we assume a training set $\mathbf{x}_{\mathcal{D}} = \{x_i, y_i\}_{i=1}^{N}$ drawn from a nonlinear function $y = f(x) + \epsilon$ contaminated by mean-zero noise $\epsilon$. We wish to approximate a locally linear model $\boldsymbol{\beta} = \begin{bmatrix} \beta_1 & \beta_0 \end{bmatrix}^T$ of this function, i.e., the slope and intercept of the tangent at a query point $x_q$, and subsequently make a prediction $y_q = \begin{bmatrix} x_q & 1 \end{bmatrix} \boldsymbol{\beta}$. For this purpose, we assume the existence of a spatially localized weighting kernel $w_i = k(x_i, x_q, h)$ that assigns a weight to every training point according to its Euclidean distance from the query point. The Gaussian RBF kernel $w_i = \exp\left(-0.5h\,(x_i - x_q)^2\right)$ is a popular choice, but as will be shown below, not always the most convenient formulation. The bandwidth $h$ of the kernel is a crucial parameter that determines the quality of fit of the locally linear model. If $h$ is too large, we may overfit the data, and if it is too small, we may oversmooth. In general, $h$ needs to be chosen as a function of the local curvature of $f(x)$ and the data density around the query point. If we can find a good bandwidth as a function of $x_q$, nonlinear function approximation can be solved accurately and efficiently. Our goal is to find a Bayesian formulation of determining $\boldsymbol{\beta}$ and $h$ simultaneously in an EM-like algorithm.

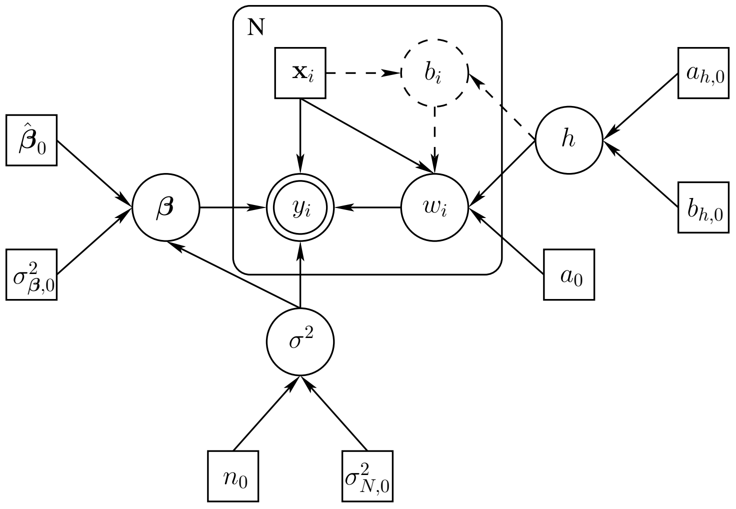

Figure 3.18: Graphical model for Bayesian supersmoothing. The dotted path indicates a dependency via the variable $b_i$, which strictly speaking does not introduce any additional stochasticity, but is a deterministic function of the random variable $h$ and the observed $\mathbf{x}_i$.

$$y_i|x_i, w_i, \boldsymbol{\beta}, \sigma^2 \sim \text{Normal}\left(y_i; \mathbf{x}_i^T\boldsymbol{\beta}, \frac{\sigma^2}{w_i}\right) \tag{3.17}$$

$$\boldsymbol{\beta}|\sigma^2 \sim \text{Normal}\left(\boldsymbol{\beta}; \boldsymbol{\beta}_0, \boldsymbol{\Sigma}_{\boldsymbol{\beta}}\sigma^2\right) \tag{3.18}$$

$$\sigma^2 \sim \text{Scaled-Inv}_{\chi^2}\left(\sigma^2; n_0, \sigma^2_{N,0}\right) \tag{3.19}$$

$$w_i|b_i \sim \text{Gamma}\left(w_i; a, b_i\right) \tag{3.20}$$

$$b_i = b_i(h, x_i, x_q) \qquad (b_i \text{ is a deterministic function}) \tag{3.21}$$

$$h \sim \text{Gamma}\left(h; a_h, b_h\right) \tag{3.22}$$

The distributions for $y_i$, $\boldsymbol{\beta}$ and $\sigma^2$ are standard for Bayesian weighted regression, which assumes heteroscedastic variance (Gelman et al. 1995). However, classic Bayesian weighted regression does not take into account how the weights are generated. For locally weighted regression, heteroscedastic variance is modeled as an effect of the weighting kernel, i.e., as growing noise variance proportional to the distance of a data point away from the query point. In order to obtain a probabilistic formulation, we introduce a conditional Gamma distribution over each weight:

$$\begin{aligned} p(w_i|h) &= \frac{\left[b_i\left(x_i, x_q, h\right)\right]^{a_0}}{\Gamma\left(a_0\right)} w_i^{a_0} \exp\left(-w_i b_i\left(x_i, x_q, h\right)\right) \\ b_i\left(x_i, x_q, h\right) &= \frac{1}{k\left(x_i, x_q, h\right)} \end{aligned}$$

which implies:

$$\begin{aligned} \langle w_i \rangle &= \frac{a_0}{b_i\left(x_i, x_q, h\right)} = a_0 k\left(x_i, x_q, h\right) \\ \mathrm{Var}\left(w_i\right) &= a_0 k\left(x_i, x_q, h\right)^2 \end{aligned} \tag{3.23}$$

There are some important observations concerning equation (3.23). The expectation of a weight is just the weighting kernel $k$ scaled by $a_0$. This scaling is harmless in weighted regression since a uniform scaling of all weights does not affect the estimation of the locally linear model. The variance of the weights however, is proportional to the squared value of the kernel $k$. Thus data points with a tiny weight will have an even tinier variance, while data points with larger weights will have more variance. This nonlinear dependence of the variance on the distance from the query point is quite useful: at a point very far away from the query point, the kernel value is close to zero, and we should rightfully be confident that this point is irrelevant to the local regression. However data that receive a significant activation of the kernel $k$ should be scrutinized carefully.

### 3.3.1 An EM-Like Learning Algorithm

In order to derive a learning algorithm for the graphical model of figure 3.18, we shall employ the factorial variational approximation discussed in chapter 2. The log joint distribution over the variables in the graphical model can be written as:

$$\begin{aligned}
\ln p(\mathbf{x}_{\mathcal{D}}, \mathbf{x}_{\mathcal{H}}; \boldsymbol{\phi}) = &-\frac{N}{2}\ln\sigma^2 + \sum_{i=1}^{N}\left[\frac{1}{2}\ln w_i - \frac{w_i}{2\sigma^2}\left(y_i - \boldsymbol{\beta}^T\mathbf{x}_i\right)^2\right] \\
&+ \sum_{i=1}^{N}\Big[a_0 \ln b_i\left(x_i, x_q, h\right) + (a_0 - 1)\ln w_i - w_i b_i\left(x_i, x_q, h\right)\Big] \\
&- \frac{1}{2}\ln|\boldsymbol{\Sigma}_{\boldsymbol{\beta},0}| - \frac{1}{2}\ln\sigma^2 - \frac{1}{2\sigma^2}\left(\boldsymbol{\beta} - \hat{\boldsymbol{\beta}}_0\right)^T\boldsymbol{\Sigma}_{\boldsymbol{\beta},0}^{-1}\left(\boldsymbol{\beta} - \hat{\boldsymbol{\beta}}_0\right) \\
&- \left(\frac{n_0}{2} + 1\right)\ln\sigma^2 - \frac{n\sigma_{N,0}^2}{2\sigma^2} + (a_{h,0} - 1)\ln h - b_{h,0}h + const_{\mathbf{x}_{\mathcal{D}},\mathbf{x}_{\mathcal{H}}}
\end{aligned}$$

Our factorial variational approximation for this model is of the form:

$$Q(\mathbf{x}_{\mathcal{H}}) = Q(\boldsymbol{\beta}, \sigma^2)Q(h)\prod_{i=1}^{N}Q(w_i) \tag{3.24}$$

Using the formula for the updates of the distributions under the factorial assumption in equation 2.6, we can derive the following updates for the distributions over the regression parameters:

$$\begin{aligned}
\boldsymbol{\Sigma}_{\boldsymbol{\beta}} &= \left(\sum_{i=1}^{N}\langle w_i\rangle\,\mathbf{x}_i\mathbf{x}_i^T + \boldsymbol{\Sigma}_{\boldsymbol{\beta},0}^{-1}\right)^{-1} \\
\hat{\boldsymbol{\beta}} &= \boldsymbol{\Sigma}_{\boldsymbol{\beta}}\left(\sum_{i=1}^{N}\langle w_i\rangle\,y_i\mathbf{x}_i + \boldsymbol{\Sigma}_{\boldsymbol{\beta},0}^{-1}\hat{\boldsymbol{\beta}}_0\right)
\end{aligned} \tag{3.25}$$

and the noise variance:

$$\sigma_N^2 = \frac{\sum_{i=1}^{N} \langle w_i \rangle \left( y_i - \hat{\boldsymbol{\beta}}^T \mathbf{x}_i \right)^2 + \left( \hat{\boldsymbol{\beta}} - \hat{\boldsymbol{\beta}}_0 \right)^T \boldsymbol{\Sigma}_{\boldsymbol{\beta},0}^{-1} \left( \hat{\boldsymbol{\beta}} - \hat{\boldsymbol{\beta}}_0 \right) + n_0 \sigma_{N,0}^2}{n_0 + N}$$
$$n = n_0 + N \tag{3.26}$$

Even more interesting is the posterior distribution over the weights $w_i$ which becomes:

$$\begin{aligned} a &= a_0 + \frac{1}{2} \\ b_i &= \frac{1}{2\sigma_N^2} \left( y_i - \hat{\boldsymbol{\beta}}^T \mathbf{x}_i \right)^2 + \frac{1}{2} \mathbf{x}_i{}^T \boldsymbol{\Sigma}_{\boldsymbol{\beta}} \mathbf{x}_i + \langle b_i \left( x_i, x_q, h \right) \rangle \\ \langle w_i \rangle &= \frac{a}{b_i} = \frac{a_0 + \frac{1}{2}}{\frac{1}{2\sigma_N^2} \left( y_i - \hat{\boldsymbol{\beta}}^T \mathbf{x}_i \right)^2 + \frac{1}{2} \mathbf{x}_i{}^T \boldsymbol{\Sigma}_{\boldsymbol{\beta}} \mathbf{x}_i + \langle b_i \left( x_i, x_q, h \right) \rangle} \end{aligned} \tag{3.27}$$

And finally, the log posterior of the bandwidth $h$ can be written as:

$$\ln Q(h) = a_0 \sum_{i=1}^{N} \ln b_i \left( x_i, x_q, h \right) - \sum_{i=1}^{N} \langle w_i \rangle \, b_i \left( x_i, x_q, h \right) + \left( a_{h,0} - 1 \right) \ln h - b_{h,0} h + const_h \tag{3.28}$$

As an obvious problem, equation (3.28) does not have a compatible form for a log-Gamma distribution in $h$ when using the general formulation $b_i = 1/k \left( x_i, x_q, h \right)$. We therefore have to investigate concrete formulations of weighting kernels. In particular we consider the following popular choices, (Atkeson et al. 1997):

$$k = \exp \left( -\frac{1}{2} h \left( x_i - x_q \right)^2 \right) \tag{3.29}$$

$$k = \left(1 + h\left(x_i - x_q\right)^p\right)^{-1} \tag{3.30}$$

$$k = \begin{cases} \left(1 - h\left(x_i - x_q\right)^2\right)^p & \text{if } h\left(x_i - x_q\right)^2 \leq 1 \\ 0 & \text{otherwise} \end{cases} \tag{3.31}$$

Where $p$ is a positive even integer. In order to be conjugate with the Gamma distribution in $h$, we can only accept terms in equation (3.28) that are linear or log-linear in $h$. None of the kernels in (3.29)–(3.31) fulfills this requirement. Indeed, only a kernel that is *linear* in $h$ would ever result in linear and log-linear terms. Unfortunately, such a kernel is ineffective for bandwidth adaptation in weighted regression, as the bandwidth would just act as a scale parameter on all weights. By inspecting equation (3.25) under the assumption of uninformative priors, it becomes apparent that such a scaling would have no effect on estimating the local linear model's regression parameters $\boldsymbol{\beta}$. Therefore, in order to find an analytical update for the posterior distribution of $h$, we will thus have to resort to further approximations. For our kernels in (3.29)–(3.31), the potentially problematic terms in equation (3.28) are respectively:

$$\sum_{i=1}^{N} \left[\frac{1}{2} a_0 h\left(x_i - x_q\right)^2 - \langle w_i \rangle \exp\left(\frac{1}{2}\left(x_i - x_q\right)^2\right)\right] \tag{3.32}$$

$$\sum_{i=1}^{N} \left[a_0 \ln\left(1 + h\left(x_i - x_q\right)^p\right) - \langle w_i \rangle \left(1 + h\left(x_i - x_q\right)^p\right)\right] \tag{3.33}$$

$$\sum_{i=1}^{N} \left[-a_0 p \ln\left(1 - h\left(x_i - x_q\right)^2\right) - \langle w_i \rangle \left(1 - h\left(x_i - x_q\right)^2\right)^{-p}\right] \tag{3.34}$$

While equation (3.34) has no linear or log-linear terms in $h$, both equations (3.32) and (3.33) seem more promising, as the terms involve only concave/convex nonlinearities, which can be easily approximated by a bound. However, equation (3.32) has a subtle additional problem: the sign on the first summand is positive, while in a log-Gamma distribution, the terms linear in $h$ should be negative. This could potentially lead to negative parameters in the posterior which are a result of the approximating process (which indeed occurs when realizing the algorithm with a Gaussian kernel). We therefore proceed with the kernel corresponding to equation (3.33), and with some foresight towards the final algorithm, we choose the following more general parameterization:

$$k(x_i, x_q, h) = \frac{1}{b_i\left(x_i, x_q, h\right)} \qquad \text{where} \qquad b_i = s\Big(1 + h\left(x_i - x_q\right)^p\Big) \tag{3.35}$$

Using the variational approach suggested by Jaakkola & Jordan (2000), we can bound the problematic first term in equation (3.33) as:

$$\ln\Big(1 + h\left(x_i - x_q\right)^p\Big) \geq \lambda_i \ln\Big(h\left(x_i - x_q\right)^p\Big) - \lambda_i \frac{\lambda_i}{1 - \lambda_i} + \ln\left(\frac{1}{1 - \lambda_i}\right)$$

where the $\lambda_i$ are the variables that parameterize a family of lower bounds, and which must be individually optimized to ensure a tight bound. With this approximation, equation (3.28) simplifies, and the following updates to the posterior distribution over $h$ can be derived:

$$\begin{aligned}
\ln Q(h) &= a_0 \sum_{i=1}^{N} \lambda_i \ln h - s \sum_{i=1}^{N} \langle w_i \rangle \, h \, (x_i - x_q)^p + (a_{h,0} - 1) \ln h - b_{h,0} h \\
a_h &= a_{h,0} + a_0 \sum_{i=1}^{N} \lambda_i \qquad (3.36) \\
b_h &= s \sum_{i=1}^{N} \langle w_i \rangle \, (x_i - x_q)^p + b_{h,0}
\end{aligned}$$

Finally, the variational parameters $\lambda_i$ need to be optimized. Fortunately, this optimization decomposes into decoupled optimizations for each $\lambda_i$ of the form:

$$\frac{\partial}{\partial \lambda_i} \left( \lambda_i \left\langle \ln h \, (x_i - x_q)^p \right\rangle - \lambda_i \ln \frac{\lambda_i}{1 - \lambda_i} + \ln \left( \frac{1}{1 - \lambda_i} \right) \right) = 0 \qquad (3.37)$$

for which the solution is:

$$\lambda_i = \frac{\varphi_i}{1 + \varphi_i} \qquad \text{where} \qquad \varphi_i = (x_i - x_q)^p \, \frac{1}{2} \psi \, (a_h) b_h$$

where $\psi(\cdot)$ is the digamma function. We can therefore write the final EM-like procedure as:

**E-Step:** Apply equations (3.25), (3.26), (3.27) and (3.36)

**M-Step:** Apply equation (3.37)

### 3.3.2 Bayesian Supersmoothing Evaluations

We evaluated Bayesian supersmoothing in several synthetic one-dimensional data sets. In all simulations, we chose the prior parameters to be:

$$a_{h,0} = 0.1, b_{h,0} = 1e-4, a_0 = 10, n_0 = 10, \sigma^2_{N,0} = 0.1, \hat{\boldsymbol{\beta}}_0 = \mathbf{0}, \boldsymbol{\Sigma}_{\boldsymbol{\beta},0} = 1e6\mathbf{I}$$

This choice of priors corresponds to a rather uninformative initial bias that $h = 1000$ and that we believe to have seen $n_0 = 10$ points with variance $\sigma^2_{N,0}$, prior to fitting our model. For the regression parameters we have a highly uninformative distribution (effectively no bias). The particular values selected for initialization were, on one hand, motivated by providing numerical stability to the algorithm even if there were no points falling within the range of the locally linear model, and on the other hand, by our desire to start out with a moderately small weighting kernel. For weighted regression, there is, in most cases, a local maximum for the algorithm when performing global linear regression, and it is this local maximum that we try to avoid in our algorithm.

A more important initialization is the scale $s$ of the weighting kernel in equation (3.35). On inspection of the posterior distribution over the weights in equation (3.27), one realizes that the weight update is influenced by three terms; the original kernel weight, the variance of the regression parameters, and the squared standardized residual error of a data point. The term with the variance of the regression parameters $\mathbf{x}_i{}^T\boldsymbol{\Sigma}_{\boldsymbol{\beta}}\mathbf{x}_i$ is inversely proportional to the number of data points contributing to the locally linear model (c.f. equation (3.25)), and drops quickly to zero for moderate amounts of data. Thus, the denominator of the posterior update of a data point's weight in equation (3.27) is primarily a tradeoff between the standardized error of the data point and its prior weight. If the standardized error were to dominate this update, our prior weighting would be ignored — empirically, we notice that this leads to overfitting. In contrast, if the standardized error residual were ignored, we will oversmooth. We choose $s = 0.01$ as a good tradeoff between residual error and prior kernel weight. Given that both the kernel weight and the standardized residual error are always in the same range of values, $s$ does not need to be adjusted or each data set and can be considered to be a one-time model design constant. In order to have lighter tails on the weighting kernel we choose $p = 4$ in equation (3.35).

We evaluated Bayesian supersmoothing on three different data sets (see figure 3.19) and compared it to locally weighted regression (LWR) with a globally optimized Gaussian weighting kernel using leave-one-out cross validation (Atkeson et al. 1997). The first data set is generated using the equation:

$$y(x) = x - \sin^3\left(2\pi x^3\right)\cos\left(2\pi x^3\right)\exp\left(x^4\right)$$

with additive i.i.d. noise of 0.1 standard deviation. This function has strongly different frequency components in different parts of the data space. As figure 3.19(a) shows, LWR overfits the data in low-frequency areas in order to accommodate the high-frequency region at the right of the plot. Bayesian supersmoothing correctly adjusts the bandwidth $h$ with the curvature of the function and does not display any overfitting or underfitting trends.

The very sparse data set in figure 3.19(b) was generated from an initial step function with a linear trail-off, and a suddenly noisy section of the function. Bayesian supersmoothing properly varies the bandwidth to account for the sudden changes in the function and the noisy regions. In comparison to LWR, it manages to chisel out the corners of the step function more accurately while properly smoothing out the noisy regions.

Figure 3.19(c) illustrates that the a high amount of noise in the classic Old Faithful data set (characterizing the eruption timing of the famous geyser in Yellowstone National Park), does not mislead Bayesian supersmoothing towards overfitting. The fitting results are comparable to LWR and the data fits published in (Hastie & Tibshirani 1990).

In general one can conclude that Bayesian supersmoothing adjusts the bandwidth in all examples over orders of magnitude in order to accommodate the data set at hand. The lower sub-plot of each example in figure 3.19 illustrates this local bandwidth adaptation as a function of location in the input space.

While we have focused on seemingly trivial one-dimensional function fitting, we believe that this is a crucial step towards multi-dimensional settings. As was demonstrated by D'Souza et al. (2004) with the Bayesian backfitting algorithm (a topic of chapter 4), it is possible to treat multivariate regression problems in a decomposable fashion by solving them as a succession of univariate regressions. It is straightforward to combine these two algorithms into a unified supervised learning framework.

It must be noted however, that our current realization of Bayesian supersmoothing requires further refinement. As an odd feature of Bayesian weighted regression (Gelman et al. 1995), equation (3.26) updates $\sigma_N^2$ by dividing by $n_0 + N$. Interestingly, this implies that even a data point which is very far away from the query point (and which therefore should have a very small weight) will have an effect of reducing our posterior variance at the query point. A variant of the formulation which enforces that $\sum_{i=1}^{N} w_i = N$ shows promise at countering this undesirable behavior.

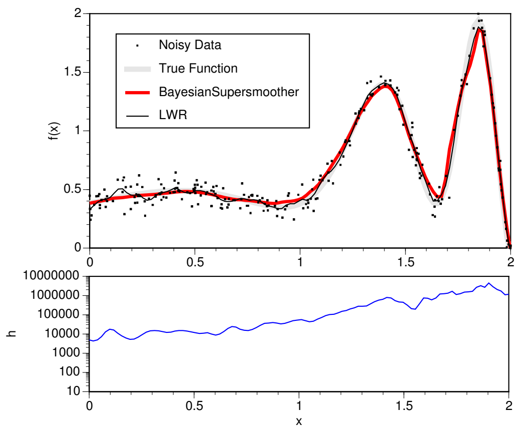

(a) Data with varying frequency properties

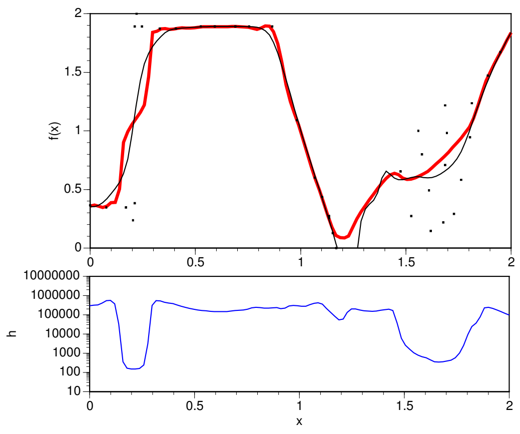

(b) Data with discontinuities

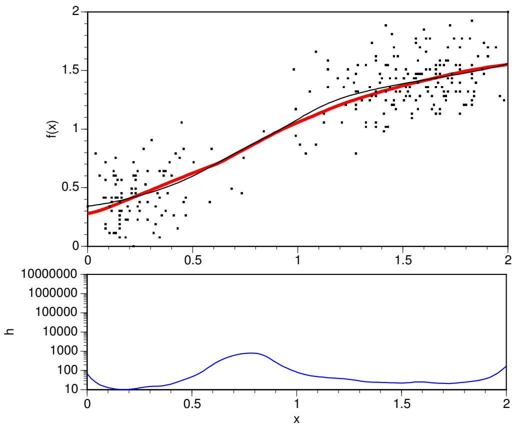

(c) “Old Faithful” data set

Figure 3.19: Each subplot shows the performance of Bayesian supersmoothing at appropriately estimating the kernel distance metric based upon which the desired function is predicted. The top graph in each subplot shows the prediction, while the bottom shows the kernel bandwidth parameter as a function of position in the input space.

# Chapter 4

# The Quest for Computational Tractability

Real-world data obtained, for instance, from neuroscience, chemometrics, data mining, or sensor-rich environments, is frequently extremely high-dimensional, severely underconstrained, and often interspersed with large amounts of irrelevant and/or redundant features. Combined with the inevitable measurement noise, efficient learning from such data still poses significant computational challenges to state-of-the-art supervised learning algorithms, even in linear settings. While traditional supervised learning techniques such as partial least squares (PLS) regression (Wold 1975), or backfitting (Hastie & Tibshirani 1990, Hastie & Tibshirani 2000) are often quite efficient and robust for these problems, they lack a probabilistic interpretation and cannot easily provide analytical measures of predictive distributions or the evidence of data as needed for model selection. On the other hand, while recent algorithms in supervised learning compute such information, they lack computational efficiency as, for instance, in Gaussian process regression or support vector learning.

This chapter presents algorithms that are specifically designed to perform Bayesian model selection when operating on high-dimensional data in underconstrained situations,

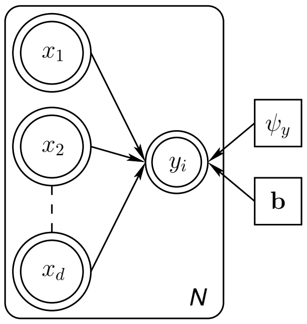

Figure 4.1: Graphical model for linear regression. Note the fan-in, which causes the estimates of the individual regression coefficients $b_m$ to become coupled in the posterior.

while maintaining the computational efficiency and robustness of more traditional statistical techniques. Section 4.1 reviews traditional regression techniques that are designed to operate on high-dimensional data. In particular, we review the well-known statistical regression technique of *backfitting*, and highlight its efficacy as a robust and efficient family of supervised learning algorithms. Section 4.2 also reviews some valuable methods for speeding up statistical computation by structuring data and partial statistics that make lookup extremely efficient. In section 4.3 we provide a novel probabilistic derivation of backfitting within the framework of the EM algorithm. This in turn allows us to generalize this algorithm within the Bayesian framework and perform sophisticated model selection through the paradigm of evidence maximization. Finally we show that the framework of *sparse Bayesian learning* (Tipping 2001) can be derived as a special case of Bayesian backfitting, and can benefit significantly from its robustness and scalability.

## 4.1 Computationally Tractable Linear Regression

We begin by examining the graphical model for linear regression as shown in figure 4.1, which corresponds to the following generative model:

$$y = \mathbf{b}^T \mathbf{x} + \epsilon \tag{4.1}$$

where, for successive samples from this model, we assume the $\epsilon$ are i.i.d. distributed as $\epsilon \sim \text{Normal}(\epsilon; 0, \psi_y)$. Given a data set of observed tuples $\mathbf{x}_{\mathcal{D}} = \{(\mathbf{x}_i, y_i)\}_{i=1}^N$ our goal is to estimate the optimal linear coefficients $\mathbf{b} = \begin{bmatrix} b_1 & b_2 & \dots & b_d \end{bmatrix}^T$ which combine the input dimensions to produce the output $y$.

It is easy to see that under our current noise model, the optimal estimate of the regression parameters (in a least-squares or maximum-likelihood sense) is given by:

$$\mathbf{b}_{\text{OLS}} = \left(\mathbf{X}^T \mathbf{X}\right)^{-1} \mathbf{X}^T \mathbf{y} \tag{4.2}$$

where $\mathbf{X}$ denotes a matrix whose rows contain the $\mathbf{x}_i$ and $\mathbf{y}$ is a column vector containing the corresponding $y_i$. Equation (4.2) is also known as the ordinary least squares (OLS) solution. From our discussion of inference in graphical models in chapter 2, we know that the cost of inference depends crucially on the structure of the model. In particular a fan-in of the type observed from $\mathbf{x}$ to $y$ in figure 4.1 couples all the regression coefficients in the posterior inference (as the moralization step in section 2.2.1 revealed) — a fact reflected in the need to evaluate the covariance matrix $\mathbf{X}^T\mathbf{X}$ in equation (4.2). With an increasing number of fan-in variables in the graphical model (or equivalently, an increasing input dimensionality $d$), evaluation of the solution in equation (4.2) becomes increasingly computationally expensive (approximately $O(d^3)$) and numerically brittle. While one can attempt to reduce the complexity by efficient matrix inversion techniques (Belsley, Kuh & Welsch 1980), solutions to this problem typically fall into one of two categories:

1. Those that try to find a low-dimensional, full-rank representation of the data which captures the salient information required to perform the regression.

2. Those that deal with the complete dimensionality, but structure computations as efficiently and robustly as possible (for example, by performing successive inexpensive univariate regressions).

Sections 4.1.1 and 4.1.2 discuss some of the more popular methods that are representative of these two classes.

### 4.1.1 Dimensionality Reduction for Regression

Often the information relevant to predicting the output $y$ can be localized to a low-dimensional manifold within the domain of $\mathbf{x}$. The methods discussed in this section rely on the assumption that by performing a dimensionality reduction on the input space, the resulting lower dimensional manifold captures sufficient information to accurately predict the output.

#### 4.1.1.1 Principal Component Regression

The underlying assumption of principal component regression (PCR) (Massey 1965) is that the low-dimensional subspace which explains the most variance in the $\mathbf{x}$ also captures the most essential information required to predict $y$. Starting with the empirical covariance matrix $\mathbf{\Sigma}_{\text{PCR}}$ of the input data:

$$\mathbf{\Sigma}_{\text{PCR}} = \frac{1}{N-1} \sum_{i=1}^{N} \mathbf{x}_i \mathbf{x}_i^T \tag{4.3}$$

we compute its eigen-decomposition:

$$\mathbf{\Sigma}_{\text{PCR}} \mathbf{v}_i = \lambda_i \mathbf{v}_i \tag{4.4}$$

where $\mathbf{v}_i$ is each eigenvector, and $\lambda_i$ the corresponding eigenvalue. By projecting the input $\mathbf{x}$ onto the principal $K$ eigenvectors (i.e., the eigenvectors with the largest eigenvalues) in the columns of the projection matrix $\mathbf{U} \equiv \begin{bmatrix} \mathbf{v}_1 & \mathbf{v}_2 & \ldots & \mathbf{v}_K \end{bmatrix}$, we can compute the regression solution as follows:

$$\mathbf{b}_{\text{PCR}} = \left(\mathbf{U}^T \mathbf{X}^T \mathbf{X} \mathbf{U}\right)^{-1} \mathbf{U}^T \mathbf{X}^T \mathbf{y} \tag{4.5}$$

Note that as a result of the projection onto the orthogonal eigenvectors $\mathbf{v}_1, \ldots, \mathbf{v}_K$, the matrix $\left(\mathbf{U}^T \mathbf{X}^T \mathbf{X} \mathbf{U}\right)$ in equation (4.5) is diagonal, and hence trivial to invert — the brunt of the computation having already been expended in the eigen-decomposition step. Hence PCR essentially reduces the multivariate regression to a set of independent univariate regressions along each of the orthogonal principal component directions.

A serious drawback of PCR is that is based purely on variance in the input data (Schaal, Vijayakumar & Atkeson 1998). The regression solution is therefore highly sensitive to common preprocessing operations such as *sphering*, which modify the perceived variance of each input dimension. Hence, low-variance input dimensions which are nevertheless important predictors of the output may be discarded in favor of high-variance, but irrelevant dimensions. If however, we operate on the joint space $\mathbf{z} = \begin{bmatrix} \mathbf{x}^T & y \end{bmatrix}^T$ of the data we can take the output into consideration when determining the appropriate lower-dimensional manifold.

#### 4.1.1.2 Joint-Space Factor Analysis for Regression

Factor analysis (FA) (Everitt 1984, Ghahramani & Hinton 1997) is a density estimation technique which assumes that the observed data $\mathbf{z}$ is generated from a lower dimensional process characterized by $K$ *latent* or *hidden* variables $\mathbf{v}$ as follows:

$$\mathbf{z}_i = \mathbf{W}\mathbf{v}_i + \boldsymbol{\epsilon}_i \qquad \text{where } 1 \leq i \leq N \tag{4.6}$$

If we assume that the latent variables are independently distributed as:

$$\mathbf{v}_i \sim \text{Normal}\left(\mathbf{v}_i; \mathbf{0}, \mathbf{I}\right)$$

$$\boldsymbol{\epsilon}_i \sim \text{Normal}\left(\boldsymbol{\epsilon}_i; \mathbf{0}, \boldsymbol{\Psi}\right)$$

then the factor loadings $\mathbf{W}$, and the diagonal noise variance matrix $\boldsymbol{\Psi}$ can be easily estimated using EM (Ghahramani & Hinton 1997), or Bayesian (Ghahramani & Beal 2000) techniques. In joint-space factor analysis for regression (JFR), we define:

$$\mathbf{z} \equiv \begin{bmatrix} \mathbf{x} \\ \\ y \end{bmatrix} \quad \text{and} \quad \mathbf{W} \equiv \begin{bmatrix} \mathbf{W}_{\mathbf{x}} \\ \\ \mathbf{W}_y \end{bmatrix} \quad \text{and} \quad \boldsymbol{\Psi} \equiv \begin{bmatrix} \boldsymbol{\Psi}_{\mathbf{x}} & \mathbf{0} \\ \\ \mathbf{0}^T & \psi_y \end{bmatrix} \tag{4.7}$$

Once we estimate $\mathbf{W}$ and $\boldsymbol{\Psi}$ for the joint data space of $\mathbf{z}$, we can condition $\mathbf{y}$ on $\mathbf{x}$, and marginalize out the latent variables $\mathbf{v}$ to obtain:

$$\langle y|\mathbf{x}\rangle = \underbrace{\mathbf{W}_y \left(\mathbf{I} + \mathbf{W}_{\mathbf{x}}^T \boldsymbol{\Psi}_{\mathbf{x}}^{-1} \mathbf{W}_{\mathbf{x}}\right)^{-1} \mathbf{W}_{\mathbf{x}}^T \boldsymbol{\Psi}_{\mathbf{x}}^{-1}}_{\mathbf{b}_{\text{JFR}}^T} \mathbf{x} \tag{4.8}$$

or equivalently:

$$\mathbf{b}_{\text{JFR}} = \boldsymbol{\Psi}_{\mathbf{x}}^{-1} \mathbf{W}_{\mathbf{x}} \left(\mathbf{I} + \mathbf{W}_{\mathbf{x}}^T \boldsymbol{\Psi}_{\mathbf{x}}^{-1} \mathbf{W}_{\mathbf{x}}\right)^{-1} \mathbf{W}_y^T \tag{4.9}$$

Note that the required matrix inversion of $\left(\mathbf{I} + \mathbf{W}_{\mathbf{x}}^T \boldsymbol{\Psi}_{\mathbf{x}}^{-1} \mathbf{W}_{\mathbf{x}}\right)$ is of the order of the *latent* dimensionality $K$, which makes this method computationally attractive for problems in which the underlying latent variable manifold is known to be relatively low dimensional (i.e. $K \ll d$).

#### 4.1.1.3 Joint-Space Principal Component Regression

Tipping & Bishop (1999) show the relationship between probabilistic versions of factor analysis and principal component analysis. In particular they show that Factor Analysis reduces to PCA under the assumption of isotropic output noise (i.e. $\mathbf{\Psi} = \sigma^2\mathbf{I}$). Importantly, they demonstrate that the maximum likelihood solution for $\mathbf{W}$ satisfies:

$$\mathbf{W} = \mathbf{U}(\mathbf{\Lambda} - \sigma^2\mathbf{I})^{1/2}\mathbf{R} \tag{4.10}$$

where (as before), $\mathbf{U}$ is a $d \times K$ matrix of principal eigenvectors, $\mathbf{\Lambda}$ is the diagonal matrix of corresponding eigenvalues, and $\mathbf{R}$ is an arbitrary rotation matrix. Given this result, we can simplify the regression solution for JFR in equation (4.8), and derive the following joint-space principal component regression (JPCR) solution:

$$\mathbf{b}_{\text{JPCR}} = \mathbf{U}_{\mathbf{x}} \left[ \mathbf{I} - \frac{\mathbf{U}_y^T\mathbf{U}_y}{\mathbf{U}_y\mathbf{U}_y^T - 1} \right] \mathbf{U}_y^T \tag{4.11}$$

Note that since $\mathbf{U}_y$ is a $1 \times K$ row vector, the matrix inversion in equation (4.11) reduces to a scalar division.

#### 4.1.1.4 Kernel Dimensionality Reduction for Regression

Recently, Fukumizu et al. (2004) have suggested the following method to achieve dimensionality reduction for regression. Assume that $\begin{bmatrix} \mathbf{U} & \mathbf{V} \end{bmatrix}$ is the $d$-dimensional orthogonal matrix, where $\mathbf{U}$ spans the subspace of $\mathbf{x}$ "relevant" to predicting $y$, and $\mathbf{V}$ spans the orthogonal "irrelevant" subspace.

If we define $\mathbf{x}_R = \mathbf{U}^T\mathbf{x}$ and $\mathbf{x}_{\setminus R} = \mathbf{V}^T\mathbf{x}$, then kernel dimensionality reduction seeks to find the subspace which minimizes $I(y|\mathbf{x}_R, \mathbf{x}_{\setminus R}|\mathbf{x}_R)$, where $I(x_1, x_2)$ denotes mutual information defined by:

$$I(x_1, x_2) = \int\int p(x_1, x_2) \log \frac{p(x_1, x_2)}{p(x_1)p(x_2)} dx_1 dx_2$$

This concept is extended to the more general case of reproducing kernel Hilbert spaces on the domains of $y$, $\mathbf{x}_R$, and $\mathbf{x}_{\setminus R}$ endowed with Gaussian kernels.

It should be stressed that as with the other methods described in this section, kernel dimensionality reduction requires that the latent dimensionality $K$ be a known quantity. In general however, unless explicit meta-level knowledge of the data can be brought to bear, the estimation of this quantity requires expensive cross-validation to avoid overfitting.

### 4.1.2 Efficient Decomposition Methods for Regression

Instead of seeking a low-dimensional version of the problem, the methods described in this section seek to structure the computation in such a way that the problem is decomposed into computationally efficient sub-problems. For example, by decomposing the multivariate regression problem into successive univariate regressions, one can create robust, iterative methods which do not suffer from the difficulties of matrix inversion for underconstrained data sets.

#### 4.1.2.1 Partial Least Squares Regression

```
1: Initialize: $\mathbf{X}_{\text{res}} = \mathbf{X}$, $\mathbf{y}_{\text{res}} = \mathbf{y}$
2: for $k = 1$ to $K$ do          //$K \leq d$ where $d$ is max. input dimensionality
3:     $\mathbf{v}_k \leftarrow \mathbf{X}_{\text{res}}^T \mathbf{y}_{\text{res}}$          //correlation direction
4:     $\mathbf{s}_k \leftarrow \mathbf{X}_{\text{res}} \mathbf{v}_k$          //project input
5:     $\beta_k \leftarrow \mathbf{s}_k^T \mathbf{y}_{\text{res}} / \left(\mathbf{s}_k^T \mathbf{s}_k\right)$          //univariate regression
6:     $\mathbf{y}_{\text{res}} \leftarrow \mathbf{y}_{\text{res}} - \beta_k \mathbf{s}_k$          //compute residual output
7:     $\mathbf{X}_{\text{res}} \leftarrow \mathbf{X}_{\text{res}} - \mathbf{s}_k \mathbf{p}_k^T$ where $\mathbf{p}_k \equiv \mathbf{X}_{\text{res}}^T \mathbf{s}_k / \left(\mathbf{s}_k^T \mathbf{s}_k\right)$          //compute residual input
8: end for
```

**Algorithm 3:** Partial Least Squares Regression

In section 4.1.1.1, we noted that PCR projected the input data onto a particular set of directions — the principal eigenvectors. This choice resulted in perfect decorrelation of the projected components, and hence the coefficients of optimal regression vector $\mathbf{b}_{\text{PCR}}$ fall out of inexpensive univariate regressions along each projection direction. Obtaining the eigenvectors however, is an $O(d^3)$ operation, and it is here that PCR must expend the bulk of its computation.

Partial least squares (PLS) regression (Wold 1975) is a technique which is extensively used in high-dimensional and severely underconstrained domains such as chemometrics (Frank & Friedman 1993). Rather than compute the covariance structure of the input space, as is done in PCR, PLS iteratively chooses its projection directions $\mathbf{v}_k$ (at the $k$th iteration) according to the direction of maximum *correlation* between the (current residual) input and the output. Computation of each projection direction is $O(d)$ in the dimensionality of the data, making PLS a highly efficient algorithm. As shown in algorithm 3, successive iterations create orthogonal projection directions by removing the component of the input data used in the last projection (c.f. steps 6 and 7). PLS requires no expensive matrix inversion or eigen-decomposition and thus is well suited to the very high-dimensional, yet severely underconstrained datasets in applications such as near infra-red (NIR) spectrometry (Frank & Friedman 1993) and humanoid robot control (Vijayakumar et al. 2000).

The number of projection directions found by PLS is only bound by the dimensionality of the data, with each univariate regression on successive projection components further serving to reduce the residual error. Using all $d$ projections is equivalent to performing OLS regression. Hence to avoid overfitting, the algorithm is typically stopped after $K$ projection components are found, where $K$ is determined empirically using cross-validation. It can be shown that if the distribution of the input data is spherical (i.e. has covariance structure $\sigma^2\mathbf{I}$), then PLS only requires a single projection to optimally reconstruct the output. Note that steps 6 and 7 of algorithm 3 choose the reduced input data $\mathbf{X}_{res}$ in such a way that the resulting data vectors have minimal norms, and thus push the distribution of $\mathbf{X}_{res}$ to become more spherical.

#### 4.1.2.2 Backfitting

```
1: Init: $\mathbf{X} = [\mathbf{x}_1 \dots \mathbf{x}_N]^T, \mathbf{y} = \left[y_1 \dots y_N\right]^T, g_{m,i} = g_m(\mathbf{x}_i;\theta_m), \mathbf{g}_m = [g_{m,1} \dots g_{m,N}]^T$
2: repeat
3:   for $m = 1$ to $d$ do
4:     $\mathbf{r}_m \leftarrow \mathbf{y} - \sum_{k \neq m} \mathbf{g}_k$          //compute partial residual (fake target)
5:     $\theta_m \leftarrow \arg\min_{\theta_m} \left(\mathbf{g}_m - \mathbf{r}_m\right)^2$          //optimize to fit partial residual
6:   end for
7: until convergence of $\boldsymbol{\theta}_m$
```

**Algorithm 4:** Backfitting

Backfitting (Hastie & Tibshirani 1990) is another very general framework for estimating additive models of the form $y(\mathbf{x}) = \sum_{m=1}^{d} g_m(\mathbf{x};\theta_m)$, where the functions $g_m$ are adjustable basis functions (e.g. splines), parameterized by $\theta_m$. As shown in algorithm 4, backfitting decomposes the statistical estimation problem into $d$ individual estimation problems by creating "fake supervised targets" for each function $g_m$. At the cost of an iterative procedure, this strategy effectively reduces the computational complexity of fan-ins, and allows easier numerical robustness control since no matrix inversion is involved.

For all its computational attractiveness, backfitting presents two serious drawbacks. Firstly, there is no guarantee that the iterative procedure outlined in algorithm 4 will converge as this is heavily dependent on the nature of the functions $g_m$. Secondly, the updates have no probabilistic interpretation, making backfitting difficult to insert into the current framework of statistical learning which emphasizes confidence measures, model selection, and predictive distributions. It should be mentioned that a Bayesian version of backfitting has been proposed in (Hastie & Tibshirani 2000). This algorithm however, relies on Gibbs sampling, which is more applicable when dealing with the non-parametric spline models discussed there, and is quite useful when one wishes to generate samples from the posterior additive model.

In practice, a large class of methods can be traced to have algorithmic underpinnings similar to those of backfitting. For example, in the case of linear regression ($\mathbf{X}^T\mathbf{X}\mathbf{b} = \mathbf{X}^T\mathbf{y}$), Gauss-Seidel/Jacobi updates are a natural specialization of the general backfitting algorithm:

$$b_m = \frac{\sum_{i=1}^{N} \overbrace{\left( y_i - \sum_{k \neq m}^{d} b_k x_{ik} \right)}^{\text{partial residual}} x_{ik}}{\sum_{i=1}^{N} x_{ik}^2} \tag{4.12}$$

where $\mathbf{x}_m = \begin{bmatrix} x_{1m} & \cdots & x_{Nm} \end{bmatrix}^T$, i.e. the vector of $m$th dimension entries, while $\mathbf{X}_{\bar{m}}$ denotes the data matrix with the $m$th dimension removed, and $\mathbf{b}_{\bar{m}}$ denotes the regression coefficient vector with the $m$th coefficient removed. The well-known cascade-correlation neural network architecture (Fahlman & Lebiere 1990) can also be seen to have similar algorithmic underpinnings; the addition of each new hidden unit can be considered to be the tuning of an additional basis function in the sequence, with the previous basis functions being locked to their previously tuned forms.

## 4.2 Data Structures for Fast Statistics

Significant computational gains can be achieved by using smarter data structures to organize the information required for statistical analysis. Examples of these include KD-trees and ball-trees (Friedman et al. 1977, Gray & Moore 2001, Omohundro 1991), which allow caching of sufficient statistics over recursively smaller regions of the data space, and AD-trees (Moore & Lee 1998, Komarek & Moore 2000) which speed up computations involving conjunctive queries and "counting" statistics.

KD-trees (Friedman et al. 1977) are data structures which partition the input space into hyper-rectangular regions. The root node contains the bounding box of the entire data set, and each non-leaf node has two children which partition the parents space by splitting the bounding box along its longest dimension (see figure 4.2). Splitting stops when the bounding boxes reach a certain minimum size, or when the number of points in a box reaches a minimum value. The key computational saving results from *annotating* each node of the tree with specific statistics about the data in the partition of space rooted at that node. For example, caching the bounding box of the data in each node

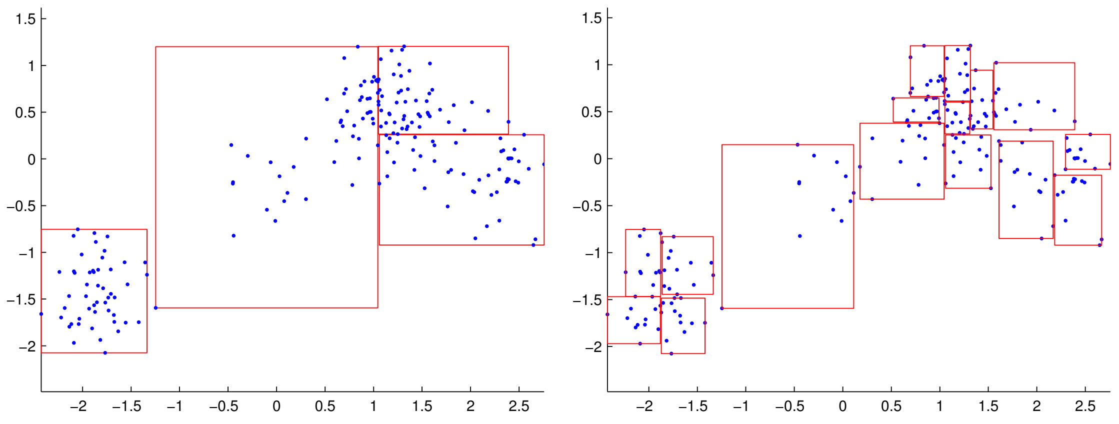

Figure 4.2: This figure shows the bounding boxes of the data stored at level 2 and level 4 nodes of a KD-tree. The tree is created by recursively splitting the hyper-rectangles along the median of longest dimension of the enclosed data. Bounding box information (as well as other statistics) are cached at each node and help speed up querying the structure.

allows eliminating a significant number of explicit comparisons when answering nearest-neighbor queries. In this way, for each query, only a fraction of the leaves in the tree are visited resulting in sub-linear computational complexity for most operations that typically require at least linear time.

A similar computational saving is achievable for kernel density estimation if we are willing to sacrifice a small amount of accuracy. Given the bounding boxes of the nodes in the KD-tree, we can bound the minimum and maximum value of the kernel function (assuming a monotonically decreasing function) within a hyper-rectangle. If the difference between the minimum and maximum is less than a tolerance value $\epsilon$, we can skip the evaluation of each query point within the node and approximate it by an average value. This achieves significant savings when the query points are the data points themselves, as

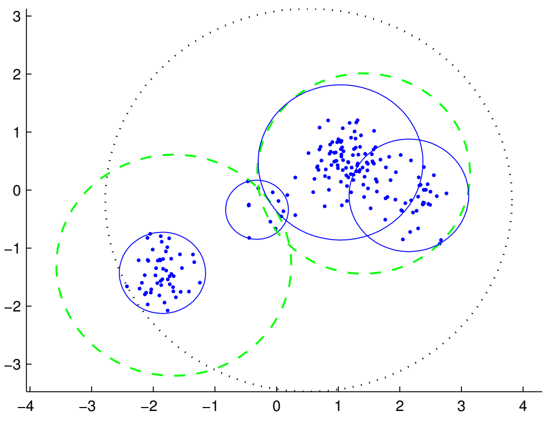

(a) Ball-tree

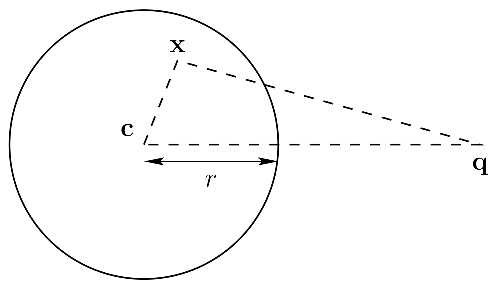

(b) Triangle inequality

Figure 4.3: The left figure shows the nodes at root, first and second levels of a ball tree (dotted, dashed and solid balls respectively). The right illustrates the triangle inequality used to derive computationally efficient bounds on the distance between an arbitrary query point and the points within a ball.

is frequently the case in settings where we evaluate the data on kernels that are centered at the data points; so-called $N$-body problems (Gray & Moore 2001).

KD-trees suffer in higher dimensional spaces since as the dimensionality increases, one observes that most of the volume is concentrated in a thin shell at the outer edges of the space. Metric-trees and ball-trees (Omohundro 1991) are an alternative that are robust to high-dimensional problems, and that do not necessarily require a Euclidean space, but merely one in which the triangle inequality holds (Moore 2000). This property allows us to derive simple yet computationally efficient bounds on the distances between a query point $\mathbf{q}$, and any point $\mathbf{x}$ belonging to a ball of radius $r$:

$$\|\mathbf{q}-\mathbf{x}\| \leq |\mathbf{q}-\mathbf{c}\| + r$$

$$\|\mathbf{q}-\mathbf{x}\| \geq |\mathbf{q}-\mathbf{c}\| - r$$

These distance bounds are then used in a manner similar to the bounding boxes of KD-trees to reduce the number of comparisons required to be performed with the actual data points.

AD-trees (Moore & Lee 1998) are an efficient representation for statistical methods which rely on "counting" occurrences of records satisfying sets of conjunctive queries over the record attributes. Traditional representation schemes for such data include precomputing answers to each query, which are stored in so-called *contingency tables.* This method is useful in creating probability tables for Bayes nets, and in conjunctive rule learning algorithms such as decision tree learning. Potential uses for statistical machine translation are obvious when we use the popular TF-IDF (term-frequency, inverse-document-frequency) representation of documents.

AD-trees allow the precomputed answers to queries which are available in contingency tables to be stored in a fraction of the memory requirements. For data sets in which records arrive incrementally or in which the initial cost of constructing the AD-tree is too high, an incremental version is also possible (Komarek & Moore 2000).

## 4.3 A Probabilistic Derivation of Backfitting

Consider the graphical model shown in figure 4.4(a). This model generalizes our discussion in section 4.1, such that the input "dimensions" of figure 4.1 are replaced by arbitrary

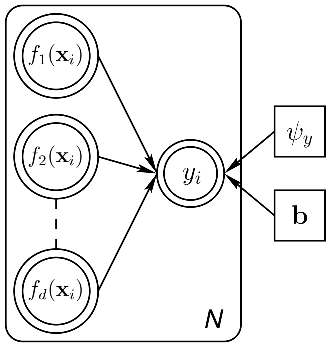

(a) Graphical model for Generalized Linear Regression.

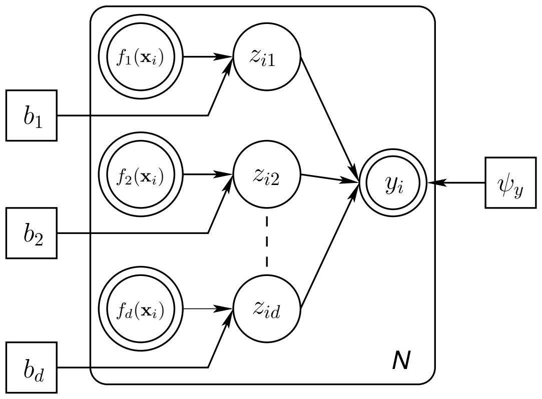

(b) Graphical model for Probabilistic Backfitting.

Figure 4.4: We modify the original graphical model for generalized linear regression by inserting hidden variables $z_{im}$ in each branch of the fan-in. This modified model can be solved using the EM framework to derive a probabilistic version of backfitting.

basis functions $f_m(\mathbf{x})$ of the input — a model commonly known as *generalized* linear regression (GLR) (Hastie & Tibshirani 1990). Our goal remains the same: given a data set $\mathbf{x}_{\mathcal{D}} = \{(\mathbf{x}_i, y_i)\}_{i=1}^{N}$, we wish to determine the most likely values of $b_m$ which linearly combine the basis functions $f_m$ to generate the output $y$.

We also noted in section 4.1.2.2, that the backfitting family of algorithms is an efficient set of methods which, under the right circumstances, is extremely robust since it requires no expensive matrix inversion, and thus avoids the numerical pitfalls therein. A drawback of the backfitting procedure is that it does not stem from a generative probabilistic model, which limits its application in current Bayesian machine learning frameworks. In this section we will describe how a probabilistic version of backfitting can be derived by making a simple structural modification to the graphical model for standard generalized linear regression. The statistical model corresponding to figure 4.4(a) can be written as follows:

$$y|\mathbf{x} \sim \text{Normal}\left(y; \sum_{m=1}^{d} b_m f_m\left(\mathbf{x}; \boldsymbol{\theta}_m\right), \psi_y\right)$$

i.e., multiple predictors $f_m(\mathbf{x}; \boldsymbol{\theta}_m)$ (where $1 \leq m \leq d$) that are generated by an adjustable non-linear transformation with parameters $\boldsymbol{\theta}_m$ and that are fed linearly to an output $y$ by an inner product with a regression vector $\mathbf{b} = \begin{bmatrix} b_1 & b_2 & \cdots & b_d \end{bmatrix}^T$ plus additive noise $\epsilon$. As we mentioned in section 4.1, estimating $\mathbf{b}$ is an $O(d^3)$ task. A simple modification of the graphical model of figure 4.4(a), however, enables us to create the desired algorithmic decoupling of the predictor functions, and gives backfitting a probabilistic interpretation. Consider the introduction of random variables $z_{im}$ as shown in figure 4.4(b). These variables are analogous to the output of the $g_m$ function of algorithm 4, and can also be interpreted as an unknown *fake target* for each branch of the regression fan-in. For the derivation of our algorithm, we assume the following conditional distributions for each variable in the model:

$$\begin{aligned} y_i|\mathbf{z}_i &\sim \text{Normal}\left(y_i; \mathbf{1}^T \mathbf{z}_i, \psi_y\right) \\ z_{im}|\mathbf{x}_i &\sim \text{Normal}\left(z_{im}; b_m f_m(\mathbf{x}_i), \psi_{zm}\right) \end{aligned} \tag{4.13}$$

where $\mathbf{1} = [1, 1, \ldots, 1]^T$. It needs to be emphasized that now, the regression coefficients $b_m$ are *behind* the fan-in. With this modification in place, we are essentially in a situation where we wish to optimize the parameters $\boldsymbol{\phi} = \left\{ \{b_m, \psi_{zm}\}_{m=1}^{d}, \psi_y \right\}$, given that we have observed variables $\mathbf{x}_{\mathcal{D}} = \{(\mathbf{x}_i, y_i)\}_{i=1}^{N}$ and that we have unobserved variables $\mathbf{x}_{\mathcal{H}} = \{\mathbf{z}_i\}_{i=1}^{N}$ in our graphical model. This situation fits very naturally into the framework of maximum-likelihood estimation via the EM algorithm discussed in section 2.2.2.

### 4.3.1 An EM Algorithm for Probabilistic Backfitting

Given our modified statistical model represented by the graphical model of figure 4.4(b), we wish to estimate the parameters $b_m$ and (possibly) optimize the individual functions $f_m(\mathbf{x}; \boldsymbol{\theta}_m)$ with respect to the parameters $\boldsymbol{\theta}_m$. This is easily formulated as an EM algorithm, which maximizes the *incomplete* log likelihood $\ln p(\mathbf{x}_{\mathcal{D}}; \boldsymbol{\phi})$ which, from figure 4.4(a), can be expressed as:

$$\ln p(\mathbf{x}_{\mathcal{D}}; \boldsymbol{\phi}) = \ln p(\mathbf{y}|\mathbf{X}; \mathbf{b}, \boldsymbol{\Psi}_{\mathbf{z}}, \psi_y) = -\frac{N}{2} \ln \psi_y - \frac{1}{2} \sum_{i=1}^{N} \left( y_i - \mathbf{b}^T \mathbf{f}(\mathbf{x}_i) \right)^2 + const \quad (4.14)$$

The EM algorithm however, operates by maximizing the expected *complete* log likelihood $\langle \ln p(\mathbf{x}_{\mathcal{D}}, \mathbf{x}_{\mathcal{H}}; \boldsymbol{\phi}) \rangle$, where:

$$
\begin{aligned}
\ln p(\mathbf{x}_{\mathcal{D}}, \mathbf{x}_{\mathcal{H}}; \boldsymbol{\phi}) &= \ln p(\mathbf{y}, \mathbf{Z}|\mathbf{X}; \mathbf{b}, \boldsymbol{\Psi}_{\mathbf{z}}, \psi_y) \\
&= -\frac{N}{2}\ln\psi_y - \frac{1}{2\psi_y}\sum_{i=1}^{N}\left(y_i - \mathbf{1}^T\mathbf{z}_i\right)^2 \\
&\quad - \sum_{m=1}^{d}\left[\frac{N}{2}\ln\psi_{zm} + \frac{1}{2\psi_{zm}}\sum_{i=1}^{N}\big(z_{im} - b_m f_m(\mathbf{x}_i; \boldsymbol{\theta}_m)\big)^2\right] + const
\end{aligned}
\tag{4.15}
$$

Using the procedure outlined in section 2.2.2, we can derive (see appendix B.4) the following EM update equations:

$$
\begin{aligned}
&\textbf{M-Step}: && \textbf{E-Step}: \\
b_m &= \frac{\sum_{i=1}^{N}\langle z_{im}\rangle f_m(\mathbf{x}_i)}{\sum_{i=1}^{N} f_m(\mathbf{x}_i)^2} & \mathbf{1}^T\boldsymbol{\Sigma}_{\mathbf{z}}\mathbf{1} &= \left(\sum_{m=1}^{d}\psi_{zm}\right)\left[1 - \frac{1}{s}\left(\sum_{m=1}^{d}\psi_{zm}\right)\right] \\
\psi_y &= \frac{1}{N}\sum_{i=1}^{N}\left(y_i - \mathbf{1}^T\langle\mathbf{z}_i\rangle\right)^2 + \mathbf{1}^T\boldsymbol{\Sigma}_{\mathbf{z}}\mathbf{1} & \sigma_{zm}^2 &= \psi_{zm}\left(1 - \frac{1}{s}\psi_{zm}\right) \\
\psi_{zm} &= \frac{1}{N}\sum_{i=1}^{N}\left(\langle z_{im}\rangle - b_m f_m(\mathbf{x}_i)\right)^2 + \sigma_{zm}^2 & \langle z_{im}\rangle &= b_m f_m(\mathbf{x}_i) + \frac{1}{s}\psi_{zm}\left(y_i - \mathbf{b}^T\mathbf{f}(\mathbf{x}_i)\right)
\end{aligned}
$$

where we define $s \equiv \psi_y + \sum_{m=1}^{d}\psi_{zm}$. In addition, the parameters $\boldsymbol{\theta}_m$ of each function $f_m$ can be updated by setting:

$$
\sum_{i=1}^{N}\Big(\langle z_{im}\rangle - b_m f_m\left(\mathbf{x}_i; \boldsymbol{\theta}_m\right)\Big)\frac{\partial f_m\left(\mathbf{x}_i; \boldsymbol{\theta}_m\right)}{\partial\boldsymbol{\theta}_m} = 0 \tag{4.16}
$$

and solving for $\boldsymbol{\theta}_m$. As this step depends on the particular choice of $f_m$, e.g., splines, kernel smoothers, parametric models, etc., we will not pursue it any further and just note that *any* statistical approximation mechanism could be used.

Two items in the above EM algorithm are of special interest. First, all equations in both the expectation and maximization steps are algorithmically $O(d)$ where $d$ is the number of predictor functions $f_m$. Second, if we substitute the expression for $\langle z_{im} \rangle$ in the maximization equation for $b_m$ we get the following update equation:

$$b_m^{(n+1)} = b_m^{(n)} + \frac{\psi_{zm}}{s} \frac{\sum_{i=1}^{N} \left( y_i - \sum_{k=1}^{d} b_k^{(n)} f_k(\mathbf{x}_i) \right) f_m(\mathbf{x}_i)}{\sum_{i=1}^{N} f_m(\mathbf{x}_i)^2} \tag{4.17}$$

Thus each EM cycle updates the $m$th regression coefficient by an amount proportional to the correlation between the $m$th predictor and the residual error. Hence the residual can be interpreted as forming a "fake target" for the $m$th branch of the fan-in. As the next section shows, this enables us to place this algorithm in the context of *backfitting*.

### 4.3.2 Relating Traditional and Probabilistic Backfitting

To understand equation (4.17) as probabilistic backfitting, we note that backfitting can be viewed as a formal Gauss-Seidel algorithm; an equivalence that becomes exact in the special case of linear models (Hastie & Tibshirani 1990). For the linear system $\mathbf{F}^T\mathbf{F}\mathbf{b} = \mathbf{F}^T\mathbf{y}$, the Gauss-Seidel updates for the individual $b_m$ are:

$$b_m = \frac{\sum_{i=1}^{N} \left( y_i - \sum_{k \neq m}^{d} b_k f_k(\mathbf{x}_i) \right) f_m(\mathbf{x}_i)}{\sum_{i=1}^{N} f_m(\mathbf{x}_i)^2} \tag{4.18}$$

Note that equation (4.18) — if used naively — only guarantees convergence for very specially structured matrices. An extension to the Gauss-Seidel algorithm adds a fraction $(1-\omega)$ of $b_m$ to the update and gives us the well-known *relaxation* algorithms:

$$b_m^{(n+1)} = (1-\omega)b_m^{(n)} + \omega \frac{\sum_{i=1}^{N}\left(y_i - \sum_{k\neq m}^{d} b_k f_k(\mathbf{x}_i)\right) f_m(\mathbf{x}_i)}{\sum_{i=1}^{N} f_m(\mathbf{x}_i)^2} \tag{4.19}$$

which has improved convergence rates for *over-relaxation* $(1 < \omega < 2)$, or improved stability for *under-relaxation* $(0 < \omega < 1)$. For $\omega = 1$, the standard Gauss-Seidel/backfitting of equation (4.18) is recovered. The appropriate value of $\omega$ which allows the iterations to converge, while still maintaining a reasonable convergence rate can only be determined by treating equation (4.18) as a discrete dynamical system, and analyzing the eigenvalues of its system matrix — an $O(d^3)$ task. If however, we set $\omega = \omega_m = \psi_{zm}/s$ in equation (4.19), it can be shown that (after some algebraic rearrangement,) we obtain exactly our EM update in equation (4.17), i.e., we indeed derive a probabilistic version of backfitting.

It should be mentioned that a similar EM algorithm and model structure has been proposed in the context of signal processing (Feder & Weinstein 1988), but we believe this is the first time that the connection of this probabilistic derivation to the backfitting algorithm has been demonstrated. As we will show in section 4.4, this allows us to place this class of methods within a much wider framework of Bayesian model complexity estimation.

### 4.3.3 Convergence of Probabilistic Backfitting

In general, for any maximum likelihood problem, the EM algorithm guarantees monotonic increase in the incomplete likelihood, but does not guarantee that the final solution is the global maximum. This section tries to answer the following questions:

1. What is the point of convergence of the probabilistic backfitting EM algorithm?
2. Are there local maxima (globally suboptimal solutions) in its likelihood space?

The answers to both questions depend on the fact that the incomplete likelihood (or marginalized complete likelihood) function for *linear* regression in equation (4.14) has a (possibly non-unique, but convex) global maximum corresponding to the OLS solution of equation 4.2, but no local maxima. Could the introduction of the hidden variables and additional parameters in equation (4.15) introduce *local* maxima in the likelihood landscape? Note that for examining convergence properties, we only focus on the estimation of the parameters $\boldsymbol{\phi} = [\mathbf{b}, \psi_{z1}, \ldots, \psi_{zd}, \psi_y]^T$, as the functions $f_m$ cannot be treated in general without knowing their structure. We start with the assumption that we have reached a stationary point $\boldsymbol{\phi}^*$ in the EM algorithm, which implies:

$$\left.\frac{\partial \left\langle \ln p(\mathbf{y}, \mathbf{Z}|\mathbf{X}; \boldsymbol{\phi})\right\rangle}{\partial \boldsymbol{\phi}}\right|_{\boldsymbol{\phi}=\boldsymbol{\phi}^*} = \mathbf{0} \tag{4.20}$$

Using Jensen's inequality, it is easy to show that for an arbitrary distribution $Q(\mathbf{Z})$ over the hidden variables:

$$\ln p(\mathbf{y}|\mathbf{X}; \boldsymbol{\phi}) \geq \left\langle \ln p(\mathbf{y}, \mathbf{Z}|\mathbf{X}; \boldsymbol{\phi})\right\rangle_{Q(\mathbf{Z})} + \mathcal{H}\left[Q(\mathbf{Z})\right] = \mathcal{F}(Q, \boldsymbol{\phi}) \tag{4.21}$$

where $\mathcal{H}[\cdot]$ denotes entropy. EM performs a coordinate ascent; alternately maximizing $\mathcal{F}$ w.r.t. $Q$ (in the E-step) and $\boldsymbol{\phi}$ (in the M-step). Differentiating $\mathcal{F}(Q, \boldsymbol{\phi})$ w.r.t. $\boldsymbol{\phi}$ at the stationary point $\boldsymbol{\phi}^*$, and noting that the entropy term $\mathcal{H}[Q(\mathbf{Z})]$ is independent of $\boldsymbol{\phi}$, gives:

$$\left.\frac{\partial \mathcal{F}(Q, \boldsymbol{\phi})}{\partial \boldsymbol{\phi}}\right|_{\boldsymbol{\phi}=\boldsymbol{\phi}^*} = \left.\frac{\partial \langle \ln p(\mathbf{y}, \mathbf{Z}|\mathbf{X}; \boldsymbol{\phi}) \rangle}{\partial \boldsymbol{\phi}}\right|_{\boldsymbol{\phi}=\boldsymbol{\phi}^*} = \mathbf{0} \tag{4.22}$$

Note however, that the preceding E-step sets $Q(\mathbf{Z})$ to the true posterior distribution $p(\mathbf{Z}|\mathbf{y}, \mathbf{X}; \boldsymbol{\phi}^*)$ which raises the lower bound in equation (4.21) to an equality — i.e. $\ln p(\mathbf{y}|\mathbf{X}; \boldsymbol{\phi}) = \mathcal{F}(Q, \boldsymbol{\phi})$ — from which it follows that:

$$\left.\frac{\partial \ln p(\mathbf{y}|\mathbf{X}; \boldsymbol{\phi})}{\partial \boldsymbol{\phi}}\right|_{\boldsymbol{\phi}=\boldsymbol{\phi}^*} = \left.\frac{\partial \mathcal{F}(Q, \boldsymbol{\phi})}{\partial \boldsymbol{\phi}}\right|_{\boldsymbol{\phi}=\boldsymbol{\phi}^*} = 0 \tag{4.23}$$

i.e. we have reached a maximum in the *incomplete* likelihood as well. Given that the *incomplete* log likelihood $\ln p(\mathbf{y}|\mathbf{X}; \boldsymbol{\phi})$ in equation (4.14) has *only* a global maximum (i.e., the OLS solution), reaching the stationary point of equation (4.20) in our EM algorithm for probabilistic backfitting must correspond to finding the OLS solution. Therefore, probabilistic backfitting is indeed performing true linear regression with a global optimum.

## 4.4 Bayesian Backfitting

Having a probabilistic interpretation of backfitting, allows us to use a Bayesian framework to regularize its OLS solution against overfitting. We achieve this by placing a prior

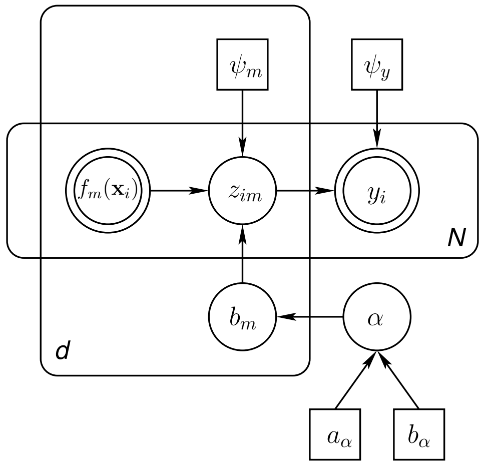

(a) Graphical model for backfitting with shrinkage prior

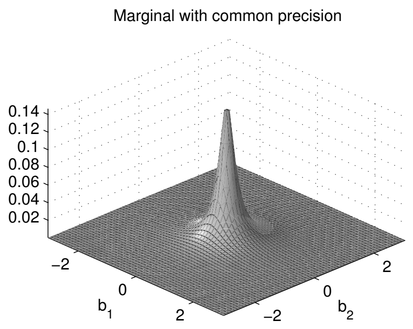

(b) Resulting marginal prior over $\mathbf{b}$

Figure 4.5: By associating a single Gamma distributed precision with the regression vector, we create a marginal prior over $\mathbf{b}$ that favors minimum-norm solutions, similar to shrinkage methods such as ridge regression.

distribution over the regression coefficients $\mathbf{b}$. As the following two sections demonstrate, our choice of prior structure results in two different, yet important forms of regularization.

### 4.4.1 Regularizing the Regression Vector Length

The graphical model for our first form of Bayesian prior is shown in figure 4.5(a). A Gaussian prior is placed over the regression coefficient vector $\mathbf{b}$ such that the variance of this prior is controlled by a single precision parameter $\alpha$. Our uncertainty in the value of this prior precision is in turn represented by a broad Gamma distribution over $\alpha$.

$$\begin{aligned} \mathbf{b}|\alpha &\sim \text{Normal}\left(\mathbf{b}; \mathbf{0}, \mathbf{I}/\alpha\right) \\ \alpha &\sim \text{Gamma}\left(\alpha; a_\alpha, b_\alpha\right) \end{aligned} \tag{4.24}$$

Our choice of Gamma prior is motivated by two reasons. Being a scale parameter, an uninformative distribution over $\alpha$ must be uniform over a *log* scale (corresponding to Jeffrey's prior) (Gelman et al. 1995, Jeffreys 1946), a requirement that is met by the appropriate choice of Gamma distribution parameters ($a_\alpha, b_\alpha \to 0$). Also, the Gamma distribution is analytically convenient, being a conjugate distribution for the Gaussian precision. As the graphical model in figure 4.5(a) shows, our set of unobserved random variables in the model is now $\mathbf{x}_\mathcal{H} = \left\{\mathbf{b}, \alpha, \{\mathbf{z}_i\}_{i=1}^N\right\}$, and we are especially interested in obtaining posterior distributions over the variables $\mathbf{b}$ and $\alpha$. The joint probability over this model extends that in equation (4.15) as follows:

$$\begin{aligned} \ln p(\mathbf{x}_\mathcal{D}, \mathbf{x}_\mathcal{H}; \boldsymbol{\phi}) &= \ln p(\mathbf{y}, \mathbf{Z}, \mathbf{b}, \alpha | \mathbf{X}; \boldsymbol{\Psi}_\mathbf{z}, \psi_y, a_\alpha, b_\alpha) \\ &= -\frac{N}{2}\ln\psi_y - \frac{1}{2\psi_y}\sum_{i=1}^N \left(y_i - \mathbf{1}^T\mathbf{z}_i\right)^2 \\ &\quad - \sum_{m=1}^d \left[\frac{N}{2}\ln\psi_{zm} + \frac{1}{2\psi_{zm}}\sum_{i=1}^N \left(z_{im} - b_m f_m(\mathbf{x}_i; \boldsymbol{\theta}_m)\right)^2\right] \\ &\quad + \frac{d}{2}\ln\alpha - \frac{\alpha}{2}\sum_{m=1}^d b_m^2 \\ &\quad + (a_\alpha - 1)\ln\alpha - b_\alpha\alpha + const_{\mathbf{x}_\mathcal{D}, \mathbf{x}_\mathcal{H}} \end{aligned} \tag{4.25}$$

While the log joint posterior $\ln p(\mathbf{x}_{\mathcal{H}}|\mathbf{x}_{\mathcal{D}};\boldsymbol{\phi})$ is readily available (up to a constant additive term) from (4.25), the extraction of marginal probabilities of interest such as $p(\mathbf{b}|\mathbf{x}_{\mathcal{D}};\boldsymbol{\phi})$ is analytically intractable. We therefore use a factorial variational approximation to the true posterior, in which we assume that the posterior distribution factorizes[1]over the variables of interest, i.e. we restrict ourselves to a family of distributions of the form $Q(\mathbf{Z},\mathbf{b},\alpha) = Q(\mathbf{Z})Q(\mathbf{b})Q(\alpha)$ (Ghahramani & Beal 2000, Parisi 1988, Rustagi 1976). We can again use the methodology developed in chapter 2 to derive (see appendix B.5.1) the following updates to the individual posterior distributions:

$$\begin{aligned}
Q(\alpha) &= \text{Gamma}\left(\alpha; \hat{a}_\alpha, \hat{b}_\alpha\right) \\
Q(\mathbf{b}) &= \prod_{m=1}^{d} \text{Normal}\left(b_m; \mu_{b_m}, \sigma^2_{b_m}\right) \\
\hat{a}_\alpha &= a_\alpha + \frac{d}{2} \\
\hat{b}_\alpha &= b_\alpha + \frac{\left\langle \mathbf{b}^T\mathbf{b} \right\rangle}{2} \\
\sigma^2_{b_m} &= \left( \frac{1}{\psi_{zm}} \sum_{i=1}^{N} f_m(\mathbf{x}_i)^2 + \langle \alpha \rangle \right) \\
\mu_{b_m} &= \sigma^2_{b_m} \left( \frac{1}{\psi_{zm}} \sum_{i=1}^{N} \langle z_{im} \rangle f_m(\mathbf{x}_i) \right)
\end{aligned}$$

The form of the $Q(\mathbf{Z})$ distribution updates remains identical to that derived in section 4.3.1 with the exception that the parameters $b_m$ are replaced with the expectations $\langle b_m \rangle$, so we shall not repeat them here. However, substituting the expressions for $\langle z_{im} \rangle$

[1]This particular factorization causes the marginal posterior of $\mathbf{b}$ to be a Gaussian. An alternative (also analytically tractable) formulation $Q(\mathbf{Z},\mathbf{b},\alpha) = Q(\mathbf{Z})Q(\mathbf{b},\alpha)$ is also possible in which the resulting marginal for $\mathbf{b}$ is a student-t distribution.

in the update equations for the distribution of $Q(\mathbf{b})$ gives us the following update for the regression coefficients:

$$\begin{aligned}\langle b_m \rangle^{(n+1)} = & \left( \frac{\sum_{i=1}^{N} f_m(\mathbf{x}_i)^2}{\sum_{i=1}^{N} f_m(\mathbf{x}_i)^2 + \psi_{zm} \langle \alpha \rangle} \right) \langle b_m \rangle^{(n)} \\ & + \frac{\psi_{zm}}{s} \frac{\sum_{i=1}^{N} \left( y_i - \sum_{k=1}^{d} \langle b_k \rangle^{(n)} f_k(\mathbf{x}_i) \right) f_m(\mathbf{x}_i)}{\left( \sum_{i=1}^{N} f_m(\mathbf{x}_i)^2 + \psi_{zm} \langle \alpha \rangle \right)} \end{aligned} \quad (4.26)$$

Comparing this solution with the result derived for probabilistic backfitting in equation (4.17), we see that in absence of correlation between the residual error, and the $k$-th predictor $f_k(\mathbf{x})$, the first term of equation (4.26) automatically decays the corresponding regression coefficient to zero. This is similar in effect to *shrinkage* methods such as ridge regression.

Note however, that the structure of the marginal prior over the regression coefficients $\mathbf{b}$ in figure 4.5(b) suggests that solutions closer to the origin are favored. In fact, sharing the common precision variable $\alpha$ across all the regression coefficients results in a regularized solution which minimizes the norm $\|\mathbf{b}\|^2$ of the entire regression vector, which is in fact identical to a ridge regression solution with a single ridge parameter. In our formulation however, the estimation of the "correct" value of the ridge parameter is implicitly inferred without the need for traditionally expensive cross-validation techniques.

This form of regularization is particularly useful when there are groups of inputs supplying redundant information (for robustness across sensors, for example), since the

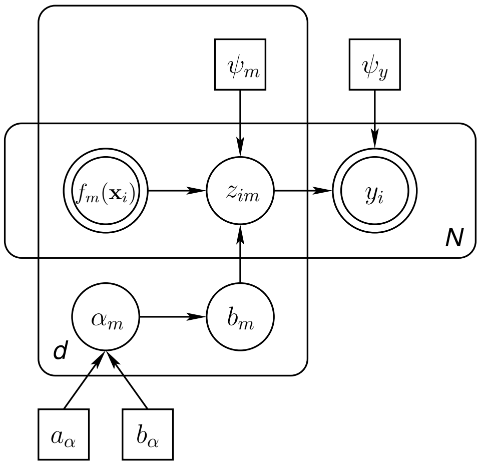

(a) Graphical model with ARD prior

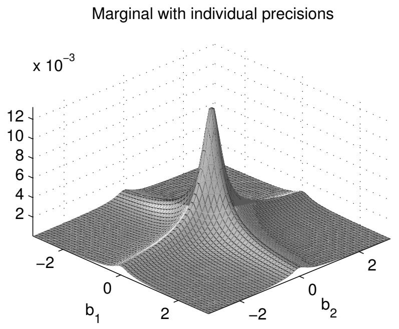

(b) Resulting marginal prior over **b**

Figure 4.6: By associating an individual Gamma distributed precision with each regression coefficient, we create a marginal prior over **b** that favors sparse solutions which lie along the (hyper)-spines of the distribution.

regression solution tends to distribute the responsibility for the output inference over all relevant input dimensions.

### 4.4.2 Regularizing the Number of Relevant Inputs

Modifying figure 4.5(a) slightly, we now place individual precision variables $\alpha_m$ over *each* of the regression parameters $b_m$, resulting in figure 4.6(a). This model structure can be captured by the following set of prior distributions:

$$\begin{aligned}\mathbf{b}|\boldsymbol{\alpha} &\sim \prod_{m=1}^{d} \text{Normal}\left(b_m; 0, 1/\alpha_m\right) \\ \boldsymbol{\alpha} &\sim \prod_{m=1}^{d} \text{Gamma}\left(\alpha; a_\alpha, b_\alpha\right)\end{aligned} \tag{4.27}$$

As the graphical model in figure 4.6(a) shows, our set of unobserved variables in the model is now $\mathbf{x}_{\mathcal{H}} = \left\{\mathbf{b}, \boldsymbol{\alpha}, \{\mathbf{z}_i\}_{i=1}^{N}\right\}$, and the modified likelihood function can be rewritten as follows:

$$\begin{aligned}
\ln p(\mathbf{x}_{\mathcal{D}}, \mathbf{x}_{\mathcal{H}}; \boldsymbol{\phi}) &= \ln p(\mathbf{y}, \mathbf{Z}, \mathbf{b}, \boldsymbol{\alpha} | \mathbf{X}; \boldsymbol{\Psi}_{\mathbf{z}}, \psi_y, a_\alpha, b_\alpha) \\
&= -\frac{N}{2} \ln \psi_y - \frac{1}{2\psi_y} \sum_{i=1}^{N} \left(y_i - \mathbf{1}^T \mathbf{z}_i\right)^2 \\
&\quad - \sum_{m=1}^{d} \left[ \frac{N}{2} \ln \psi_{zm} + \frac{1}{2\psi_{zm}} \sum_{i=1}^{N} \left(z_{im} - b_m f_m(\mathbf{x}_i; \boldsymbol{\theta}_m)\right)^2 \right] \\
&\quad + \sum_{m=1}^{d} \left[ \frac{d}{2} \ln \alpha_m - \frac{\alpha_m}{2} b_m^2 \right] \\
&\quad + \sum_{m=1}^{d} \left[ (a_\alpha - 1) \ln \alpha_m - b_\alpha \alpha_m \right] + const_{\mathbf{x}_{\mathcal{D}}, \mathbf{x}_{\mathcal{H}}}
\end{aligned} \tag{4.28}$$

Proceeding as before in section 4.4.1, we can derive the following iterative updates to the distributions of $Q(\mathbf{b})$ and $Q(\boldsymbol{\alpha})$:

$$\begin{aligned}
Q(\boldsymbol{\alpha}) &= \prod_{m=1}^{d} \text{Gamma}\left(\alpha_m; \hat{a}_\alpha, \hat{b}_\alpha^{(m)}\right) \\
Q(\mathbf{b}) &= \prod_{m=1}^{d} \text{Normal}\left(b_m; \mu_{b_m}, \sigma_{b_m}^2\right) \\
\hat{a}_\alpha &= a_\alpha + \frac{1}{2} \\
\hat{b}_\alpha^{(m)} &= b_\alpha + \frac{\left\langle b_m^2 \right\rangle}{2} \\
\sigma_{b_m}^2 &= \left( \frac{1}{\psi_{zm}} \sum_{i=1}^{N} f_m(\mathbf{x}_i)^2 + \langle \alpha_m \rangle \right)^{-1}
\end{aligned}$$

$$\mu_{b_m} = \sigma_{b_m}^2 \left( \frac{1}{\psi_{zm}} \sum_{i=1}^{N} \langle z_{im} \rangle f_m(\mathbf{x}_i) \right)$$

Deriving our update equation for the mean of the regression coefficients as we did in equation (4.26), we get:

$$\begin{aligned} \langle b_m \rangle^{(n+1)} = & \left( \frac{\sum_{i=1}^{N} f_m(\mathbf{x}_i)^2}{\sum_{i=1}^{N} f_m(\mathbf{x}_i)^2 + \psi_{zm} \langle \alpha_m \rangle} \right) \langle b_m \rangle^{(n)} \\ & + \frac{\psi_{zm}}{s} \frac{\sum_{i=1}^{N} \left( y_i - \sum_{k=1}^{d} \langle b_k \rangle^{(n)} f_k(\mathbf{x}_i) \right) f_m(\mathbf{x}_i)}{\left( \sum_{i=1}^{N} f_m(\mathbf{x}_i)^2 + \psi_{zm} \langle \alpha_m \rangle \right)} \end{aligned} \tag{4.29}$$

This solution is almost identical to that of equation (4.26), except that because of the individual precision variables, the regularization of the regression solution occurs over the magnitude of *each* regression coefficient, rather than the overall norm. This results in a regression solution that minimizes the *number* of relevant inputs required to accurately predict the output, much like the automatic relevance detection (ARD) framework in neural networks (Neal 1994). This is also intuitively apparent from the marginal prior over **b** shown in figure 4.6(b), which favors *sparse* solutions which lie along the (hyper-)spines of the distribution.

While the regularization discussed in the previous section is useful in situations where there exists *redundant* information, this form of regularization is desirable when the input contains information that is *irrelevant* to predicting the output.

Note that the graphical models of figures 4.5(a) and 4.6(a) are two extremes in a spectrum of regularization options. One can certainly conceive of models in which groups

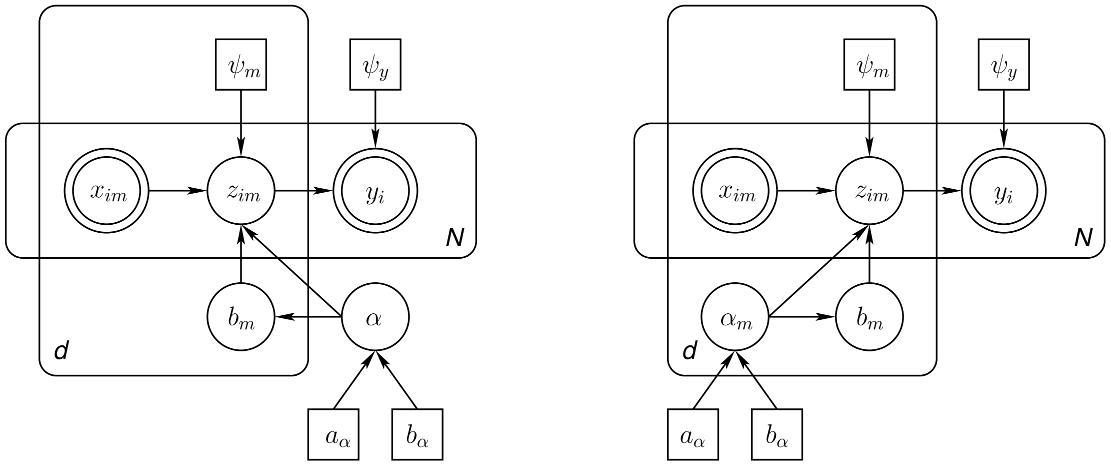

(a) Common prior (b) Individual priors

Figure 4.7: We can relax the assumption of factorization $Q(\mathbf{b})Q(\boldsymbol{\alpha})$ between the regression coefficients and their precision variables, by modifying the graphical models as shown in this figure. The marginal posterior distribution over the regression coefficients $\mathbf{b}$ can now be analytically derived as a Student t-distribution.

of regression coefficients are placed under the control of individual precision parameters. This situation may make sense, for example, when we have groups of redundant sensors providing input. It allows an irrelevant signal (set of sensors) to be eliminated if it does not contribute to the output, but at the same time, a relevant set exploits the redundancy of information within its group to provide a more robust input signal.

### 4.4.3 Alternative Posterior Factorization

In sections 4.4.1 and 4.4.2, we made the assumption that the posterior distribution factorized over the regression coefficients $b_m$ and their precisions $\alpha$ (or $\alpha_m$ in section 4.4.2). We can relax this assumption, if we make a small modification to the graphical model to retain analytical tractability. Figure 4.7(a) shows the alternative model corresponding to the one described in section 4.4.1, which can be described by the following conditional distributions:

$$\begin{aligned}
y_i|\mathbf{z}_i &\sim \text{Normal}\left(y_i; \mathbf{1}^T\mathbf{z}_i, \psi_y\right) \\
z_{im}|b_m, \alpha, x_{im} &\sim \text{Normal}\left(z_{im}; b_m x_{im}, \psi_{zm}/\alpha\right) \\
\mathbf{b}|\alpha &\sim \text{Normal}\left(\mathbf{b}; \mathbf{0}, \mathbf{I}/\alpha\right) \\
\alpha &\sim \text{Gamma}\left(\alpha; a_\alpha, b_\alpha\right)
\end{aligned} \tag{4.30}$$

The dependency of $z_{im}$ on the precision $\alpha$ may seem unnecessary, but Gelman et al. (1995) provide a justification: It is reasonable to assume that the variance in $z_{im}$ scales with the variance in $b_m$ since increasing our uncertainty in the prior value of $b_m$ should imply a corresponding increase in the uncertainty of $z_{im}$ as well. In this case, we will obtain a joint posterior distribution $Q(\mathbf{b}, \alpha)$ which is then marginalized to get the individual distributions $Q(\mathbf{b})$ and $Q(\alpha)$. The derivation (see appendix B.5.2) proceeds in a manner similar to that described in the previous sections. The crucial difference is that the marginal distribution over $\mathbf{b}$ is now a product of Student-t distributions instead of the Gaussian distributions of sections 4.4.1 and 4.4.2. The following equations summarize the marginal posteriors for the graphical model of figure 4.7(a):

$$\begin{aligned}
Q(\alpha) &= \text{Gamma}\left(\alpha; \hat{a}_\alpha, \hat{b}_\alpha\right) \\
Q(\mathbf{b}) &= \prod_{m=1}^{d} t_\nu\left(b_m; \mu_{b_m}, \sigma^2\right)
\end{aligned}$$

$$\begin{aligned}
\hat{a}_\alpha &= a_\alpha + \frac{Nd}{2} \\
\hat{b}_\alpha &= b_\alpha + \sum_{m=1}^{d} \frac{1}{2\psi_{zm}} \left[ \sum_{i=1}^{N} \left\langle z_{im}^2 \right\rangle - \left( \sum_{i=1}^{N} f_m(\mathbf{x}_i)^2 + \psi_{zm} \right)^{-1} \left( \sum_{i=1}^{N} \langle z_{im} \rangle f_m(\mathbf{x}_i) \right)^2 \right] \\
\nu &= 2\hat{a}_\alpha \\
\mu_{b_m} &= \left( \sum_{i=1}^{N} f_m(\mathbf{x}_i)^2 + \psi_{zm} \right)^{-1} \left( \sum_{i=1}^{N} \langle z_{im} \rangle f_m(\mathbf{x}_i) \right) \\
\sigma_{b_m}^2 &= \frac{\hat{b}_\alpha \psi_{zm}}{\hat{a}_\alpha} \left( \sum_{i=1}^{N} f_m(\mathbf{x}_i)^2 + \psi_{zm} \right)^{-1}
\end{aligned}$$

For the case of individual precision variables $\alpha_m$ shown in figure 4.7(b), we have the following updates:

$$\begin{aligned}
Q(\boldsymbol{\alpha}) &= \prod_{m=1}^{d} \text{Gamma}\left( \alpha_m; \hat{a}_\alpha, \hat{b}_\alpha^{(m)} \right) \\
Q(\mathbf{b}) &= \prod_{m=1}^{d} t_\nu \left( b_m; \mu_{b_m}, \sigma^2 \right) \\
\hat{a}_\alpha &= a_\alpha + \frac{N}{2} \\
\hat{b}_\alpha^{(m)} &= b_\alpha + \frac{1}{2\psi_{zm}} \left[ \sum_{i=1}^{N} \left\langle z_{im}^2 \right\rangle - \left( \sum_{i=1}^{N} f_m(\mathbf{x}_i)^2 + \psi_{zm} \right)^{-1} \left( \sum_{i=1}^{N} \langle z_{im} \rangle f_m(\mathbf{x}_i) \right)^2 \right] \\
\nu &= 2\hat{a}_\alpha \\
\mu_{b_m} &= \left( \sum_{i=1}^{N} f_m(\mathbf{x}_i)^2 + \psi_{zm} \right)^{-1} \left( \sum_{i=1}^{N} \langle z_{im} \rangle f_m(\mathbf{x}_i) \right) \\
\sigma_{b_m}^2 &= \frac{\hat{b}_\alpha^{(m)} \psi_{zm}}{\hat{a}_\alpha} \left( \sum_{i=1}^{N} f_m(\mathbf{x}_i)^2 + \psi_{zm} \right)^{-1}
\end{aligned}$$

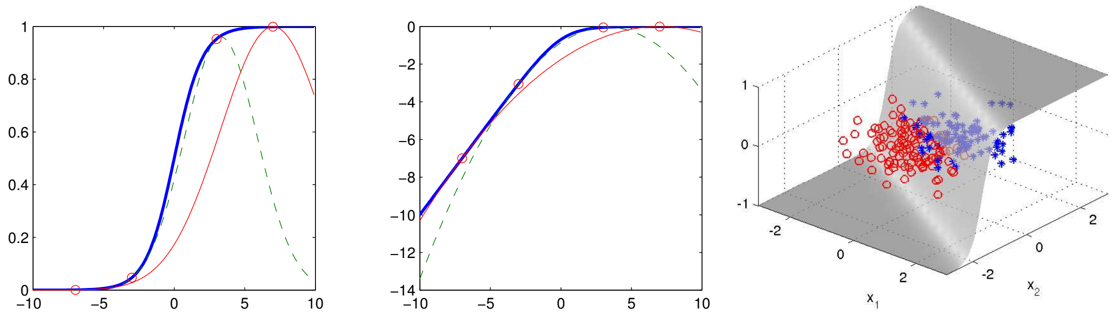

Figure 4.8: The left panel shows the logistic function (solid thick line), and two approximations with the variational parameters set to $\xi = 3$ (dashed line), and $\xi = 7$ (solid thin line). The points of tangency between the true function and the approximation are circled. The center panel shows the same plots on a log scale, while the right panel shows the classification solution to a toy problem.

This approximation can be used in conjunction with a distribution over the noise parameter $\psi_y$ to derive a form of robust regression which is less sensitive to outliers than our original formulation, in which the predictive distribution over the output is a Gaussian.

### 4.4.4 Extension to Classification

The probabilistic backfitting EM algorithm that was developed in section 4.3.1 can be adapted to handle categorical outputs $y_i \in \{-1, +1\}$ by simply changing the target conditional distribution $p(y_i|\mathbf{z}_i)$ in equation (4.13) to a Bernoulli distribution via the *sigmoid link* function $g(x) = \big(1 + \exp(-x)\big)^{-1}$. In this case, the conditional distribution can be expressed as:

$$p(y_i|\mathbf{z}_i) = \frac{1}{1 + \exp\left(-y_i \mathbf{1}^T \mathbf{z}_i\right)} = g(y_i \mathbf{1}^T \mathbf{z}_i)$$

Since this renders the posterior intractable due to non-conjugacy with $p(\mathbf{z}_i|\mathbf{x}_i)$, we follow (Jaakkola & Jordan 2000) and introduce an additional lower bound using the inequality:

$$g(x) \geq g(\xi) \exp\left\{\frac{x-\xi}{2} - \varphi(\xi)\left(x^2 - \xi^2\right)\right\}$$

where $\varphi(\xi) = \tan(\xi/2)/4\xi$, and $\xi$ is the variational parameter for the family of lower bounds to $g(x)$ (see figure 4.8). Hence we can lower bound the likelihood $p(y_i|\mathbf{z}_i)$ by the parameterized version $p(y_i|\mathbf{z}_i, \xi_i)$ as follows:

$$\begin{aligned} p(y_i|\mathbf{z}_i) &= g(y_i\mathbf{1}^T\mathbf{z}_i) \\ &\geq p(y_i|\mathbf{z}_i;\xi_i) \\ &= g(\xi_i)\exp\left\{\frac{y_i\mathbf{1}^T\mathbf{z}_i - \xi_i}{2} - \varphi(\xi_i)\left(\mathbf{z}_i^T\mathbf{1}\mathbf{1}^T\mathbf{z}_i - \xi_i^2\right)\right\} \end{aligned} \tag{4.31}$$

Note that this form still is an exponent of a quadratic in $\mathbf{z}_i$ which retains conjugacy with $p(\mathbf{z}_i|\mathbf{b};\mathbf{x}_i)$, and allows us to proceed with our EM derivation as before, with the additional step that we must optimize the $\xi_i$ parameters. We again start by writing out the log *complete* likelihood, which is the joint distribution over the known and unknown variables $\mathbf{x}_{\mathcal{D}}$ and $\mathbf{x}_{\mathcal{H}}$ in the model:

$$\begin{aligned}\ln p(\mathbf{x}_{\mathcal{D}}, \mathbf{x}_{\mathcal{H}}; \boldsymbol{\phi}) &= \sum_{i=1}^{N} \ln p(y|\mathbf{z}_i) + \sum_{i=1}^{N}\sum_{m=1}^{d} \ln p(z_{im}|\mathbf{x}_i; b_m, \psi_{zm}) \\ &\geq \sum_{i=1}^{N} \ln p(y|\mathbf{z}_i; \xi_i) + \sum_{i=1}^{N}\sum_{m=1}^{d} \ln p(z_{im}|\mathbf{x}_i; b_m, \psi_{zm}) \\ &= \sum_{i=1}^{N} \left[\ln g(\xi_i) + \frac{y_i \mathbf{1}^T \langle \mathbf{z}_i \rangle - \xi_i}{2} - \varphi(\xi_i)\left(\mathbf{1}^T \left\langle \mathbf{z}_i \mathbf{z}_i^T \right\rangle \mathbf{1} - \xi_i^2\right)\right] \\ &\quad - \sum_{m=1}^{d}\left[\frac{N}{2}\ln \psi_{zm} + \frac{1}{2\psi_{zm}} \sum_{i=1}^{N} \left(z_{im} - b_m f_m(\mathbf{x}_i; \boldsymbol{\theta}_m)\right)^2\right] + const\end{aligned} \tag{4.32}$$

As it turns out, the additional approximation only affects the E-step equations which are summarized as follows:

**E-Step** :

$$\begin{aligned}\mathbf{1}^T \boldsymbol{\Sigma}_{\mathbf{z}_i} \mathbf{1} &= \left(\sum_{m=1}^{d} \psi_{zm}\right)\left[1 - \frac{2\varphi(\xi_i)}{s_i}\left(\sum_{m=1}^{d} \psi_{zm}\right)\right] \\ \sigma_{zim}^2 &= \psi_{zm}\left(1 - \frac{2\varphi(\xi_i)}{s_i}\psi_{zm}\right) \\ \langle z_{im} \rangle &= b_m f_m(\mathbf{x}_i) + \frac{\psi_{zm}}{s_i}\left(\frac{y_i}{2} - 2\varphi(\xi_i)\sum_{m=1}^{d} b_m f_m(\mathbf{x}_i)\right)\end{aligned}$$

where $s_i = 1 + 2\varphi(\xi_i)\mathbf{1}^T \boldsymbol{\Psi}_{\mathbf{z}} \mathbf{1}$. The estimation of each $\xi_i$ can be done by differentiating the expected log likelihood w.r.t. each $\xi_i$:

$$\frac{\partial}{\partial \xi_i} \langle \ln p(\mathbf{y}, \boldsymbol{\theta}|\mathbf{X}) \rangle = \frac{\partial}{\partial \xi_i}\left[\ln g(\xi_i) + \frac{y_i \mathbf{1}^T \langle \mathbf{z}_i \rangle - \xi_i}{2} - \varphi(\xi_i)\left(\mathbf{1}^T \left\langle \mathbf{z}_i \mathbf{z}_i^T \right\rangle \mathbf{1} - \xi_i^2\right) + const_{\xi_i}\right]$$

$$= \underbrace{1 - g(\xi_i) - \frac{1}{2} + 2\xi_i \varphi(\xi_i)}_{=0} - \frac{\partial \varphi(\xi_i)}{\partial \xi_i} \left( \mathbf{1}^T \left\langle \mathbf{z}_i \mathbf{z}_i^T \right\rangle \mathbf{1} - \xi_i^2 \right)$$

Hence the likelihood is maximized by solving the following:

$$\frac{\partial \varphi(\xi_i)}{\partial \xi_i} \left( \mathbf{1}^T \left\langle \mathbf{z}_i \mathbf{z}_i^T \right\rangle \mathbf{1} - \xi_i^2 \right) = 0$$

which has solutions at $\partial\varphi(\xi_i)/\partial\xi_i = 0$ and at $\xi_i^2 = \mathbf{1}^T \left\langle \mathbf{z}_i \mathbf{z}_i^T \right\rangle \mathbf{1}$. One can show that the solution $\partial\varphi(\xi_i)/\partial\xi_i = 0$ occurs for the value $\xi_i = 0$, and actually corresponds to a *minimum* rather than a maximum of the expected log likelihood. Hence we have the admissible solutions for $\xi_i$ being:

$$\xi_i = \pm\sqrt{\mathbf{1}^T \left\langle \mathbf{z}_i \mathbf{z}_i^T \right\rangle \mathbf{1}}$$

The sign of $\xi_i$ can be chosen arbitrarily, since the likelihood is an even function of $\xi_i$, i.e. both solutions result in the likelihood taking the same maximal value (c.f. figure 4.8). Importantly, the $O(d)$ complexity of all update equations is preserved even in the extension to categorical output data, making backfitting for classification an equally robust and efficient tool as its regression counterpart.

#### 4.4.4.1 Bayesian Backfitting for Classification

Given that the functional approximation of equation (4.31) allows us to retain the conjugacy necessary for an analytical treatment, the Bayesian extensions of section 4.4 are straightforward to apply to our classification model. For the case in which we have a common shared precision parameter $\alpha$ across all regression parameters (c.f. section 4.4.1), the $b_m$ variables still have a posterior Gaussian with the mean update as follows:

$$\langle b_m \rangle^{(n+1)} = \left( \frac{\sum_{i=1}^N f_m(\mathbf{x}_i)^2}{\sum_{i=1}^N f_m(\mathbf{x}_i)^2 + \psi_{zm} \langle \alpha \rangle} \right) \langle b_m \rangle^{(n)} + \frac{\psi_{zm} \sum_{i=1}^N \frac{1}{s_i} \left( \frac{y_i}{2} - 2\varphi(\xi_i) \langle \mathbf{b} \rangle^{(n)^T} \mathbf{f}(\mathbf{x}_i) \right) f_m(\mathbf{x}_i)}{\left( \sum_{i=1}^N f_m(\mathbf{x}_i)^2 + \psi_{zm} \langle \alpha \rangle \right)}$$

For the case in which we have an individual precision parameter $\alpha_m$ over each regression parameter (c.f. section 4.4.2), the $b_m$ variables again have a posterior Gaussian with the mean update as follows:

$$\langle b_m \rangle^{(n+1)} = \left( \frac{\sum_{i=1}^N f_m(\mathbf{x}_i)^2}{\sum_{i=1}^N f_m(\mathbf{x}_i)^2 + \psi_{zm} \langle \alpha_m \rangle} \right) \langle b_m \rangle^{(n)} + \frac{\psi_{zm} \sum_{i=1}^N \frac{1}{s_i} \left( \frac{y_i}{2} - 2\varphi(\xi_i) \langle \mathbf{b} \rangle^{(n)^T} \mathbf{f}(\mathbf{x}_i) \right) f_m(\mathbf{x}_i)}{\left( \sum_{i=1}^N f_m(\mathbf{x}_i)^2 + \psi_{zm} \langle \alpha_m \rangle \right)}$$

### 4.4.5 Efficient Sparse Bayesian Learning and RVMs

The relevance vector machine was introduced by Tipping (2000) as an alternative to the popular support vector regression (SVR) method. The RVM operates in a framework similar to generalized linear regression, but uses the following generative model:

$$y(\mathbf{x}; \mathbf{b}) = \sum_{i=1}^N b_i k(\mathbf{x}, \mathbf{x}_i) + \epsilon \tag{4.33}$$

where $k(\mathbf{x}, \mathbf{x}_i)$ is a bivariate *kernel* function centered on each of the $N$ training data points $\mathbf{x}_i$, and $\mathbf{b} = \begin{bmatrix} b_1 & \dots & b_N \end{bmatrix}^T$ is a vector of regression coefficients. As in support vector regression (SVR) (Schölkopf & Smola 2000), the goal of the RVM is to accurately predict the target function, while retaining as few basis functions as possible in the linear combination. This is achieved through the framework of *sparse Bayesian learning* and the introduction of prior distributions over the precisions $\alpha_i$ of each element of $\mathbf{b}$:

$$p(\mathbf{b}, \boldsymbol{\alpha}) = \prod_{i=1}^{N} \text{Normal}\left(b_i; 0, \alpha_i^{-1}\right) \text{Gamma}\left(\alpha_i; a_\alpha, b_\alpha\right) \tag{4.34}$$

This prior structure is identical to that used in section 4.4.2, and allows us to cast the framework of sparse Bayesian learning in terms of Bayesian backfitting. Until now, we have chosen not to comment on the nature of the basis functions $f_m(\mathbf{x})$ in our model. Let us now switch to the RVM framework in which we create $N$ basis functions by centering a bivariate kernel function $k(\mathbf{x}, \mathbf{x}')$ on each individual data point. This implies:

$$f_m(\cdot) = k(\cdot, \mathbf{x}_m) \text{ for } 1 \leq m \leq d$$

and where we now have $d = N$. Notice that this transformation makes the RVM model exactly equivalent to the backfitting model of figure 4.6(a), with the notable difference that backfitting allows a significant advantage over the standard RVM in computational complexity. Note however, that while the computational complexity of a backfitting update is linear in the dimensionality of the problem, it is also linear in the number of data points i.e. $O(Nd)$. When cast into the RVM framework, setting $d = N$ makes this complexity $O(N^2)$. In particular we would like to stress the following:

- At *each* update of the $\alpha_m$ hyperparameters, the RVM requires an $O(N^3)$ Cholesky decomposition to re-estimate the regression parameters, while discarding the estimate at the previous iteration. In the backfitting-RVM however, the existing estimate of the regression parameters provides a good starting estimate, allowing the update to complete in just a handful of $O(N^2)$ iterations ($\sim$ 10 iterations were sufficient in our simulations). The saving in computation is especially evident when the number of data points (and hence the effective dimensionality) is large, and in situations where the hyperparameters require many updates before convergence.

- In the initial computations within the graphical model, it seems wasteful to spend large amounts of computation on estimating parameters accurately, when surrounding parameters (and hyperparameters) have not converged. One can structure the backfitting updates to work with partially converged estimates, such that the brunt of computation is only expended to accurately estimate a variable when one is more confident about the variables in its Markov blanket.

Figure 4.9 shows backfitting-RVM used to fit a toy data set generated using the 1-dimensional sinc function $\sin(x)/x$, as well as the popular "Banana" classification dataset (Rätsch, Onoda & Müller 2001) using the Gaussian kernel:

$$k(x_i, x_j) = \exp\left\{-\lambda\left(x_i - x_j\right)^2\right\}$$

for $\lambda > 0$. Even though backfitting-RVM is an order of magnitude faster than the standard RVM, it suffers no penalty in generalization error or its ability to sparsify the set of basis functions. Note that Tipping (2001) proposes an optimization of the distance

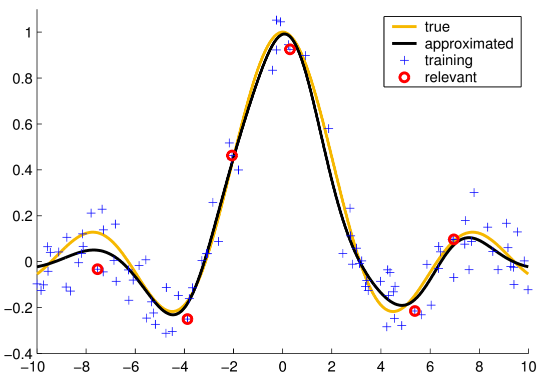

(a) Fitting the sinc function

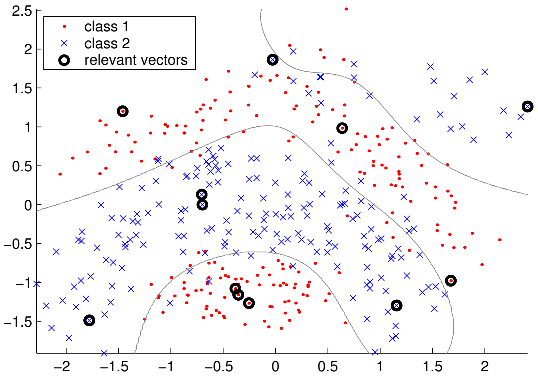

(b) Fitting the banana dataset

Figure 4.9: Fitting the sinc function using backfitting-RVM.

metric $\lambda$ that is based on gradient ascent in the log likelihood. Such a gradient can also be computed for backfitting as:

$$\frac{\partial \langle \ln p(\mathbf{y}, \mathbf{Z}|\mathbf{X}) \rangle}{\partial \lambda} = \sum_{j=1}^{N} \frac{b_j}{\psi_{zj}} \sum_{i=1}^{N} \left( \langle z_{ij} \rangle - b_j k_{ij} \right) (x_i - x_j)^2 \, k_{ij}$$

where we have abbreviated $k_{ij} = k(x_i, x_j)$. Based on our experience however, we would like to caution against unconstrained maximization of the likelihood, especially over distance metrics. Instead, we would recommend the route taken in the Gaussian process community, which is to treat these variables as hyperparameters, and place prior distributions over them. Exact solutions being typically intractable, we can either optimize them by using *maximum a posteriori* estimates (MacKay 1999), or by Monte Carlo techniques (Williams & Rasmussen 1996). Note that although a change in the distance metric would require a re-evaluation of the kernel responses at each data point, such computations can be speeded up significantly by the techniques reviewed in section 4.2.

Other optimizations suggested (Tipping 2001, Tipping & Faul 2003) include pruning the basis functions when their precision variables dictate that they are unneeded, as well as adopting a *greedy* (but potentially suboptimal) strategy in which the algorithm starts with a single basis function and adds candidates as necessary. We would like to emphasize that our implementation of the backfitting-RVM performs neither of these optimizations, although it is trivial to introduce them into our framework as well. Other variants of the RVM exist including a sequential version (Vermaak et al. 2004) which relies on generalized importance sampling to determine the number of kernels and their centers.

## 4.5 Bayesian Backfitting Experiments

We compare the use of partial least squares (PLS) and Bayesian backfitting as described in section 4.4.2 to analyze the following real-world data set collected from neuroscience. Our choice of PLS for comparison was motivated by the fact that this is a well-studied algorithm that also has $O(d)$ complexity, and is widely used on data sets in chemometrics with similar properties. The data set consists of simultaneous recordings (2400 data points) of firing-rate coded activity in 71 motor cortical neurons and the EMG of 11 muscles. The goal is to determine which neurons are responsible for the activity of each muscle. The relationship between neural and muscle activity is assumed to be linear, such that the basis functions in backfitting are simply a copy of the respective input dimensions, i.e. $f_m(\mathbf{x}) = x_m$.

A brute-force study (conducted by our research collaborators) painstakingly considered every possible combination of neurons (up to groups of 20 for computational reasons,

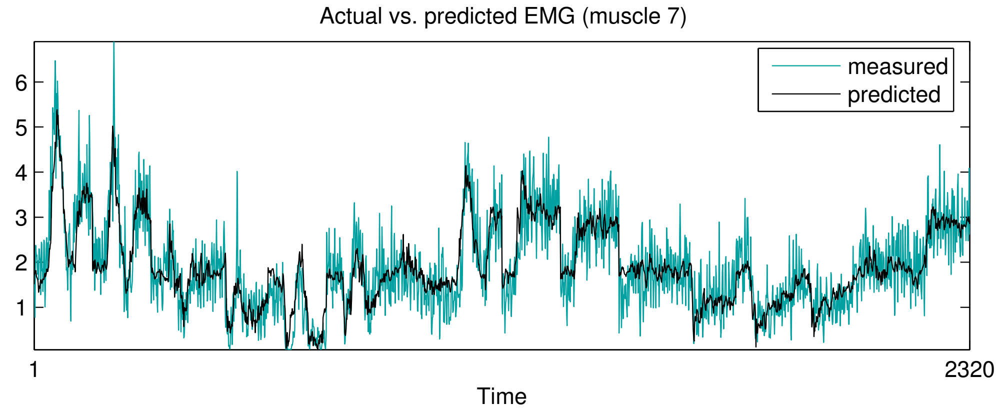

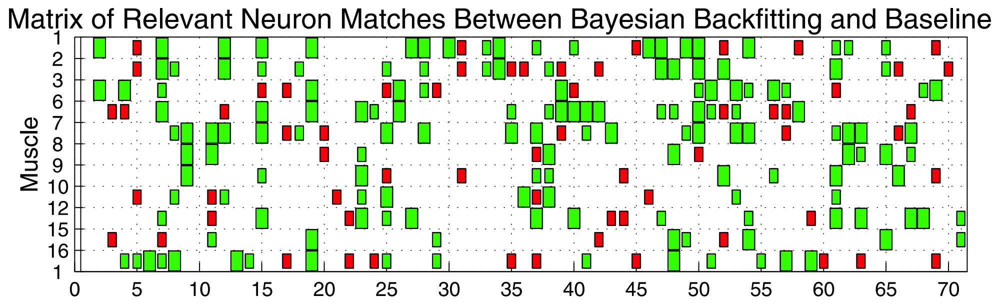

Figure 4.10: The first graph shows the EMG signal predicted by Bayesian backfitting (dark line) versus the original (light line). By pruning away unnecessary features, backfitting achieves significant noise reduction. Each row of the Hinton diagram shows the matched (green) and missed (red) neurons between the backfitting results and the baseline analysis.

i.e. even this reduced analysis required several weeks of computation on a 30-node cluster computer), to determine the optimal neuron-muscle correlation as measured on various validation sets. This study provided us with a baseline neuron-muscle correlation matrix that we hoped to duplicate with PLS and Bayesian backfitting, although with much reduced computational effort.

The results shown in Table 4.1 demonstrate two points:

| | **Bayes. back.** | **PLS** | **baseline** |
|---|---|---|---|
| neuron match | 93.6% | 18% | — |
| nMSE | 0.8446 | 1.77 | 0.84 |

Table 4.1: Results on the neuron-muscle data set

- The relevant neurons found by Bayesian backfitting contained over 93% of the neurons found by the baseline study, while PLS fails to find comparable correlations. The neuron match in backfitting is easily inferred from the resulting magnitude of the precision parameters $\alpha$, while for PLS, the neuron match was inferred based on the subspace spanned by the projections that PLS employed.

- The regression accuracy of Bayesian backfitting (as determined by 8-fold cross-validation), is comparable to that of the baseline study, while PLS' failure to find the correct correlations causes it to have significantly higher generalization errors. The analysis for both backfitting and PLS was carried out using the same validation sets as those used for the baseline analysis.

The performance of Bayesian backfitting on this particularly difficult data set shows that it is a viable alternative to traditional generalized linear regression tools. Even with the additional Bayesian inference for ARD, it maintains its algorithmic efficiency since no matrix inversion is required.

As an aside it is useful to note that Bayesian backfitting and PLS required of the order of 8 hours of computation on a standard PC[2] (compared with several weeks on a cluster for the brute-force study), and evaluated the contributions of all 71 neurons.

[2]Pentium IV class machine, 1.7GHz

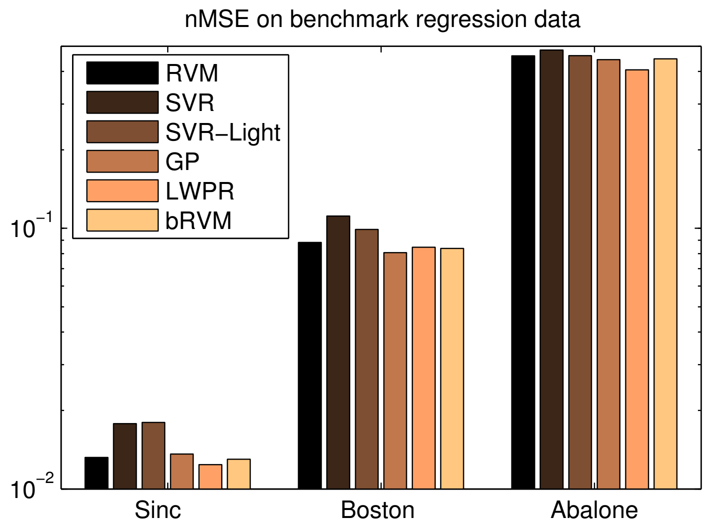

Figure 4.11: A comparison of the normalized mean squared error (nMSE) on several benchmark regression data sets. Results are statistically significant with $p < 0.05$.

### 4.5.1 Backfitting RVM Evaluation

To evaluate the generalization ability of backfitting-RVM, we compared it to other state-of-the art regression tools on the popular benchmark Boston housing and Abalone data sets[3]. For each data set, a randomly selected 20% of the data set was used as test data and the remainder for training.

Figure 4.11 shows the normalized mean squared errors on the test sets averaged over 100 experiments. The algorithms compared were the standard relevance vector machine (RVM), support vector regression (SVR)[4], SVR-Light, Gaussian process (GP) regression, locally weighted projection regression (LWPR) (Vijayakumar & Schaal 2000), and our backfitting-RVM (bRVM). Both backfitting-RVM and its standard counterpart used Gaussian kernels with distance metrics optimized by 5-fold cross-validation. The Gaussian

[3]Both available from the UCI repository
[4]RVM and SVR results adapted from (Tipping 2001)

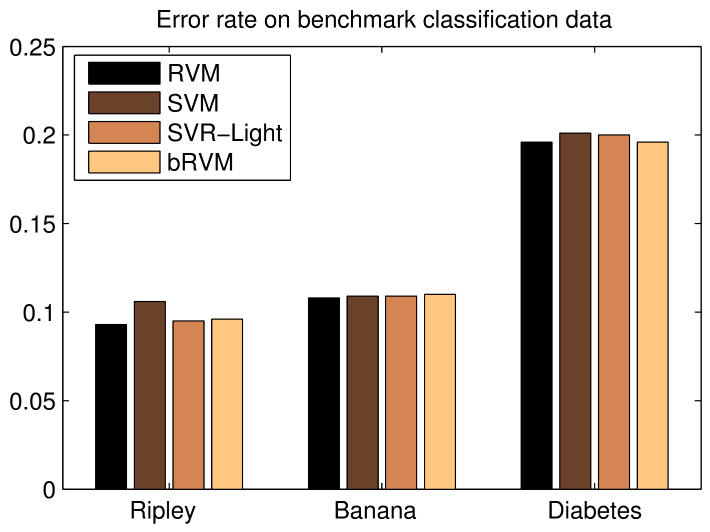

Figure 4.12: A comparison of the classification error rate (as a fraction of 1) on several benchmark data sets. Results are statistically significant with $p < 0.05$.

process algorithm used an RBF kernel with automatic hyperparameter optimization. As figure 4.11 shows, backfitting-RVM provides an extremely competitive solution in terms of generalization ability when compared to other popular regression methods.

Figure 4.12 shows the classification accuracy of RVM, SVM, SVM-Lite and our bRVM on some benchmark datasets. To aid in comparison, we trained and tested bRVM on exactly the same data used in (Tipping 2001), with the distance metrics optimized as in the regression case.

For the methods (RVM, SVM, SVM-Light and bRVM) that focus on a "sparsification" of the set of basis functions, we compared the average number of basis functions retained on each data set in the regression and classification benchmarks. Figure 4.13 shows the average number of vectors retained in the final solution on these data sets. The RVM and backfitting-RVM retain an order of magnitude fewer data points in the final solution compared to support vector machine implementations.

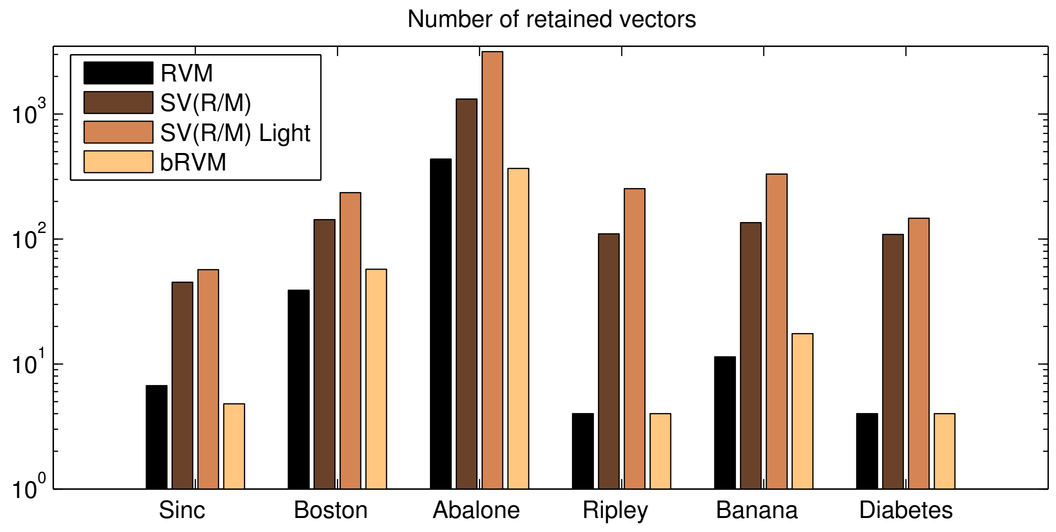

Figure 4.13: This graph compares the number of "relevant" vectors retained by the original relvance vector machine, support vector machines/regression, and our backfitting RVM. Note the log scale of the $y$-axis indicating that both versions of the RVM require an order of magnitude fewer retained vectors than support vector machines.

| | RVM | bRVM | SVM-Light | $N$ | $d$ |
|---|---|---|---|---|---|
| Sinc | 18.71s | 6.24s | 3.86s | 100 | 1 |
| Boston | 372s | 155s | 231s | 481 | 13 |
| Abalone | 2767s | 428s | 387s | 3341 | 10 |

Table 4.2: Relative computation time

The above experiments demonstrate that backfitting-RVM is a competitive regression solution when compared to other current state-of-the-art statistical methods, both in its generalization ability, and in its efficacy as a sparse Bayesian learning algorithm. However, the main advantage of backfitting-RVM is apparent only when we examine its relative computation time. Table 4.2 gives the average execution time (in seconds) required by the RVM, the backfitting-RVM, and SVM-Light for convergence of their regression parameter estimates (to 5 significant digits) on the sinc, Boston housing, and Abalone data sets. The table also shows the number of *training* data points, and their dimensionality. While

SVM-Light does better than the backfitting-RVM, we note that it retains significantly more basis vectors in the final solution. In spite of this, backfitting-RVM is within the same order of magnitude in computation time. Note that the number of $O(N^2)$ updates to $\mathbf{b}$ per update cycle of the hyperparameters is very small ($\sim 10$), since the solution from the previous update cycle is a very good starting point for the iterations of the next cycle. The results demonstrate that the backfitting-RVM can significantly gain from the iterative nature of the Bayesian backfitting generalized linear regression procedure.

# Chapter 5

# Conclusion

In the drive towards greater autonomy in intelligent systems, this dissertation contributes theory and algorithms that seek to automate the model creation process by providing a framework within which statistical model complexity is automatically derived in a tractable and efficient manner. We tackled several particularly difficult problems of model complexity estimation, for which to date, there have been no clear solutions which allow general applicability in real-world applications.

## 5.1 Summary of Dissertation Contributions

In chapter 2 we reviewed inference in graphical models and derived the factorial variational approximation as an extension to the popular EM algorithm. The factorial variational approximation is related to the mean-field approximation which has been widely used in statistical physics, and also has an interpretation as a message-passing or *propagation* algorithm (Ghahramani & Beal 2001) similar to the junction tree method. The key assumption is one of factorization in the posterior distribution over the unknown variables in the model. When applied to graphical models which have conditional distributions within the conjugate-exponential family, one can derive update equations for the posterior distributions over the hidden variables which are analytically tractable, and which ensure a monotonic decrease of the KL divergence between the true joint posterior and its factorial approximation. Non-conjugate distributions can be handled by deriving additional bounds using the theory of convex duality (Wainwright & Jordan 2003). This formulation formed the basis for the analytical update equations for models presented in later chapters.

Chapter 3 introduced three novel analytical solutions to difficult model complexity estimation problems. The first deals with the problem of estimating the complexity of mixture models. We put forward the idea that the decision to grow model complexity can be made efficiently by examining local decisions on whether to split existing components. This reduces the problem to deriving a principled splitting criterion, for which we look at the marginal likelihood comparison between the existing component, and a hypothetical model which splits the component in two. A factorial variational approximation to the marginal likelihood gives us analytically tractable update equations, such that maximizing the marginal likelihood automatically chooses the hypothesis that best models the data. We demonstrated the efficacy of this procedure by analyzing a data set consisting of human movement data, in order to determine the dimensionality of the underlying manifold.

The second algorithm presented in chapter 3 dealt with the problem of estimating the extent of the window of sufficient statistics that should be cached in online learning scenarios. This is also a model complexity problem since a very small window can explain larger parameter drifts in the model and hence more complex data sets. Getting this complexity parameter right is crucial since having a window that is too large will respond only sluggisly to rapid parameter changes, while having one that is too small will respond to noise fluctuations and fail to generalize well. We suggest a solution that is based on tracking the parameters of a drifting system using a Kalman filter. By using the anti-causal information available (Kalman *smoothing*), we can create a formulation for estimating the process noise variance, which relates to how quickly we believe the system changes with time. We show that in conjunction with the Bayesian backfitting algorithm presented in chapter 4, we can provide a principled online learning algorithm that has no open parameters to tune, and yet tracks the drifting process well.

Our final exploration of analytical tractability tackled the problem of estimating distance metrics for locally weighted learning — a problem also known as *supersmoothing.* This proves to be a particularly difficult problem in practice, since unlike the standard probabilistic formulations like mixture-of-experts, we would like the individual components to be non-competitive, in order to provide for a computationally efficient solution. This goal is accomplished by treating the kernel weights probabilistically, which also leads to interesting design questions about the kernel form such that analytical tractability is retained. By using a bound derived from the theory of convex duality, we created a simple and efficient procedure for estimating the width of the kernel, such that it adapts locally to the data without overfitting or underfitting.

Our main contribution to computationally efficient algorithms was provided in chapter 4, in which we examined the family of backfitting algorithms as a candidate for reducing the computational complexity of supervised learning problems by decomposing inference along individual features. Several efficient procedures such as cascade-correlation neural networks, and generalized Gauss-Seidel procedures can be shown to have algorithmic underpinnings that stem from the backfitting family of algorithms. Unfortunately, until now, backfitting has been ignored by the larger machine learning community since it does not have a probabilistic description. We therefore proposed the first probabilistic derivation of this family of algorithms that stems from the EM optimization procedure, and thus provides a natural analysis of its convergence properties. Moreover, given its probabilistic derivation, we can extend the algorithm to incorporate more sophisticated Bayesian inference such as automatic relevance detection.

The key advantage of Bayesian backfitting is its numerical robustness, since it requires no matrix inversion. Empirically this also results in a computational saving since updates to the distributions over the hyperparameters of the model do not require an expensive matrix inversion step to recompute regression coefficients. Each EM step has *linear* computational complexity in the number of dimensions $d$ which results in an algorithm which scales easily to high dimensional data sets. Extensions to classification and categorical outputs is easily achieved using bounds derived from the principle of convex duality. Another interesting consequence of the probabilistic derivation of backfitting is that the framework of sparse Bayesian learning, and in particular, the relevance vector machine can be derived with Bayesian backfitting at its core, thus allowing us to vastly improve on its robustness and computational scalability.

## 5.2 Opportunities for Further Research

While we hope that the algorithms presented in this dissertation are widely applicable over a large range of data sets, they are not the last word on their respective topics.

The variational approximation techniques described in this dissertation all have their roots in the theory of convex duality, allowing the derivation of several families of approximations including the factorial variational approximation, Bethe/Kikuchi approximations and cluster variation techniques. While there exists some analysis of the free-energy behaviour of these approximations (Wainwright & Jordan 2003), there is still no clear interpretaton of the implications each variant has on the outcome of the statistical analysis. MacKay (2001) suggests an interesting interpretation of the update equations that result from the variational analysis, and shows that when interpreted as a system of discrete-time dynamical equations, the interaction between the observed data and the structure of the conditional distributions can be interpreted as phase-transitions which move between models of varying complexity. The exploration of these ideas and their relation to the outcome of statistical analysis would be a topic of interesting further research.

The extension of Bayesian backfitting to classification, and the Bayesian supersmoothing algorithm both used a functional variational approximation in addition to the bound from the factorial approximation. Part of the criticism of variational methods that use functional rather than factorial bounds, is that the choice of the appropriate transformation (and hence the family of lower bound functions) seems to be more of an art than an established procedure. Also, unlike the factorial approximation in which we can cleanly quantify the tightness of the bound in terms of a KL divergence, there is no such analysis for more general functional bounds. As we noted in our derivation of Bayesian supersmoothing in section 3.3, when working outside the conjugate-exponential family, we often need to make these additional functional variational approximations, and an automated procedure for deriving tight bounds is still elusive. The software system VIBES (Variational Inference for Bayesian Networks) (Winn, Spiegelhalter & Bishop 2003) is a popular tool for performing automated variational inference in Bayesian networks of directed and undirected graphical models. While it can handle creating the appropriate factorization in models which fall within the conjugate-exponential family, it cannot yet handle the more general case of models that do not.

While our growing mixture model formulation works well in practice, it still suffers from the curse of dimensionality when used in problems with more than a few hundred dimensions. This primarily stems from the modeling of Wishart distributions over the local covariance matrices of the mixture components. At present, the only viable solution for very high-dimensional data seems to be to use local models which are axis-aligned, thus reducing the problem to modeling only the diagonal elements of the covariance matrices, which can be achieved easily with inverse Gamma distributions over each diagonal component.

Our formulation of Bayesian forgetting factors tackles the problem of learning how quickly to forget past data in online environments. It still however has the unfortunate need to rely on a *smoothing* pass to correct an overestimate in the rate of process drift. While we can reliably detect the window size of the Bayes filter in such situations, it would be desirable if we could cache and recursively update sufficient statistics, instead of keeping past data around for the duration of the window.

As we mentioned in section 3.1.4, the use of semiparametric Bayesian methods for mixture modeling growing within the machine learning community, and it would be interesting to interpret several efficient learning algorithms such as locally weighted projection regression (LWPR) within this framework. At the moment its dependence on Gibbs sampling restricts its application to relatively low-dimensional densities, but this should not prove to be a problem when adapting to methods like LWPR and backfitting since they decompose multivariate problems in to series of univariate ones, within which the semiparametric approach would still be efficient. It would also be interesting to see if this can be combined with the variational approach to deal with density functions that do not conform to the conjugate-exponential family.

# Reference List

Akaike, H. (1974), 'A new look at the statistical model identification', *IEEE Transactions on Automatic Control* **19**, 716–723.

Andrieu, C., de Freitas, N., Doucet, A. & Jordan, M. I. (2003), 'An introduction to MCMC for machine learning', *Journal of Machine Learning Research* **50**, 5–43.

Antoniak, C. E. (1974), 'Mixtures of Dirichlet processes with applications to Bayesian nonparametric problems', *The Annals of Statistics* **2**(6), 1152–1174.

Atkeson, C. G., Moore, A. W. & Schaal, S. (1997), 'Locally weighted learning', *Artificial Intelligence Review* **11**(1-5), 11–73.

Beal, M. J. (2003), Variational Algorithms for Approximate Bayesian Inference, PhD thesis, The Gatsby Computational Neurosience Unit, University College London, 17 Queen Square, London WC1N 3AR.

Beal, M. J., Ghahramani, Z. & Rasmussen, C. E. (2002), The infinite hidden markov model, *in* Dietterich, Becker & Ghahramani (2002).

Becker, S., Thrun, S. & Obermayer, K., eds (2003), *Advances in Neural Information Processing Systems 15*, Vol. 15, MIT Press, Cambridge, MA.

Belsley, D. A., Kuh, E. & Welsch, R. E. (1980), *Regression diagnostics: Identifying influential data and sources of collinearity*, Wiley, New York.

Bernardo, J. M. & Smith, A. F. M. (1994), *Bayesian Theory*, John Wiley & Sons, Inc.

Bishop, C. M. (1995), *Neural Networks for Pattern Recognition*, Oxford University Press.

Bishop, C. M. (1999*a*), Bayesian PCA, *in* M. S. Kearns, S. A. Solla & D. A. Cohn, eds, 'Advances in Neural Information Processing Systems 11', Vol. 11, MIT Press, Cambridge, MA, pp. 382–388.

Bishop, C. M. (1999*b*), Variational principle components, *in* 'Proceedings of the International Conference on Artificial Neural Networks (ICANN'99)', IEE Press, Edinburgh, pp. 509–514.

Bishop, C. M. & Winn, J. M. (2000), Non-linear Bayesian image modelling, *in* D. Vernon, ed., 'Proceedings of the 6th European Conference on Computer Vision', Vol. 1842 of *Lecture Notes in Computer Science*, Springer-Verlag.

Blackwell, D. (1973), 'Discreteness of Ferguson selections', *The Annals of Statistics* **1**(2), 356–358.

Blackwell, D. & MacQueen, J. B. (1973), 'Ferguson distributions via Pólya urn schemes', *The Annals of Statistics* **1**(2), 353–355.

Blei, D. M. & Jordan, M. I. (2004), Variational methods for the dirichlet process, *in* 'Proceedings of the 21st International Conference on Machine Learning'.

Cadez, I. V. & Smyth, P. (2001), Model complexity, goodness of fit, and diminishing returns, *in* T. Leen, T. Dietterich & V. Tresp, eds, 'Advances in Neural Information Processing Systems', Vol. 13, MIT Press, pp. 388–394.

Chuang, R. & Mendell, N. R. (1997), 'The approximate null distribution of the likelihood ratio test for a mixture of two bivariate normal distributions with equal variance', *Communications in Statistics — Simulation and Computation* **26**, 631–648.

Chun, F., Handjani, S. & Jungreis, D. (2003), 'Generalizations of Pólya's urn problem', *Annals of Combinatorics* **7**(2), 141–154.

de Freitas, J. F. G., Niranjan, M. & Gee, A. H. (1999), Regularization in sequential learning algorithms, *in* 'Advances in Neural Information Processing Systems', Vol. 10, MIT Press, pp. 458–464.

Dempster, A. P., Laird, N. M. & Rubin, D. B. (1977), 'Maximum likelihood from incomplete data via the EM algorithm', *Journal of the Royal Statistical Society. Series B (Methodological)* **39**(1), 1–38.

Deutscher, J., Blake, A. & Reid, I. (2000), Articulated body motion capture by annealed particle filtering, *in* 'Proceedings of the IEEE Conference on Computer Vision and Pattern Recognition', Vol. 2, pp. 126–133.

Dietterich, T., Becker, S. & Ghahramani, Z., eds (2002), *Advances in Neural Information Processing Systems 14*, Vol. 14, MIT Press, Cambridge, MA.

Doucet, A., de Freitas, N. & Gordon, N. J., eds (2001), *Sequential Monte Carlo Methods in Practice*, Statistics for Engineering and Information Science, Springer-Verlag, New York.

D'Souza, A., Vijayakumar, S. & Schaal, S. (2001), Are internal models of the entire body learnable?, *in* 'Society for Neuroscience Abstracts', Vol. 27. Program No. 406.2.

D'Souza, A., Vijayakumar, S. & Schaal, S. (2004), The Bayesian backfitting relevance vector machine, *in* 'Proceedings of the 21st International Conference on Machine Learning', ACM Press.

Escobar, M. D. (1994), 'Estimating normal means with a Dirichlet process prior', *Journal of the American Statistical Association* **89**(425), 268–277.

Escobar, M. D. & West, M. (1995), 'Bayesian density estimation and inference using mixtures', *Journal of the American Statistical Association* **90**(430), 577–588.

Everitt, B. S. (1984), *An Introduction to Latent Variable Models*, Monographs on Statistics and Applied Probability, Chapman & Hall.

Fahlman, S. E. & Lebiere, C. (1990), The cascade-correlation learning architecture, *in* D. S. Touretzky, ed., 'Advances in Neural Information Processing Systems 2', Vol. 2, Morgan Kaufmann Publishers.

Fearnhead, P. (1998), Sequential Monte Carlo methods in filter theory, PhD thesis, Merton College, University of Oxford.

Feder, M. & Weinstein, E. (1988), 'Parameter estimation of superimposed signals using the EM algorithm', *IEEE Transactions on Acoustics, Speech and Signal Processing* **36**(4), 477–490.

Ferguson, T. S. (1973), 'A Bayesian analysis of some nonparametric problems', *The Annals of Statistics* **1**(2), 209–230.

Ferguson, T. S. (1974), 'Prior distributions on spaces of probability measures', *The Annals of Statistics* **2**(4), 615–629.

Frank, I. E. & Friedman, J. H. (1993), 'A statistical view of some chemometrics regression tools', *Technometrics* **35**(2), 109–135.

Friedman, J. H. (1984), A variable span smoother, Technical Report LCS5, Department of Statistics, Stanford University.

Friedman, J. H., Bentley, J. L. & Finkel, R. A. (1977), An algorithm for finding best matches in logarithmic expected time, *in* 'ACM Transactions on Mathematical Software', Vol. 3, pp. 209–226.

Fukumizu, K., Bach, F. R. & Jordan, M. I. (2004), 'Dimensionality reduction for supervised learning using reproducing kernel Hilbert spaces', *Journal of Machine Learning Research* **5**, 73–99.

Gelman, A., Carlin, J. B., Stern, H. S. & Rubin, D. B. (1995), *Bayesian Data Analysis*, Texts in Statistical Science, Chapman & Hall/CRC, Boca Raton, Florida.

Geman, S., Bienestock, E. & Doursal, R. (1992), 'Neural networks and the bias/variance dilemma', *Neural Computation* **4**, 1–58.

Geman, S. & Geman, D. (1984), 'Stochastic relaxation, Gibbs distributions and the Bayesian restoration of images', *IEEE Transactions on Pattern Analysis and Machine Intelligence* **6**, 721–741.

Ghahramani, Z. & Beal, M. J. (2000), Variational inference for Bayesian mixtures of factor analysers, *in* Solla, Leen & Müller (2000), pp. 509–514.

Ghahramani, Z. & Beal, M. J. (2001), Propagation algorithms for variational Bayesian learning, *in* Leen, Diettrich & Tresp (2001).

Ghahramani, Z. & Hinton, G. E. (1997), The EM algorithm for mixtures of factor analyzers, Technical Report CRG-TR-96-1, Department of Computer Science, University of Toronto, 6 King's College Road, Toronto, Canada M5S 1A4.

Ghosh, J. K. & Ramamoorthi, R. V. (2003), *Bayesian Nonparametrics*, Springer Series in Statistics, Springer-Verlag, New York, USA, chapter Dirichlet and Pólya Tree Processes, pp. 87–120.

Gordon, N. J., Salmond, D. J. & Smith, A. F. M. (1993), 'Novel approach to nonlinear/non-Gaussian Bayesian state estimation', *IEE Proceedings-F* **140**(2), 107–113.

Gray, A. & Moore, A. W. (2001), $N$-body problems in statistical learning, *in* Leen et al. (2001).

Green, P. J. (1995), 'Reversible jump Markov chain Monte Carlo computation and Bayesian model determination', *Biometrika* **82**, 711–732.

Hammersley, J. M. & Clifford, P. (1971), Markov fields on finite graphs and lattices. Unpublished.

Hastie, T. J. & Tibshirani, R. J. (1990), *Generalized Additive Models*, number 43 *in* 'Monographs on Statistics and Applied Probability', Chapman & Hall.

Hastie, T. J. & Tibshirani, R. J. (2000), 'Bayesian backfitting', *Statistical Science* **15**(3), 196–213.

Hastie, T. J., Tibshirani, R. J. & Friedman, J. H. (2001), *The Elements of Statistical Learning: Data Mining, Inference, and Prediction*, Springer Series in Statistics, Springer-Verlag.

Hastings, W. K. (1970), 'Monte Carlo sampling methods using Markov chains and their applications', *Biometrika* **57**, 97–109.

Hurvich, C. & Tsai, C. (1976), 'Regression and time series model selection in small samples', *Biometrika* **76**, 297–307.

Ishwaran, H. & James, L. F. (2001), 'Gibbs sampling methods for stick-breaking priors', *Journal of the American Statistical Association* **96**(453), 161–173.

Ishwaran, H. & James, L. F. (2002), 'Approximate Dirichlet process computing in finite normal mixtures: Smoothing and prior information', *Journal of Computational and Graphical Statistics* **11**(3), 1–26.

Ishwaran, H. & Zarepour, M. (2002), 'Exact and approximate sum-representations for the Dirichlet process', *Canadian Journal of Statistics* **30**, 269–283.

Jaakkola, T. S. & Jordan, M. I. (2000), 'Bayesian parameter estimation via variational methods', *Statistics and Computing* **10**(1), 25–37.

Jeffreys, H. (1946), 'An invariant form for the prior probability in estimation problems', *Journal of the Royal Statistical Society. Series A* **186**, 453–461.

Jordan, M. I., Ghahramani, Z., Jaakkola, T. S. & Saul, L. K. (1999), An introduction to variational methods for graphical models, *in* M. I. Jordan, ed., 'Learning in Graphical Models', MIT Press, pp. 105–161.

Jordan, M. I. & Jacobs, R. A. (1994), 'Hierarchical mixtures of experts and the EM algorithm', *Neural Computation* **6**(2), 181–214.

Kalman, R. E. (1960), 'A new approach to linear filtering and prediction problems', *Transactions of the ASME — Journal of Basic Engineering* **82**, 35–45.

Kawato, M. (1999), 'Internal models for motor control and trajectory planning', *Current Opinion in Neurobiology* **9**, 718–727.

Komarek, P. & Moore, A. W. (2000), A dynamic adaptation of AD-trees for efficient machine learning on large data sets, *in* P. Langley, ed., 'International Conference on Machine Learning', pp. 495–502.

Lauritzen, S. L. (1996), *Graphical Models*, Vol. 17 of *Oxford Statistical Science Series*, Oxford Science Publications.

Lauritzen, S. L. & Spiegelhalter, D. J. (1988), 'Local computations with probabilities on graphical structures and their applications to expert systems (with discussion)', *Journal of the Royal Statistical Society. Series B (Methodological)* **50**(2), 157–224.

Leen, T. K., Diettrich, T. G. & Tresp, V., eds (2001), *Advances in Neural Information Processing Systems 13*, Vol. 13, MIT Press, Cambridge, MA.

Li, J. Q. & Barron, A. R. (2001), Mixture density estimation, *in* Leen et al. (2001), pp. 279–285.

Ljung, L. & Söderström, T. (1983), *Theory and Practice of Recursive Identification*, MIT Press, Cambridge, Massachusets.

MacEachern, S. N. & Müller, P. (1998), 'Estimating mixture of Dirichlet process models', *Journal of Computational and Graphical Statistics* **7**, 223–238.

MacKay, D. J. C. (1999), 'Comparison of approximate methods for handling hyperparameters', *Neural Computation* **11**(5), 1035–1068.

MacKay, D. J. C. (2001), Local minima, symmetry breaking, and model pruning in variational free energy minimization. Unpublished.

MacKay, D. J. C. (2003*a*), *Information Theory, Inference and Learning Algorithms*, Cambridge University Press, chapter Monte Carlo Methods, pp. 357–386.

MacKay, D. J. C. (2003*b*), *Information Theory, Inference and Learning Algorithms*, Cambridge University Press, chapter Variational Methods, pp. 422–436.

Massey, W. F. (1965), 'Principal component regression in exploratory statistical research', *Journal of the American Statistical Association* **60**, 234–246.

McLachlan, G. & Peel, D. (2000), *Finite Mixture Models*, Wiley series in probability and statistics, John Wiley & Sons, Inc., New York, NY.

Mendell, N. R., Finch, S. J. & Thode, H. C. (1993), 'Where is the likelihood ratio test powerful for detecting two component mixtures?', *Biometrics* **49**, 907–915.

Mengerson, K. & Robert, C. P. (1996), Testing for mixtures: A Bayesian entropy approach, *in* J. O. Berger, J. M. Bernardo, A. P. Dawid, D. V. Lindley & A. F. M. Smith, eds, 'Bayesian Statistics', Vol. 5, Oxford University Press.

Metropolis, N., Rosenbluth, A. W., Rosenbluth, M. N., Teller, A. H. & Teller, E. (1953), 'Equation of state calculations by fast computing machines', *Journal of Chemical Physics* **21**, 1087–1092.

Minagawa, A., Tagawa, N. & Tanaka, T. (2002), 'SMEM algorithm is not fully compatible with maximum likelihood framework', *Neural Computation* **14**, 1261–1266.

Mitchell, T. M. (1997), *Machine Learning*, WCB/McGraw Hill.

Moore, A. W. (2000), The anchors hierarchy: Using the triangle inequality to survive high-dimensional data, *in* 'Proceedings of the Twelfth International Conference on Uncertainty in Artificial Intelligence', AAAI Press, pp. 397–405.

Moore, A. W. & Lee, M. S. (1998), 'Cached sufficient statistics for efficient machine learning with large datasets', *Journal of Artificial Intelligence Research* **8**, 67–91.

Motwani, R. & Raghavan, P. (1995), *Randomized Algorithms*, Cambridge University Press.

Neal, R. M. (1994), Bayesian Learning for Neural Networks, PhD thesis, Dept. of Computer Science, University of Toronto.

Neal, R. M. (1998), Markov chain sampling methods for Dirichlet process mixture models, Technical Report 9815, Department of Statistics, University of Toronto, Toronto, Canada.

Neal, R. M. & Hinton, G. E. (1998), A view of the EM algorithm that justifies incremental, sparse, and other variants, *in* M. I. Jordan, ed., 'Learning in Graphical Models', Kluwer Academic Publishers, Dordecht, The Netherlands, pp. 355–368.

Omohundro, S. M. (1991), Bumptrees for efficient function, constraint and classification learning, *in* R. Lippmann, J. Moody & D. S. Touretzky, eds, 'Advances in Neural Information Processing Systems 3', Vol. 3, Morgan Kaufmann Publishers, pp. 693–699.

Paciorek, C. J. & Schervish, M. J. (2004), Nonstationary covariance functions for Gaussian process regression, *in* Thrun, Saul & Schölkopf (2004).

Parisi, G. (1988), *Statistical Field Theory*, Vol. 66 of *Frontiers in Physics*, Addison-Wesley, Redwood City, CA.

Pearl, J. (1988), *Probabilistic Reasoning in Intelligent Systems: Networks of Plausible Inference*, Morgan Kaufmann Publishers.

Pitman, J. & Yor, M. (1997), 'The two-parameter Poisson-Dirichlet distribution derived from a stable subordinator', *The Annals of Statistics* **25**(2), 855–900.

Poggio, R. & Girosi, F. (1990), 'Regularization algorithms for learning that are equivalent to multilayer networks', *Science* **247**, 213–225.

Proakis, J. G., Rader, C. M., Ling, F., Nikias, C. L., Moonen, M. & Proudler, I. K. (2002), *Algorithms for Statistical Signal Processing*, Prentice Hall, Upper Saddle River, New Jersey.

Rasmussen, C. E. (2000), The infinite Gaussian mixture model, *in* Solla et al. (2000), pp. 554–560.

Rasmussen, C. E. & Ghahramani, Z. (2002), Infinite mixtures of gaussian process experts, *in* Dietterich et al. (2002).

Rätsch, G., Onoda, T. & Müller, K.-R. (2001), 'Soft margins for AdaBoost', *Machine Learning* **42**(3), 287–320.

Richardson, S. & Green, P. J. (1997), 'On Bayesian analysis of mixtures with an unknown number of components', *Journal of the Royal Statistical Society. Series B (Methodological)* **59**, 731–792.

Rissanen, J. (1978), 'Modelling by shortest data description', *Automatica* **14**, 465–471.

Rissanen, J. (1996), 'Fisher information and stochastic complexity', *IEEE Transactions on Information Theory* **42**(1), 40–47.

Roeder, K. & Wasserman, L. (1995), Practical Bayesian density estimation using mixtures of normals, Technical Report 633, Department of Statistics, Carnegie Mellon University.

Rubin, D. B. (1988), Using the SIR algorithm to simulate posterior distributions, *in* J. Bernado, M. H. DeGroot, D. V. Lindley & A. F. M. Smith, eds, 'Bayesian Statistics 3', Oxford University Press, pp. 395–403.

Rustagi, J. S. (1976), *Variational Methods in Statistics*, Vol. 121 of *Mathematics in Science and Engineering*, Academic Press, New York.

Sato, M. (2001), 'Online model selection based on the variational Bayes', *Neural Computation* **13**(7), 1649–1681.

Saul, L. K., Jaakkola, T. S. & Jordan, M. I. (1996), 'Mean field theory for sigmoid belief networks', *Journal of Artificial Intelligence Research* **4**, 61–76.

Schaal, S. & Atkeson, C. G. (1998), 'Constructive incremental learning from only local information', *Neural Computation* **10**, 2047–2084.

Schaal, S. & Sternad, D. (2001), 'Origins and violations of the 2/3 power law in rhythmic 3d movements', *Experimental Brain Research* **136**, 60.

Schaal, S., Vijayakumar, S. & Atkeson, C. G. (1998), Local dimensionality reduction, *in* M. I. Jordan, M. S. Kearns & S. A. Solla, eds, 'Advances in Neural Information Processing Systems 10', Vol. 10, MIT Press, Cambridge, MA, pp. 633–639.

Schölkopf, B. & Smola, A. J. (2000), *Learning with Kernels — Support Vector Machines, Regularization, Optimization, and Beyond*, Adaptive Computation and Machine Learning, MIT Press.

Schwarz, G. (1978), 'Estimation the dimension of a model', *The Annals of Statistics* **6**, 461–464.

Sethuraman, J. (1994), 'A constructive definition of Dirichlet priors', *Statistica Sinica* **4**, 639–650.

Smyth, P. (2000), 'Model selection for probabilistic clustering using cross validated likelihood', *Statistics and Computing* **10**, 63–72.

Solla, S. A., Leen, T. K. & Müller, K.-R., eds (2000), *Advances in Neural Information Processing Systems 12*, Vol. 12, MIT Press, Cambridge, MA.

Stone, M. (1974), 'Cross-validatory choice and assessment of statistical predictions', *Journal of the Royal Statistical Society. Series B (Methodological)* **36**(1), 111–147.

Stone, M. & Brooks, R. J. (1990), 'Continuum regression: Cross-validated sequentially constructed prediction embracing ordinary least squares, partial least squares and principal components regression', *Journal of the Royal Statistical Society. Series B (Methodological)* **52**(2), 237–269.

Sykacek, P. & Roberts, S. J. (2003), Adaptive classification by variational Kalman filtering, *in* Becker, Thrun & Obermayer (2003), pp. 737–744.

Thrun, S. (2002), Particle filters in robotics, *in* 'Proceedings of the International Conference on Uncertainty in Artificial Intelligence (UAI 2002)'.

Thrun, S., Saul, L. K. & Schölkopf, B., eds (2004), *Advances in Neural Information Processing Systems 16*, Vol. 16, MIT Press, Cambridge, MA.

Tipping, M. E. (2000), The relevance vector machine, *in* Solla et al. (2000).

Tipping, M. E. (2001), 'Sparse Bayesian learning and the relevance vector machine', *Journal of Machine Learning Research* **1**, 211–244.

Tipping, M. E. & Bishop, C. M. (1999), 'Mixtures of probabilistic principal component analysers', *Neural Computation* **11**(2), 443–482.

Tipping, M. E. & Faul, A. C. (2003), Fast marginal likelihood maximization for sparse Bayesian models, *in* C. M. Bishop & B. J. Frey, eds, 'Proceedings of the Ninth International Workshop on Artificial Intelligence and Statistics'.

Ueda, N. & Nakano, R. (1998), 'Deterministic annealing EM algorithm', *Neural Networks* **11**, 271–282.

Ueda, N., Nakano, R., Ghahramani, Z. & Hinton, G. E. (1999), SMEM algorithm for mixture models, *in* M. S. Kearns, S. A. Solla & D. A. Cohn, eds, 'Advances in Neural Information Processing Systems', Vol. 11, MIT Press.

Vapnik, V. N. (1982), *Estimation of Dependences Based on Empirical Data*, Springer-Verlag, Berlin.

Vapnik, V. N. (1995), *The Nature of Statistical Learning Theory*, Springer-Verlag, New York.

Vermaak, J., Godsill, S. J. & Doucet, A. (2004), Sequential Bayesian kernel regression, *in* Thrun et al. (2004).

Vijayakumar, S., D'Souza, A. & Schaal, S. (2004), 'Incremental online learning in high dimensions', *Neural Computation* . (submitted).

Vijayakumar, S., D'Souza, A., Shibata, T., Conradt, J. & Schaal, S. (2000), 'Statistical learning for humanoid robots', *Autonomous Robots* **12**, 55–69.

Vijayakumar, S. & Schaal, S. (2000), An $O(n)$ algorithm for incremental real time learning in high dimensional space, *in* 'Proceedings of the Seventeenth International Conference on Machine Learning (ICML2000)', Stanford, CA, pp. 1079–1086.

Wainwright, M. J. & Jordan, M. I. (2003), Graphical models, exponential families, and variational inference, Technical Report 649, Department of Statistics, University of California, Berkeley.

Williams, C. K. I. (1997), Prediction with Gaussian processes: From linear regression to linear prediction and beyond, Technical Report NCRG/97/012, Neural Computing Research Group, Dept. of Computer Science & Applied Mathematics, Aston University, Birmingham B4 7ET, United Kingdom.

Williams, C. K. I. & Rasmussen, C. E. (1996), Gaussian processes for regression, *in* D. S. Touretzky, M. C. Mozer & M. E. Hasselmo, eds, 'Advances in Neural Information Processing Systems 8', Vol. 8, MIT Press, Cambridge, MA, pp. 514–520.

Winn, J. M., Spiegelhalter, D. J. & Bishop, C. M. (2003), VIBES: A variational inference engine for Bayesian networks, *in* Becker et al. (2003), pp. 793–800.

Wold, H. (1975), Soft modeling by latent variables: The nonlinear iterative partial least squares approach, *in* J. Gani, ed., 'Perspectives in Probability and Statistics, Papers in Honour of M. S. Bartlett', Academic Press, London, pp. 520–540.

Wu, C. F. J. (1983), 'On the convergence properties of the EM algorithm', *The Annals of Statistics* **11**(1), 95–103.

Zhang, Y.-J. & Liu, Z.-Q. (2002), 'Self-splitting competitive learning: A new on-line clustering paradigm', *IEEE Transactions on Neural Networks* **13**(2), 369–380.

# Appendix A

# Some Useful Results

## A.1 Schur Complements

If we partition $\mathbf{M} = \begin{bmatrix} \mathbf{A} & \mathbf{B} \\ \mathbf{C} & \mathbf{D} \end{bmatrix}$ then we can write the following Schur complements:

$$\begin{aligned} \mathbf{M_A} &= \mathbf{D} - \mathbf{C}\mathbf{A}^{-1}\mathbf{B} \\ \mathbf{M_D} &= \mathbf{A} - \mathbf{B}\mathbf{D}^{-1}\mathbf{C} \\ -\mathbf{M_B} &= \mathbf{C} - \mathbf{D}\mathbf{B}^{-1}\mathbf{A} \qquad \text{if } \mathbf{B}^{-1} \text{ exists} \\ -\mathbf{M_C} &= \mathbf{B} - \mathbf{A}\mathbf{C}^{-1}\mathbf{D} \qquad \text{if } \mathbf{C}^{-1} \text{ exists} \end{aligned}$$

This allows us to express the inverse of $\mathbf{M}$ as follows:

$$\mathbf{M}^{-1} = \begin{bmatrix} \mathbf{M}_\mathbf{D}^{-1} & -\mathbf{M}_\mathbf{B}^{-1} \\ -\mathbf{M}_\mathbf{C}^{-1} & \mathbf{M}_\mathbf{A}^{-1} \end{bmatrix}$$

Importantly if $\mathbf{B}$ and $\mathbf{C}$ are singular, then we can obtain $\mathbf{M}_\mathbf{B}^{-1}$ and $\mathbf{M}_\mathbf{D}^{-1}$ in terms of benign inversions by using the property that $\mathbf{M}\mathbf{M}^{-1} = \mathbf{I}$ and $\mathbf{M}^{-1}\mathbf{M} = \mathbf{I}$ to realize:

$$\begin{aligned} \mathbf{C}\mathbf{M}_\mathbf{D}^{-1} &= \mathbf{D}\mathbf{M}_\mathbf{C}^{-1} \\ \mathbf{M}_\mathbf{B}^{-1}\mathbf{D} &= \mathbf{M}_\mathbf{D}^{-1}\mathbf{B} \end{aligned}$$

These results prove highly useful when computing partial matrix inversions, such as those required when conditioning multivariate Gaussian distributions.

## A.2 Some Important Expectations

Frequently we are required to compute the expectation $\langle \ln x \rangle$ where $x$ is distributed according to a Beta (conjugate for Binomial probability), Dirichlet (conjugate for Multinomial probability vector), Gamma (conjugate for Gaussian precision), or Wishart (conjugate for multivariate Gaussian precision). These are frequently expressed in terms of the *digamma* function:

$$\psi(a) = \left.\frac{d \ln \Gamma(x)}{dx}\right|_{x=a}$$

where the Gamma function $\Gamma(x)$ is an interpolant to the factorial defined as:

$$\Gamma(x) = \int_0^\infty t^{(x-1)} \exp(-t) dt$$

for $x > 0$. For integer values of $x$, $\Gamma(x) = (x-1)!$

- To compute $\langle \ln x \rangle$ for $x \sim \text{Beta}\,(x; a, b)$ consider:

$$\begin{aligned}\text{Beta}\,(x; a, b) &= \frac{\Gamma\,(a+b)}{\Gamma(a)\Gamma(b)} x^{a-1} \left(1-x\right)^{b-1} \\ &= \frac{1}{Z} x^{a-1} \left(1-x\right)^{b-1}\end{aligned}$$

where:

$$\begin{aligned}Z &= \frac{\Gamma(a)\Gamma(b)}{\Gamma\,(a+b)} \\ &= \int_0^1 x^{a-1} \left(1-x\right)^{b-1} dx\end{aligned}$$

Differentiating w.r.t. the parameter $a$ we get:

$$\begin{aligned}\frac{d}{da} Z &= \frac{d}{da} \int_0^1 x^{a-1} \left(1-x\right)^{b-1} dx \\ &= \int_0^1 \left(\ln x\right) x^{a-1} \left(1-x\right)^{b-1} dx \\ &= Z \left\langle \ln x \right\rangle\end{aligned}$$

Hence:

$$\begin{aligned}\langle \ln x \rangle &= \frac{1}{Z} \frac{d}{da} Z \\ &= \frac{d}{da} \ln Z\end{aligned}$$

$$
\begin{aligned}
&= \frac{d}{da}\left(\Gamma(a) + \Gamma(b) - \Gamma(a+b)\right) \\
&= \psi(a) - \psi(a+b)
\end{aligned}
$$

- The Dirichlet is a generalization of the beta distribution to a multinomial probability vector $\mathbf{x}$:

$$\text{Dirichlet}\left(\mathbf{x};\mathbf{u}\right) = \frac{\Gamma\left(\sum_i u_i\right)}{\prod_i \Gamma\left(u_i\right)} \prod_i x_i^{u_i - 1}$$

A property of the Dirichlet distribution is that each component $x_i$ is marginally distributed as:

$$x_i \sim \text{Beta}\left(x_i; u_i, \sum_{j \neq i} u_j\right)$$

Thus the result above for the Beta distribution allows us to infer that:

$$\langle \ln x_i \rangle = \psi(u_i) - \psi\left(\sum_j u_j\right)$$

- To compute $\langle \ln x \rangle$ for $x \sim \text{Gamma}\left(x; a, b\right)$ consider:

$$
\begin{aligned}
\text{Gamma}\left(x; a, b\right) &= \frac{b^a}{\Gamma(a)} x^{(a-1)} \exp(-bx) \\
&= \frac{1}{Z} x^{(a-1)} \exp(-bx)
\end{aligned}
$$

where:

$$
\begin{aligned}
Z &= \frac{\Gamma(a)}{b^a} \\
&= \int_0^\infty x^{(a-1)} \exp(-bx) dx
\end{aligned}
$$

Differentiating w.r.t. the parameter $a$ we get:

$$
\begin{aligned}
\frac{d}{da} Z &= \frac{d}{da} \int_0^\infty x^{(a-1)} \exp(-bx) dx \\
&= \int_0^\infty (\ln x) x^{(a-1)} \exp(-bx) dx \\
&= Z \langle \ln x \rangle
\end{aligned}
$$

Hence:

$$\begin{aligned}\langle \ln x \rangle &= \frac{1}{Z}\frac{d}{da}Z \\ &= \frac{d}{da}\ln Z \\ &= \frac{d}{da}\big(\ln \Gamma(a) - a\ln b\big) \\ &= \psi\left(a\right) - \ln b\end{aligned}$$

- For a symmetric positive definite matrix $\mathbf{X} \sim \mathrm{Wishart}_\nu\left(\mathbf{X};\mathbf{S}\right)$ we often require $\langle \ln |\mathbf{X}| \rangle$. Consider:

  $$\begin{aligned}\mathrm{Wishart}_\nu\left(\mathbf{X};\mathbf{S}\right) &= \frac{|\mathbf{S}|^{-\nu/2}}{2^{\nu d/2}\pi^{d(d-1)/4}\prod_i^d \Gamma\left(\frac{\nu+1-i}{2}\right)} |\mathbf{X}|^{(\nu-d-1)/2} \exp\left\{-\frac{1}{2}\,\mathrm{Tr}\left[\mathbf{S}^{-1}\mathbf{X}\right]\right\} \\ &= \frac{1}{Z}|\mathbf{X}|^{(\nu-d-1)/2} \exp\left\{-\frac{1}{2}\,\mathrm{Tr}\left[\mathbf{S}^{-1}\mathbf{X}\right]\right\}\end{aligned}$$

  where:

  $$\begin{aligned}Z &= \frac{2^{\nu d/2}\pi^{d(d-1)/4}\prod_i^d \Gamma\left(\frac{\nu+1-i}{2}\right)}{|\mathbf{S}|^{-\nu/2}} \\ &= \int_{\mathbf{O}}^{\infty} |\mathbf{X}|^{(\nu-d-1)/2} \exp\left\{-\frac{1}{2}\,\mathrm{Tr}\left[\mathbf{S}^{-1}\mathbf{X}\right]\right\} d\mathbf{X}\end{aligned}$$

  Differentiating w.r.t. the parameter $\nu$ we get:

  $$\begin{aligned}\frac{d}{d\nu}Z &= \frac{d}{d\nu}\int_{\mathbf{O}}^{\infty} |\mathbf{X}|^{(\nu-d-1)/2} \exp\left\{-\frac{1}{2}\,\mathrm{Tr}\left[\mathbf{S}^{-1}\mathbf{X}\right]\right\} d\mathbf{X} \\ &= \int_{\mathbf{O}}^{\infty} \left(\ln|\mathbf{X}|\right) |\mathbf{X}|^{(\nu-d-1)/2} \exp\left\{-\frac{1}{2}\,\mathrm{Tr}\left[\mathbf{S}^{-1}\mathbf{X}\right]\right\} d\mathbf{X} \\ &= Z\left\langle \ln|\mathbf{X}|\right\rangle\end{aligned}$$

  Hence:

  $$\begin{aligned}\langle \ln|\mathbf{X}| \rangle &= \frac{1}{Z}\frac{d}{d\nu}Z \\ &= \frac{d}{d\nu}\ln Z \\ &= \frac{d}{d\nu}\left(\frac{\nu d}{2}\ln 2 + \frac{d(d-1)}{4}\ln\pi + \sum_i^d \ln\Gamma\left(\frac{\nu+1-i}{2}\right) + \frac{\nu}{2}\ln|\mathbf{S}|\right)\end{aligned}$$

$$= \sum_{i}^{d} \psi \left( \frac{\nu + 1 - i}{2} \right) + \frac{d}{2} \ln 2 + \frac{1}{2} \ln |\mathbf{S}|$$

# Appendix B

# Derivations

## B.1 Factorial Variational Approximation

Let us start with the lower bound derived in equation (2.4) of section 2.2.2. We know that maximizing the lower bound implies maximizing the functional $\mathcal{F}(Q, \boldsymbol{\phi})$ over the space of probability distributions $Q(\mathbf{x}_{\mathcal{H}})$. Let us consider a simple example in which $\mathbf{x}_{\mathcal{H}} = \{x_1, x_2, x_3\}$, and furthermore assume that $Q(\mathbf{x}_{\mathcal{H}})$ factors over the individual variables $x_i$ as $Q(\mathbf{x}_{\mathcal{H}}) = Q_1(x_1)Q_2(x_2)Q_3(x_3)$. The calculus of variations (see (Rustagi 1976) for example,) allows us to derive a very elegant and general update mechanism for the individual factored distributions in our variational approximation.

For the ease of notation, in the rest of this derivation we shall use the symbol $Q_i$ to denote $Q_i(x_i)$. Hence for our current example, the functional $\mathcal{F}(Q, \boldsymbol{\phi})$ is of the form:

$$\mathcal{F}(Q, \boldsymbol{\phi}) = \int Q_1 Q_2 Q_3 \ln \frac{p(\mathbf{x}_{\mathcal{D}}, \mathbf{x}_{\mathcal{H}}; \boldsymbol{\phi})}{Q_1 Q_2 Q_3} dx_1 dx_2 dx_3 \tag{B.1}$$

Maximizing $\mathcal{F}(Q, \boldsymbol{\phi})$ is actually a constrained maximization since we must ensure that $\int Q(\mathbf{x}_{\mathcal{H}}) d\mathbf{x}_{\mathcal{H}} = 1$. This constraint can be incorporated into the integrand by the use of Lagrange multipliers. We therefore define a new function $z(\mathbf{x}_{\mathcal{H}})$ and derive a differential constraint as follows:

$$\begin{aligned} z(\mathbf{x}_{\mathcal{H}}) &= \int_{-\infty}^{\mathbf{x}_{\mathcal{H}}} Q_1(x_1')Q_2(x_2')Q_3(x_3') dx_1' dx_2' dx_3' \\ \dot{z} - Q_1 Q_2 Q_3 &= 0 \qquad \text{s.t. } z(-\infty) = 0 \text{ and } z(\infty) = 1 \end{aligned} \tag{B.2}$$

with the end point constraints being $z(-\infty) = 0$ and $z(\infty) = 1$. If we let $g(Q_1, Q_2, Q_3, \mathbf{x}_{\mathcal{H}})$ represent the integrand in equation (B.1), then we can incorporate the differential constraint of equation (B.2) using the Lagrange multiplier $\lambda$ as folows:

$$g_a(Q_1, Q_2, Q_3, \mathbf{x}_{\mathcal{H}}, z, \lambda) = Q_1 Q_2 Q_3 \ln \frac{p(\mathbf{x}_{\mathcal{D}}, \mathbf{x}_{\mathcal{H}}; \boldsymbol{\phi})}{Q_1 Q_2 Q_3} + \lambda(\dot{z} - Q_1 Q_2 Q_3) \tag{B.3}$$

Using this constrained integrand, maximizing the functional $\mathcal{F}(Q, \boldsymbol{\phi})$ w.r.t. each of the distributions $Q_i$ involves solving the following Euler equations:

$$\frac{\partial g_a}{\partial Q_i} - \frac{d}{d\mathbf{x}_{\mathcal{H}}}\left(\frac{\partial g_a}{\partial \dot{Q}_i}\right) = 0 \tag{B.4}$$

$$\frac{\partial g_a}{\partial z} - \frac{d}{d\mathbf{x}_{\mathcal{H}}}\left(\frac{\partial g_a}{\partial \dot{z}}\right) = 0 \tag{B.5}$$

where we denote $\dot{Q}_i = dQ_i/d\mathbf{x}_{\mathcal{H}}$. Substituting from equation (B.3) in equation (B.5) we get $d\lambda/d\mathbf{x}_{\mathcal{H}} = \mathbf{0}$. This implies that the Lagrange multiplier $\lambda$ is not a function of any of the hidden variables — an important result that will be used in the following steps. Similarly substituting from equation (B.3) in equation (B.4) and performing the differentiation with $Q_i = Q_1$ we get:

$$Q_2Q_3\left[\ln p(\mathbf{x}_{\mathcal{D}}, \mathbf{x}_{\mathcal{H}}; \boldsymbol{\phi}) - \ln Q_1 - \ln Q_2Q_3\right] - Q_2Q_3 - \lambda Q_2Q_3 = 0 \tag{B.6}$$

Integrating the above equation w.r.t. $x_2$ and $x_3$ we get:

$$\langle \ln p(\mathbf{x}_{\mathcal{D}}, \mathbf{x}_{\mathcal{H}}; \boldsymbol{\phi})\rangle_{Q_2Q_3} - \ln Q_1 - \int Q_2Q_3 \ln Q_2Q_3 dx_2 dx_3 - 1 - \lambda = 0 \tag{B.7}$$

Solving for $Q_1$ we get:

$$Q_1 = \frac{\exp\langle \ln p(\mathbf{x}_{\mathcal{D}}, \mathbf{x}_{\mathcal{H}}; \boldsymbol{\phi})\rangle_{Q_2Q_3}}{\exp\left(1 + \lambda + \int Q_2Q_3 \ln Q_2Q_3 dx_2 dx_3\right)}$$

The denominator is independent of $x_1$ since we have shown that $\lambda$ is not a function of the hidden variables, and our assumed independence $Q(\mathbf{x}_{\mathcal{H}}) = Q_1(x_1)Q_2(x_2)Q_3(x_3)$ implies that $Q_2Q_3$ is also independent of $\theta 1$. Hence the denominator can be treated as simply a normalizing constant, and we can express the solution for the individual $Q_i$ that maximizes the functional $\mathcal{F}(Q, \boldsymbol{\phi})$ under the assumed factorization as:

$$Q_i(x_i) = \frac{\exp\langle \ln p(\mathbf{x}_{\mathcal{D}}, \mathbf{x}_{\mathcal{H}}; \boldsymbol{\phi})\rangle_{Q_{k\neq i}}}{\int \exp\langle \ln p(\mathbf{x}_{\mathcal{D}}, \mathbf{x}_{\mathcal{H}}; \boldsymbol{\phi})\rangle_{Q_{k\neq i}} dx_i}$$

or equivalently:

$$\ln Q_i(x_i) = \langle \ln p(\mathbf{x}_{\mathcal{D}}, \mathbf{x}_{\mathcal{H}}; \boldsymbol{\phi})\rangle_{Q_{k\neq i}} + const_{x_i}$$

where $\langle\cdot\rangle_{Q_{k\neq i}}$ denotes expectation taken w.r.t. all distributions $Q_k$ except $Q_i$.

### B.1.1 Solution for Partial Factorization

Let us drop the assumption of complete factorization for now and examine how our solution changes when the factorization is partial. Suppose our current example had the partial factorization $Q(\mathbf{x}_{\mathcal{H}}) = Q_{12}(x_1, x_2)Q_3(x_3) = Q_1(x_1|x_2)Q_2(x_2)Q(x_3)$, then if we were trying to find a solution for $Q_1$ we would not be able to separate the $\ln Q_1$ term out of the integral as we have done in eq. (B.7), due to the fact that $Q_1 = Q_1(x_1|x_2)$ and has a dependency on $x_2$. Our only way out of the problem is to infer the joint distribution $Q_{12}(x_1, x_2)$, and hope to be able to factor the resulting distribution into $Q_1(x_1|x_2)Q_2(x_2)$.

The final solution also changes if we were trying to maximize the functional w.r.t. $Q_2$. We would proceed as if we assumed full factorization as before and arrive at the following equation which is analogous to equation (B.7)

$$\langle \ln p(\mathbf{x}_\mathcal{D}, \mathbf{x}_\mathcal{H}; \boldsymbol{\phi}) \rangle_{Q_1 Q_3} - \ln Q_2 - \int Q_1 Q_3 \ln Q_1 Q_3 dx_1 dx_3 - 1 - \lambda = 0$$

In this situation however, we must keep in mind that $Q_1$ is actually $Q_1(x_1|x_2)$ and hence has a dependency on $x_2$. Now when we solve for $Q_2$ we should take care to place all of the terms in the equation that have a dependency on $x_2$ in the numerator. We then arrive at the equation:

$$Q_2(x_2) \propto \exp\left( \langle \ln p(\mathbf{x}_\mathcal{D}, \mathbf{x}_\mathcal{H}; \boldsymbol{\phi}) \rangle_{Q_1 Q_3} - \int Q_1(x_1|x_2) \ln Q_1(x_1|x_2) dx_1 \right)$$

or equivalently

$$\ln Q_2 = \langle \ln p(\mathbf{x}_\mathcal{D}, \mathbf{x}_\mathcal{H}; \boldsymbol{\phi}) \rangle_{Q_1 Q_3} + \text{entropy}\left\{ Q_1(x_1|x_2) \right\} + const$$

Note that this method gives exactly the same result as the equivalent method of using the simple factorial approximation to determine the update for the joint posterior $Q(x_1, x_2)$ and subsequently marginalizing out $x_1$ to obtain $Q(x_2)$.

## B.2 Variational Approximation for Mixture Models

For convenience, we will repeat the log probability of the of the statistical model represented by figure 3.1:

$$\begin{aligned}
\ln p(\mathbf{x}_\mathcal{D}, \mathbf{x}_\mathcal{H}; \mathcal{M}_2) = \sum_{i=1}^{N} & s_{i1} \left[ \frac{1}{2} \ln |\mathbf{P}_1| - \frac{1}{2} (\mathbf{x}_i - \boldsymbol{\mu}_1)^T \mathbf{P}_1 (\mathbf{x}_i - \boldsymbol{\mu}_1) + \ln \zeta \right] \\
& + s_{i2} \left[ \frac{1}{2} \ln |\mathbf{P}_2| - \frac{1}{2} (\mathbf{x}_i - \boldsymbol{\mu}_2)^T \mathbf{P}_2 (\mathbf{x}_i - \boldsymbol{\mu}_2) + \ln (1 - \zeta) \right] \\
& + \sum_{m=1,2} \left[ \frac{d}{2} \ln \alpha_0 + \frac{1}{2} \ln |\mathbf{P}_m| - \frac{\alpha_0}{2} \boldsymbol{\mu}_m{}^T \mathbf{P}_m \boldsymbol{\mu}_m \right] \\
& + \sum_{m=1,2} \left[ \left( \frac{\nu - d - 1}{2} \right) \ln |\mathbf{P}_m| - \frac{1}{2} \operatorname{Tr} \left[ \mathbf{R}^{-1} \mathbf{P}_m \right] \right] \\
& + (u_1 - 1) \ln \zeta + (u_2 - 1) \ln (1 - \zeta) + const_{\mathbf{x}_\mathcal{D}, \mathbf{x}_\mathcal{H}}
\end{aligned} \tag{B.8}$$

If we assume the factorization $Q(\mathbf{x}_{\mathcal{H}}) = Q(\boldsymbol{\mu}, \mathbf{P})Q(\mathbf{S})Q(\zeta)$, we can use the results derived in appendix B.1, to obtain the update equations for the marginal distributions over each set of factored variables.

- For $Q(\zeta)$:

$$\ln Q(\zeta) = \left(u_1 + \sum_{i=1}^{N} \langle s_{i1} \rangle - 1\right) \ln \zeta + \left(u_2 + \sum_{i=1}^{N} \langle s_{i2} \rangle - 1\right) \ln(1-\zeta) + const_{\zeta} \quad \text{(B.9)}$$

  From equation (B.9) we can infer the following:

$$\begin{aligned} Q(\zeta) &= \text{Beta}\left(\zeta; \tilde{u}_1, \tilde{u}_2\right) \\ \tilde{u}_1 &= u_1 + \sum_{i=1}^{N} \langle s_{i1} \rangle \\ \tilde{u}_2 &= u_2 + \sum_{i=1}^{N} \langle s_{i2} \rangle \end{aligned}$$

- For $Q(\boldsymbol{\mu}_m, \mathbf{P}_m)$:

$$\begin{aligned} \ln Q(\boldsymbol{\mu}_m, \mathbf{P}_m) = \frac{1}{2} \left(\sum_{i=1}^{N} \langle s_{im} \rangle\right) \ln |\mathbf{P}_m| - \frac{1}{2} \sum_{i=1}^{N} \langle s_{im} \rangle \left(\mathbf{x}_i - \boldsymbol{\mu}_m\right)^T \mathbf{P}_m \left(\mathbf{x}_i - \boldsymbol{\mu}_m\right) \\ + \frac{1}{2} \ln |\mathbf{P}_m| - \frac{\alpha_0}{2} \boldsymbol{\mu}_m^T \mathbf{P}_m \boldsymbol{\mu}_m + \left(\frac{\nu - d - 1}{2}\right) \ln |\mathbf{P}_m| \\ - \frac{1}{2} \text{Tr}\left[\mathbf{S}^{-1} \mathbf{P}_m\right] + const_{\boldsymbol{\mu}_m, \mathbf{P}_m} \end{aligned} \quad \text{(B.10)}$$

  From equation (B.10) we can infer the following:

$$\begin{aligned} Q(\boldsymbol{\mu}_m, \mathbf{P}_m) &= \text{Normal}\left(\boldsymbol{\mu}_m; \mathbf{m}_{\boldsymbol{\mu}}^{(m)}, \boldsymbol{\Sigma}_{\boldsymbol{\mu}}^{(m)}\right) \text{Wishart}_{\tilde{\nu}_m}\left(\mathbf{P}_m; \tilde{\mathbf{R}}_m\right) \\ \bar{\mathbf{x}}_m &= \frac{\sum_{i=1}^{N} \langle s_{im} \rangle \mathbf{x}_i}{\sum_{i=1}^{N} \langle s_{im} \rangle} \\ \boldsymbol{\Sigma}_{\boldsymbol{\mu}}^{(m)} &= \left(\sum_{i=1}^{N} \langle s_{im} \rangle + \alpha_0\right)^{-1} \mathbf{P}_m^{-1} \\ \mathbf{m}_{\boldsymbol{\mu}}^{(m)} &= \boldsymbol{\Sigma}_{\boldsymbol{\mu}_m} \left(\sum_{i=1}^{N} \langle s_{im} \rangle\right) \mathbf{P}_m \bar{\mathbf{x}}_m = \frac{\sum_{i=1}^{N} \langle s_{im} \rangle}{\sum_{i=1}^{N} \langle s_{im} \rangle + \alpha_0} \bar{\mathbf{x}}_m \end{aligned}$$

$$\tilde{\mathbf{R}}_m^{-1} = \mathbf{R}^{-1} + \sum_{i=1}^{N} \langle s_{im} \rangle (\mathbf{x}_i - \bar{\mathbf{x}}_m)(\mathbf{x}_i - \bar{\mathbf{x}}_m)^T + \frac{\sum_{i=1}^{N} \langle s_{im} \rangle \alpha_0}{\sum_{i=1}^{N} \langle s_{im} \rangle + \alpha_0} \bar{\mathbf{x}}_m \bar{\mathbf{x}}_m^T$$

$$\tilde{\nu}_m = \nu + \sum_{i=1}^{N} \langle s_{im} \rangle$$

- For $Q(\mathbf{S})$:

  $$\ln Q(s_{i1} = 1) = \frac{1}{2} \langle \ln |\mathbf{P}_1| \rangle - \frac{1}{2} \left\langle (\mathbf{x}_i - \boldsymbol{\mu}_1)^T \mathbf{P}_1 (\mathbf{x}_i - \boldsymbol{\mu}_1) \right\rangle + \langle \ln \zeta \rangle + const_{s_{i1}}$$

  Similarly,

  $$\ln Q(s_{i2} = 1) = \frac{1}{2} \langle \ln |\mathbf{P}_2| \rangle - \frac{1}{2} \left\langle (\mathbf{x}_i - \boldsymbol{\mu}_2)^T \mathbf{P}_2 (\mathbf{x}_i - \boldsymbol{\mu}_2) \right\rangle + \langle \ln(1 - \zeta) \rangle + const_{s_{i2}}$$

  The expectation $\left\langle (\mathbf{x}_i - \boldsymbol{\mu}_m)^T \mathbf{P}_m (\mathbf{x}_i - \boldsymbol{\mu}_m) \right\rangle$ is deceptively simple. Expanding the quadratic as follows:

  $$\left\langle (\mathbf{x}_i - \boldsymbol{\mu}_m)^T \mathbf{P}_m (\mathbf{x}_i - \boldsymbol{\mu}_m) \right\rangle = \mathbf{x}_i{}^T \langle \mathbf{P}_m \rangle \mathbf{x}_i - 2\mathbf{x}_i^T \langle \mathbf{P}_m \boldsymbol{\mu}_m \rangle + \left\langle \boldsymbol{\mu}_m^T \mathbf{P} \boldsymbol{\mu}_m \right\rangle$$

  we notice that the only tricky expectations are $\langle \mathbf{P}_m \boldsymbol{\mu}_m \rangle$ and $\left\langle \boldsymbol{\mu}_m^T \mathbf{P} \boldsymbol{\mu}_m \right\rangle$, which simplify considerably on consideration of the update equations for $Q(\boldsymbol{\mu}_m, \mathbf{P}_m)$ giving:

  $$\begin{aligned} \left\langle (\mathbf{x}_i - \boldsymbol{\mu}_m)^T \mathbf{P}_m (\mathbf{x}_i - \boldsymbol{\mu}_m) \right\rangle = {} & \left(\mathbf{x}_i - \langle \boldsymbol{\mu}_m | \mathbf{P}_m \rangle\right)^T \langle \mathbf{P}_m \rangle \left(\mathbf{x}_i - \langle \boldsymbol{\mu}_m | \mathbf{P}_m \rangle\right) \\ & + \langle \mathrm{Cov}\left(\boldsymbol{\mu}_m | \mathbf{P}_m\right) \mathbf{P}_m \rangle \end{aligned}$$

## B.3 Variational Approximation for Forgetting Rates

For convenience, we will repeat the log probability of the of the statistical model represented by figure 3.12:

$$\begin{aligned} \ln p(\mathbf{y}, \mathbf{w}, \lambda, \psi_y | \mathbf{x}) = & \sum_{n=1}^{N} \Bigg[ \frac{1}{2} \ln \frac{\psi_y}{2\pi} - \frac{\psi_y}{2} (y_n - w_n x_n)^2 \\ & + \frac{1}{2} \ln \frac{\lambda}{2\pi} - \frac{\lambda}{2} (w_n - w_{n-1})^2 \Bigg] \\ & + \frac{1}{2} \ln \frac{\zeta_0}{2\pi} - \frac{\zeta_0}{2} (w_0 - \hat{w}_0)^2 \\ & + a_\lambda \ln b_\lambda - \ln \Gamma(a_\lambda) + (a_\lambda - 1) \ln \lambda - b_\lambda \lambda \\ & + a_\psi \ln b_\psi - \ln \Gamma(a_\psi) + (a_\psi - 1) \ln \psi_y - b_\psi \psi_y \end{aligned} \tag{B.11}$$

If we assume the factorization $Q(\mathbf{x}_{\mathcal{H}}) = Q(\mathbf{w})Q(\lambda, \psi_y)$, then from the graph structure in figure 3.12 we can see that this factorization also results in the factorization $Q(\lambda, \psi_y) = Q(\lambda)Q(\psi_y)$. Hence, we can use the results derived in appendix B.1, to obtain the update equations for the following marginal distributions:

- For $Q(\psi_y)$:

$$\ln Q(\psi_y) = \frac{N}{2}\ln\psi_y - \frac{\psi_y}{2}\sum_{n=1}^{N}\left\langle (y_n - w_n x_n)^2 \right\rangle_N + (a_\psi - 1)\ln\psi_y - b_\psi\psi_y + const_{\psi_y} \quad \text{(B.12)}$$

From equation (B.12) we can infer the following:

$$\begin{aligned} Q(\psi_y) &= \text{Gamma}\left(\psi_y; \hat{a}_\psi, \hat{b}_\psi\right) \\ \hat{a}_\psi &= a_\psi + \frac{N}{2} \\ \hat{b}_\psi &= b_\psi + \frac{1}{2}\sum_{n=1}^{N}\left\langle (y_n - w_n x_n)^2 \right\rangle_N \\ &= b_\psi + \frac{1}{2}\sum_{n=1}^{N}\left[\left(y_n - \langle w_n\rangle_N x_n\right)^2 + \frac{1}{\varphi_n}\right] \end{aligned}$$

- For $Q(\lambda)$:

$$\ln Q(\lambda) = \frac{N}{2}\ln\lambda - \frac{\lambda}{2}\sum_{n=1}^{N}\left\langle (w_n - w_{n-1})^2 \right\rangle_N + (a_\lambda - 1)\ln\lambda - b_\lambda\lambda + const_\lambda \quad \text{(B.13)}$$

From equation (B.13) we can infer the following:

$$\begin{aligned} Q(\lambda) &= \text{Gamma}\left(\lambda; \hat{a}_\lambda, \hat{b}_\lambda\right) \\ \hat{a}_\lambda &= a_\lambda + \frac{N}{2} \\ \hat{b}_\lambda &= b_\lambda + \frac{1}{2}\sum_{n=1}^{N}\left\langle (w_n - w_{n-1})^2 \right\rangle_N \\ &= b_\lambda + \frac{1}{2}\sum_{n=1}^{N}\left[\left(\langle w_n\rangle_N - \langle w_{n-1}\rangle_N\right)^2 + \frac{1}{\varphi_n} + \frac{1}{\varphi_{n-1}} - 2\,\text{Cov}\left(w_{n-1}, w_n\right)\right] \end{aligned}$$

In order to estimate the $\text{Cov}\left(w_{n-1}, w_n\right)$ term we must consider the joint posterior distribution of $(w_{n-1}, w_n)$, which can be written as:

$$Q(w_{n-1}, w_n|\mathbf{x}_{\mathcal{D}_{1:N}}) = \frac{Q\left(w_n|w_{n-1}\right) Q\left(w_{n-1}|\mathbf{x}_{\mathcal{D}_{1:n-1}}\right)}{\int Q\left(w_n|w_{n-1}\right) Q\left(w_{n-1}|\mathbf{x}_{\mathcal{D}_{1:n-1}}\right) dw_{n-1}} Q(w_n|\mathbf{x}_{\mathcal{D}_{1:N}})$$

where

$$\begin{aligned} Q\left(w_n|w_{n-1}\right) &= \text{Normal}\left(w_n; w_{n-1}, 1/\lambda\right) \\ Q\left(w_{n-1}|\mathbf{x}_{\mathcal{D}_{1:n-1}}\right) &= \text{Normal}\left(w_{n-1}; \langle w_{n-1}\rangle_{n-1}, 1/\zeta_{n-1}\right) \\ Q(w_n|\mathbf{x}_{\mathcal{D}_{1:N}}) &= \text{Normal}\left(w_n; \langle w_n\rangle_N, 1/\varphi_N\right) \end{aligned}$$

Since all the distributions involved are Gaussian, it is easy to show that the resulting joint distribution $Q(w_{n-1}, w_n|\mathbf{x}_{\mathcal{D}_{1:N}})$ is also Gaussian, and using Schur complements (see appendix A.1), we can derive the off-diagonal covariance term:

$$\text{Cov}(w_{n-1}, w_n) = \frac{\langle\lambda\rangle\left(\zeta_{n-1} + \langle\lambda\rangle\right)}{\varphi_{n-1}\left[\varphi_n\left(\zeta_{n-1} + \langle\lambda\rangle\right) + \langle\lambda\rangle^2\right]}$$

## B.4 Derivation of Probabilistic Backfitting

To derive an EM solution to probabilistic backfitting, we begin with the complete log likelihood of equation (4.15):

$$\begin{aligned} \ln p(\mathbf{x}_{\mathcal{D}}, \mathbf{x}_{\mathcal{H}}; \boldsymbol{\phi}) = &-\frac{N}{2}\ln\psi_y - \frac{1}{2\psi_y}\sum_{i=1}^{N}\left(y_i - \mathbf{1}^T\mathbf{z}_i\right)^2 \\ &- \sum_{m=1}^{d}\left[\frac{N}{2}\ln\psi_{zm} + \frac{1}{2\psi_{zm}}\sum_{i=1}^{N}\left(z_{im} - b_m f_m(\mathbf{x}_i; \boldsymbol{\theta}_m)\right)^2\right] + const \end{aligned}$$

Taking expectations w.r.t. $p(\mathbf{x}_{\mathcal{H}}|\mathbf{x}_{\mathcal{D}}; \boldsymbol{\phi})$ where $\mathbf{x}_{\mathcal{H}} = \{\mathbf{Z}\}$, and differentiating with respect to each of the parameters $\boldsymbol{\phi} = \left\{\{b_m, \psi_{zm}\}_{m=1}^{d}, \psi_y\right\}$ we get the following M-step equations:

$$\begin{aligned} b_m &= \frac{\sum_{i=1}^{N}\langle z_{im}\rangle f_m(\mathbf{x}_i)}{\sum_{i=1}^{N} f_m(\mathbf{x}_i)^2} \\ \psi_y &= \frac{1}{N}\left[\sum_{i=1}^{N} y_i^2 - 2\mathbf{1}^T\sum_{i=1}^{N} y_i\langle\mathbf{z}_i\rangle + \mathbf{1}^T\left(\sum_{i=1}^{N}\left\langle\mathbf{z}_i\mathbf{z}_i^T\right\rangle\right)\mathbf{1}\right] \\ \psi_{zm} &= \frac{1}{N}\left[\sum_{i=1}^{N}\left\langle z_{im}^2\right\rangle - 2b_m\sum_{i=1}^{N}\langle z_{im}\rangle f_m(\mathbf{x}_i) + b_m^2\sum_{i=1}^{N} f_m(\mathbf{x}_i)^2\right] \end{aligned}$$

The expectations $\langle \mathbf{z}_i \rangle$, $\langle \mathbf{z}_i \mathbf{z}_i^T \rangle$, $\langle z_{im} \rangle$ and $\langle z_{im}^2 \rangle$ which feature in the above equations must be evaluated w.r.t. the posterior distribution $p(\mathbf{x}_H | \mathbf{x}_\mathcal{D}; \boldsymbol{\phi})$. Using Bayes rule, the posterior distribution over the hidden variables $\mathbf{Z}$ can be evaluated as follows:

$$\begin{aligned}
\ln p(\mathbf{z}_i | y_i, \mathbf{x}_i) &= \ln p(y_i | \mathbf{z}_i) + \ln(\mathbf{z}_i | \mathbf{x}_i) + const \\
&= -\frac{1}{2\psi_y} \left( y_i - \mathbf{1}^T \mathbf{z}_i \right)^2 - \frac{1}{2} \big( \mathbf{z}_i - \mathbf{B}\mathbf{f}(\mathbf{x}_i) \big)^T \boldsymbol{\Psi}_\mathbf{z}^{-1} \big( \mathbf{z}_i - \mathbf{B}\mathbf{f}(\mathbf{x}_i) \big) + const \\
&= -\frac{1}{2} \left[ \mathbf{z}_i^T \left( \frac{1}{\psi_y} \mathbf{1}\mathbf{1}^T + \boldsymbol{\Psi}_z^{-1} \right) \mathbf{z}_i - 2\mathbf{z}_i^T \left( \frac{1}{\psi_y} \mathbf{1} y_i + \boldsymbol{\Psi}_z^{-1} \mathbf{B}\mathbf{f}(\mathbf{x}_i) \right) + \dots \right] \\
&\quad + const
\end{aligned}$$

where we define $\mathbf{B} \equiv \text{diag}\,[b_1 \cdots b_d]$, and $\boldsymbol{\Psi}_\mathbf{z} \equiv \text{diag}\,[\psi_{z1} \cdots \psi_{zd}]$. Since this expression is quadratic in $\mathbf{z}_i$, we can infer that the posterior distribution of $\mathbf{z}_i$ is Gaussian with the following parameters:

$$\begin{aligned}
\mathbf{z}_i | y_i, \mathbf{x}_i &\sim \text{Normal}\left( \mathbf{z}_i; \boldsymbol{\Sigma}_{\mathbf{z}|y,\mathbf{x}}, \boldsymbol{\mu}_{\mathbf{z}_i} \right) \\
\boldsymbol{\Sigma}_{\mathbf{z}|y,\mathbf{x}} &= \left( \frac{1}{\psi_y} \mathbf{1}\mathbf{1}^T + \boldsymbol{\Psi}_z^{-1} \right)^{-1} \qquad \text{(B.14)} \\
\boldsymbol{\mu}_{\mathbf{z}_i} &= \boldsymbol{\Sigma}_{\mathbf{z}|y,\mathbf{x}} \left( \frac{1}{\psi_y} \mathbf{1} y_i + \boldsymbol{\Psi}_z^{-1} \mathbf{B}\mathbf{f}(\mathbf{x}_i) \right)
\end{aligned}$$

Applying the Sherman-Morrison-Woodbury matrix inversion lemma[1]to the expression in equation (B.14) we get:

$$\begin{aligned}
\boldsymbol{\Sigma}_{\mathbf{z}|y,\mathbf{x}} &= \boldsymbol{\Psi}_z - \frac{\boldsymbol{\Psi}_z \mathbf{1}\mathbf{1}^T \boldsymbol{\Psi}_z}{\psi_y + \mathbf{1}^T \boldsymbol{\Psi}_z \mathbf{1}} \qquad \text{(B.15)} \\
\boldsymbol{\mu}_{\mathbf{z}_i} &= \left( \boldsymbol{\Psi}_z - \frac{\boldsymbol{\Psi}_z \mathbf{1}\mathbf{1}^T \boldsymbol{\Psi}_z}{\psi_y + \mathbf{1}^T \boldsymbol{\Psi}_z \mathbf{1}} \right) \left( \frac{1}{\psi_y} \mathbf{1} y_i + \boldsymbol{\Psi}_z^{-1} \mathbf{B}\mathbf{f}(\mathbf{x}_i) \right) \\
&= \left( \frac{\boldsymbol{\Psi}_z \mathbf{1}}{\psi_y + \mathbf{1}^T \boldsymbol{\Psi}_z \mathbf{1}} \right) y_i + \left( \mathbf{B} - \frac{\boldsymbol{\Psi}_z \mathbf{1}\mathbf{1}^T \mathbf{B}}{\psi_y + \mathbf{1}^T \boldsymbol{\Psi}_z \mathbf{1}} \right) \mathbf{f}(\mathbf{x}_i) \qquad \text{(B.16)}
\end{aligned}$$

Although these equations appear to require quadratic computational complexity, we note that we are only required to compute the terms $\mathbf{1}^T \langle \mathbf{z}_i \rangle$, $\mathbf{1}^T \langle \mathbf{z}_i \mathbf{z}_i^T \rangle \mathbf{1}$, $\langle z_{im} \rangle$, and $\langle z_{im}^2 \rangle$. Using the parameters of the posterior distribution derived in equations (B.15) and (B.16), and defining $s = \psi_y + \mathbf{1}^T \boldsymbol{\Psi}_z \mathbf{1}$, we can derive the following E-step equations:

[1]$(\mathbf{XRY} + \mathbf{A})^{-1} = \mathbf{A}^{-1} - \mathbf{A}^{-1}\mathbf{X}(\mathbf{R}^{-1} + \mathbf{Y}\mathbf{A}^{-1}\mathbf{X})^{-1}\mathbf{Y}\mathbf{A}^{-1}$

$$
\begin{aligned}
\mathbf{1}^T \langle \mathbf{z}_i \rangle &= \frac{1}{s}\left(\sum_{m=1}^{d} \psi_{zm}\right) y_i + \left(1 - \frac{1}{s}\left(\sum_{m=1}^{d} \psi_{zm}\right)\right) \mathbf{b}^T \mathbf{f}(\mathbf{x}_i) \\
&= \frac{1}{s}\left[\left(\sum_{m=1}^{d} \psi_{zm}\right) + \psi_y \mathbf{b}^T \mathbf{f}(\mathbf{x}_i)\right]
\end{aligned} \tag{B.17}
$$

$$
\begin{aligned}
\mathbf{1}^T \left\langle \mathbf{z}_i \mathbf{z}_i^T \right\rangle \mathbf{1} &= \sum_{m=1}^{d} \psi_{zm} - \frac{1}{s}\left(\sum_{m=1}^{d} \psi_{zm}\right)^2 + \left(\mathbf{1}^T \langle \mathbf{z}_i \rangle\right)^2 \\
&= \frac{\psi_y}{s}\left(\sum_{m=1}^{d} \psi_{zm}\right) + \left(\mathbf{1}^T \langle \mathbf{z}_i \rangle\right)^2
\end{aligned} \tag{B.18}
$$

$$
\langle z_{im} \rangle = b_m x_{im} + \frac{1}{s}\psi_{zm}\left(y_i - \mathbf{b}^T \mathbf{f}(\mathbf{x}_i)\right) \tag{B.19}
$$

$$
\left\langle z_{im}^2 \right\rangle = \psi_{zm} - \frac{1}{s}\psi_{zm}^2 + \langle z_{im} \rangle^2 \tag{B.20}
$$

This allows us to derive the following EM update equations:

**M-Step** :

$$
b_m = \frac{\sum_{i=1}^{N} \langle z_{im} \rangle f_m(\mathbf{x}_i)}{\sum_{i=1}^{N} f_m(\mathbf{x}_i)^2}
$$

$$
\psi_y = \frac{1}{N}\sum_{i=1}^{N}\left(y_i - \mathbf{1}^T \langle \mathbf{z}_i \rangle\right)^2 + \mathbf{1}^T \boldsymbol{\Sigma}_{\mathbf{z}} \mathbf{1}
$$

$$
\psi_{zm} = \frac{1}{N}\sum_{i=1}^{N}\left(\langle z_{im} \rangle - b_m f_m(\mathbf{x}_i)\right)^2 + \sigma_{zm}^2
$$

**E-Step** :

$$
\mathbf{1}^T \boldsymbol{\Sigma}_{\mathbf{z}} \mathbf{1} = \left(\sum_{m=1}^{d} \psi_{zm}\right)\left[1 - \frac{1}{s}\left(\sum_{m=1}^{d} \psi_{zm}\right)\right]
$$

$$
\sigma_{zm}^2 = \psi_{zm}\left(1 - \frac{1}{s}\psi_{zm}\right)
$$

$$
\langle z_{im} \rangle = b_m f_m(\mathbf{x}_i) + \frac{1}{s}\psi_{zm}\left(y_i - \mathbf{b}^T \mathbf{f}(\mathbf{x}_i)\right)
$$

where we define $s \equiv \psi_y + \sum_{m=1}^{d} \psi_{zm}$

## B.5 Variational Approximation for Bayesian Backfitting

### B.5.1 Regularizing the Regression Vector Length

Starting with the joint distribution outlined in equation (4.25), we can use the same procedure outlined in previous sections to obtain update equations for the marginal posterior distributions:

$$\begin{aligned}
\ln p(\mathbf{x}_{\mathcal{D}}, \mathbf{x}_{\mathcal{H}}; \boldsymbol{\phi}) = &-\frac{N}{2}\ln\psi_y - \frac{1}{2\psi_y}\sum_{i=1}^{N}\left(y_i - \mathbf{1}^T\mathbf{z}_i\right)^2 \\
&-\sum_{m=1}^{d}\left[\frac{N}{2}\ln\psi_{zm} + \frac{1}{2\psi_{zm}}\sum_{i=1}^{N}\left(z_{im} - b_m f_m(\mathbf{x}_i; \boldsymbol{\theta}_m)\right)^2\right] \\
&+\frac{d}{2}\ln\alpha - \frac{\alpha}{2}\sum_{m=1}^{d} b_m^2 \\
&+(a_\alpha - 1)\ln\alpha - b_\alpha\alpha + const_{\mathbf{x}_{\mathcal{D}}, \mathbf{x}_{\mathcal{H}}}
\end{aligned}$$

We assume the factorization $Q(\mathbf{b}, \alpha, \mathbf{Z}) = Q(\mathbf{b})Q(\alpha)Q(\mathbf{Z})$ which allows us to derive the following update equations:

- For $Q(\alpha)$:

$$\ln Q(\alpha) = \frac{d}{2}\ln\alpha - \frac{\alpha}{2}\sum_{m=1}^{d} b_m^2 + (a_\alpha - 1)\ln\alpha - b_\alpha\alpha + const_\alpha \tag{B.21}$$

From equation (B.21) we can infer the following:

$$\begin{aligned}
Q(\alpha) &= \text{Gamma}\left(\alpha; \hat{a}_\alpha, \hat{b}_\alpha\right) \\
\hat{a}_\alpha &= a_\alpha + \frac{d}{2} \\
\hat{b}_\alpha &= b_\alpha + \frac{\left\langle \mathbf{b}^T\mathbf{b} \right\rangle}{2}
\end{aligned}$$

- For $Q(\mathbf{b})$:

$$\ln Q(\mathbf{b}) = -\sum_{m=1}^{d}\left[\frac{1}{2\psi_{zm}}\sum_{i=1}^{N}\left(z_{im} - b_m f_m(\mathbf{x}_i; \boldsymbol{\theta}_m)\right)^2\right] - \frac{\alpha}{2}\sum_{m=1}^{d} b_m^2 + const_{\mathbf{b}} \tag{B.22}$$

From equation (B.22) we can infer the following:

$$\begin{aligned}
Q(\mathbf{b}) &= \prod_{m=1}^{d}\text{Normal}\left(b_m; \mu_{b_m}, \sigma_{b_m}^2\right) \\
\sigma_{b_m}^2 &= \left(\frac{1}{\psi_{zm}}\sum_{i=1}^{N} f_m(\mathbf{x}_i)^2 + \langle\alpha\rangle\right) \\
\mu_{b_m} &= \sigma_{b_m}^2\left(\frac{1}{\psi_{zm}}\sum_{i=1}^{N}\langle z_{im}\rangle f_m(\mathbf{x}_i)\right)
\end{aligned}$$

### B.5.2 Alternative Posterior Factorization

The joint distribution over all variables in the model of figure 4.7(a) is:

$$\begin{aligned}\ln p(\mathbf{x}_{\mathcal{D}}, \mathbf{x}_{\mathcal{H}}; \boldsymbol{\phi}) = &-\frac{N}{2}\ln\psi_y - \frac{1}{2\psi_y}\sum_{i=1}^{N}\left(y_i - \mathbf{1}^T\mathbf{z}_i\right)^2 \\ &+ \frac{N}{2}\sum_{m=1}^{d}\ln\frac{\alpha}{\psi_{zm}} - \sum_{m=1}^{d}\frac{\alpha}{2\psi_{zm}}\sum_{i=1}^{N}\left(z_{im} - b_m f_m(\mathbf{x}_i)\right)^2 \\ &+ \frac{d}{2}\ln\alpha - \frac{\alpha}{2}\mathbf{b}^T\mathbf{b} \\ &+ (a_\alpha - 1)\ln\alpha - b_\alpha\alpha + const_{\mathbf{x}_{\mathcal{D}},\mathbf{x}_{\mathcal{H}}}\end{aligned}$$

Instead of the complete factorization assumed in sections 4.4.1 and 4.4.2, we only assume the following:

$$Q(\mathbf{b}, \alpha, \mathbf{Z}) = Q(\mathbf{b}, \alpha)Q(\mathbf{Z})$$

Even with the assumption of complete factorization relaxed, the model can still be analytically solved as follows:

- For $Q(\mathbf{b}, \alpha)$:

$$\begin{aligned}\ln Q(\mathbf{b}, \alpha) = &\frac{Nd}{2}\ln\alpha - \alpha\sum_{m=1}^{d}\frac{1}{2\psi_{zm}}\sum_{i=1}^{N}\left\langle\left(z_{im} - b_m f_m(\mathbf{x}_i)\right)^2\right\rangle \\ &+ \frac{d}{2}\ln\alpha - \frac{\alpha}{2}\mathbf{b}^T\mathbf{b} + (a_\alpha - 1)\ln\alpha - b_\alpha\alpha + const_{\mathbf{b},\alpha}\end{aligned} \tag{B.23}$$

From equation (B.23) we can deduce the following:

$$\begin{aligned}Q(\mathbf{b}, \alpha) &= Q(\alpha)\prod_{m=1}^{d} Q(b_m|\alpha) \\ Q(b_m|\alpha) &= \text{Normal}\left(b_m; \mu_{b_m}, \sigma_{b_m}^2\right) \\ \sigma_{b_m}^2 &= \frac{\psi_{zm}}{\alpha}\left(\sum_{i=1}^{N} f_m(\mathbf{x}_i)^2 + \psi_{zm}\right)^{-1} \\ \mu_{b_m} &= \left(\sum_{i=1}^{N} f_m(\mathbf{x}_i)^2 + \psi_{zm}\right)^{-1}\left(\sum_{i=1}^{N}\langle z_{im}\rangle f_m(\mathbf{x}_i)\right)\end{aligned} \tag{B.24}$$

Note that in Eq. (B.24), the posterior mean $\langle b_m|\alpha_m\rangle = \mu_{b_m}$ is actually independent of $\alpha_m$. We can now rewrite equation (B.23) in terms of the conditional posterior of $b_m$ as follows:

$$\begin{aligned}\ln Q(\mathbf{b},\alpha) = &-\frac{1}{2}\sum_{m=1}^{d}\left[\frac{1}{\sigma_{b_m}^2}\left(b_m-\mu_{b_m}\right)^2 - \frac{\mu_{b_m}^2}{\sigma_{b_m}^2} + \frac{\alpha}{\psi_{zm}}\sum_{i=1}^{N}\left\langle z_{im}^2\right\rangle\right] \\ &+\left(a_\alpha + \frac{Nd+d}{2} - 1\right)\ln\alpha - b_\alpha\alpha + const_{\mathbf{b},\alpha}\end{aligned} \tag{B.25}$$

Taking the exponent and integrating out $\mathbf{b}$ we can derive the following log marginal distribution for $\alpha$:

$$\begin{aligned}\ln Q(\alpha) &= -\frac{1}{2}\sum_{m=1}^{d}\left[-\ln 2\pi\sigma_{b_m}^2 + \frac{\alpha}{\psi_{zm}}\sum_{i=1}^{N}\left\langle z_{im}^2\right\rangle - \frac{\mu_{b_m}^2}{\sigma_{b_m}^2}\right] \\ &\quad+\left(a_\alpha + \frac{Nd+d}{2} - 1\right)\ln\alpha - b_\alpha\alpha + const_{\boldsymbol{\alpha}} \\ &= -\frac{1}{2}\sum_{m=1}^{d}\left[\frac{\alpha}{\psi_{zm}}\sum_{i=1}^{N}\left\langle z_{im}^2\right\rangle - \frac{\mu_{b_m}^2}{\sigma_{b_m}^2}\right] \\ &\quad+\left(a_\alpha + \frac{Nd}{2} - 1\right)\ln\alpha - b_\alpha\alpha + const_{\boldsymbol{\alpha}}\end{aligned}$$

We can therefore deduce that the posterior distribution over $\alpha$ is:

$$\begin{aligned}&Q(\alpha) = \text{Gamma}\left(\alpha;\hat{a}_\alpha,\hat{b}_\alpha\right) \\ &\quad\hat{a}_\alpha = a_\alpha + \frac{Nd}{2} \\ &\quad\hat{b}_\alpha = b_\alpha + \sum_{m=1}^{d}\frac{1}{2\psi_{zm}}\left[\sum_{i=1}^{N}\left\langle z_{im}^2\right\rangle - \left(\sum_{i=1}^{N}f_m(\mathbf{x}_i)^2 + \psi_{zm}\right)^{-1}\left(\sum_{i=1}^{N}\left\langle z_{im}\right\rangle f_m(\mathbf{x}_i)\right)^2\right]\end{aligned}$$

Note that instead of expressing the joint distribution $p(\mathbf{b},\alpha)$ and subsequently integrating out $\mathbf{b}$, we could also use the result derived in section 2.3.2 to directly derive the identical update equations for $Q(\alpha)$. Given the forms of the distributions $Q(b_m|\alpha)$, and $Q(\alpha)$, it is easy to show that the marginal posterior of each regression coefficient is a Student-t distribution:

$$\begin{aligned}Q(\mathbf{b}) &= \prod_{m=1}^{d} t_\nu\left(b_m;\mu_{b_m},\sigma^2\right) \\ &= \frac{\Gamma\left((\nu+1)/2\right)}{\Gamma\left(\nu/2\right)}\left(\frac{1}{\nu\pi\sigma_{b_m}^2}\right)^{1/2}\left[1+\frac{1}{\nu}\frac{\left(x-\mu_{b_m}\right)^2}{\sigma_{b_m}^2}\right]^{-(\nu+1)/2} \\ \nu &= 2\hat{a}_\alpha\end{aligned}$$

$$\mu_{b_m} = \left( \sum_{i=1}^{N} f_m(\mathbf{x}_i)^2 + \psi_{zm} \right)^{-1} \left( \sum_{i=1}^{N} \langle z_{im} \rangle f_m(\mathbf{x}_i) \right)$$

$$\sigma_{b_m}^2 = \frac{\hat{b}_\alpha \psi_{zm}}{\hat{a}_\alpha} \left( \sum_{i=1}^{N} f_m(\mathbf{x}_i)^2 + \psi_{zm} \right)^{-1}$$